Asymmetrical Three-Phase Fault Evaluation in a Distribution Network using the Genetic Algorithm and the Particle Swarm Optimisation

by

Chikomborero Shambare

A Master's Research dissertation submitted in fulfilment of the requirements for the degree of

Master of Engineering

in

Electrical and Electronic Engineering Science

in the

Faculty of Engineering and the Built Environment

at the

UNIVERSITY OF JOHANNESBURG

SUPERVISOR: Professor Yanxia Sun
CO-SUPERVISOR: Dr OdunAyo IMORU

January 2020

Declarations

I CHIKOMBORERO SHAMBARE hereby declare and confirm that this master's research dissertation is entirely my work. It has not been submitted to any other organisation or institution for academic credit by me or any other person. I have a clear understanding of what plagiarism implies and declare that this document is my work except where references and acknowledgement have been made to another person's work and the details have been included in the dissertation or the references sections.

Ethical Statement

It is not the intention of this research to criticise or endorse any of the compared short-circuit computational methods and standards. The chief aim of this dissertation is to present an in-depth analysis on the current methods (methods in use and those found in various pieces of literature) and to bring some innovations that can enhance the intelligence of modern power systems.

Signed Chikomborero Shambare Date 20 January 2020

Acknowledgements

I thank my thesis supervisors i.e. Professor Yanxia Sun and Dr OdunAyo IMORU whose continuous guidance, encouragements, constructive comments and remarks were of great help to me. I would like to thank them for being tolerant and extraordinarily patient with me. Without them and their great qualities, this thesis would not have been successful. I thank them for their great mentorship.

I would also like to give my most sincere regards to the University of Johannesburg and its entities such as the Postgraduate Research Center and the Faculty of Engineering and Built Environment for the various resources provided including conferences, seminars and workshops.

I also thank my family members, friends and colleagues for continuously motivating me during my postgraduate study period.

Abstract

Modern electric power systems are made up of three main sub-systems: generation; transmission; and distribution. The most common faults in distribution sub-systems are asymmetrical three-phase short circuit faults due to the fact that asymmetrical three-phase faults can be: line-to-line faults; two lines-to-earth faults; and single line-to-earth faults. This increases their probability of occurrence, unlike symmetrical three-phase faults which can only occur when all the three phases have been simultaneously shorted. Standard IEC 60909 and IEC 61363 provide all the basic information that is used for the detection of short circuit faults. However, the two standards use numerous estimates in their faults evaluation procedures. They estimate voltage factors (c), impedance correction factors (k), resistance to reactance ratios (R/X), resistance to impedance ratios (R/Z) and various other scaling factors for rotating machines. These IEC estimates are not evenly distributed throughout the 550kV and as such, they do not sufficiently cater for every nominal voltage. When the need arises, the user has to estimate these values accordingly. This research presents a genetic algorithm (GA) and a particle swarm optimisation (PSO) for the detection of asymmetrical three-phase short circuit faults within electric distribution networks of power systems with nominal voltages less than 550kV. GA and PSO are nature-inspired optimisation techniques. Although PSO has quick convergence, it suffers from partial optimism and premature stagnation. Some innovative coding adjustments were made in the creation of initial positions and particle distribution within the swarm. The GA struggles with: survival rates of individuals; stalling during optimisation; and proper gene replacements. Coding adjustments were also made to GA with regards to: strategic gene replacements; crossover when combining the properties of parents; and the arrangement of scores and expectation. Pattern search and Fmincon algorithms were also added to both algorithms as minimisation functions that commence after the evolutionary algorithms (EAs) terminate. The EAs were initially tested on the Rastrigin and Rosenbrock functions to ensure their efficiencies. During fault detection, the developed EAs were used to stochastically determine some of the most crucial estimates (R/X and R/Z ratios). The proposed methodology would compute these values on a case-to-case basis for every optimisation case with regards to the parameters and unique specifications of the power system. The EAs were tested on a nominal voltage that is properly catered for by Standard IEC. They obtained ratios, impedances and currents that were within an approximate range to the IEC values for that nominal voltage. This further implies that EAs can be reliably used to: stochastically determine these ratios; compute impedances; and detect fault currents for all the nominal voltages including those that are not sufficiently catered for by Standard IEC. Since R/X and R/Z ratios play a key role in determining the upstream and fault point impedances, the proposed methodology can be used to compute much more precise fault magnitudes at various network levels thereby setting up and repairing power systems sufficiently.

Keywords: Asymmetrical, Autonomy, Genetic Algorithm, Particle Swarm Optimisation, Robust, Short Circuit Fault, Standard IEC 60909, Standard IEC 61363, Stochastic.

List of Abbreviations

A	Cross-sectional area of conductors
AF	Arc Fault Hazard
AC	Alternating Current
C	Capacitance
CMs	Conventional Methods
CosØ	Power Factor in absence of harmonics
DC	Direct Current
EA	Evolutionary Algorithms
GA	Genetic Algorithm
IEC	International Electro-technical Commission
I	Current
I_{sc}	Short-circuit Current
I_{peak}	Peak Short-circuit current
I_{3P}	Symmetrical Three-Phase Current
I_{LL}	Asymmetrical Line-to-Line Fault
MGA	Modified Genetic Algorithm
MGAF	Modified Genetic Algorithm with Fmincon Hybrid function
MGAP	Modified Genetic Algorithm with Patternsearch Hybrid function
MPSO	Modified Particle Swarm Optimisation
MPSOF	Modified Particle Swarm Optimisation with Fmincon Hybrid function
MPSOP	Modified Particle Swarm Optimisation with Patternsearch Hybrid function
PSO	Particle Swarm Optimisation
R	Resistance
RMC	Reverse Motor Currents
RMS	Root Mean Square value
U	Voltage
U_{phase}	Line (Phase) Voltage
U_{sc}	Short-circuit voltage
X	Reactance
Z	Impedance

Table of Contents

List of Tables

List of Figures

CHAPTER 1

INTRODUCTION

1.1 Research background

Modern electric power systems are made up of three main sub-systems: generation; transmission; and distribution. Electricity distribution can either be by symmetrical (balanced) phase systems or asymmetrical (unbalanced) phase systems (Tleis, 2008). For balanced systems, the line voltages and the line currents are equal to each other whereas, for unbalanced systems, the line voltages and currents are not equal (Sallam et al., 2011). Unbalanced systems occur as a result of asymmetrical loads or some faults within the system and its components. Symmetrical three-phase short circuit current can be detected using the 'Direct' method or the 'Per-Unit' method. These two methods draw the system on a one-line diagram and basic electrical equations are used to calculate the fault magnitude (Das, 2017). To detect asymmetrical three-phase short circuit faults, one can apply the symmetric components technique or one can represent the system on a three-phase plane and retain the identities of all the phases and use them in the fault evaluation procedures (Tleis, 2008). Both methods give an approximate value of the asymmetrical fault current. Both methods are difficult to implement, data-intensive and not easily tractable (Cai et al., 2017). The complexity of the situation increases when more than one device is contributing to the fault (Tan, 2015).

Electrical distribution can either be by a radial system, a ring system or a meshed system (Das, 2017). In the radial and ring distribution sub-systems, it is less complicated to detect the fault current magnitude. For meshed systems, it becomes more difficult because many components feed and inter-depend in supplying the distribution zone (Han et al., 2016). Meshed systems are nowadays commonly used because of their improved reliability (Ashish, 2015). However, it is difficult to precisely detect their short circuit currents. This gives rise to using the most advanced techniques because the basic methods cannot give very precise results (Malik et al., 2011).

1.2 Motivations

There is a continuously increasing demand in the energy which is generated, transmitted and distributed by modern electric power systems (Cai et al., 2017). This increase in power causes overheating of components and rapid degradation of equipment insulation which results in unexpected equipment deterioration. Detecting short circuit faults and their magnitude becomes more complicated because of the numerous fault causes and uncertainties that come along with them. Short circuits may be generated within the system or outside the system (Mathur et al., 2015). This also makes it difficult to predict when and where they will occur and compute their magnitude. Short-circuit faults can be caused by lightning, temperature rise within the system, partial discharges within the system, a connection of two conductors caused by external bodies, faults on motors, faults on generators and ferromagnetic resonance (Das, 2012; Zhang et al.,2014). A power system is also made up of a lot of nonlinear components which present transient behaviour e.g. capacitors, inductors and transistors (Folarin et al., 2018). Due to all these factors, the conventional methods cannot swiftly handle these short circuit currents during abnormal operating conditions (Osowski et al., 2002; Sing et al., 2016). Conventional methods for detecting short circuit faults found from the literature include:

i. The Direct method, Per-Unit method and Symmetric Components Technique (Das, 2017; Sallam et al., 2011).
ii. Computer methods i.e. Time-domain fault analysis and Quasi steady-state fault analysis (Kono et al., 2016; Malik et al., 2011).
iii. Software tools e.g. Matlab, Easy-Power and ETAP (Electrical Transient Analysis Program) (Soroudi et al., 2016).

The detection of short circuit faults in the real world should consider noise and dynamic environments since they adversely affect the fault evaluation processes of these methods (Ghaderi et al., 2015). During the fault evaluation processes of the conventional methods, they try to address the problems of adaptivity to uncertain environments, parameter sensitivity, data intensity, autonomy and multi-objective optimisation (Costa et al., 2015; Debowski et al., 2009). However, they fail to do so sufficiently. The conventional methods struggle with trade-off analysis for higher dimension problems (Kono et al., 2016). For every problem, they need all the characteristics of the function i.e. the task processing periods, data dependencies and synchronisation requirements before they can begin execution (Campoccia

et al., 2007). This means that they cannot provide a valuable mean artificial creativity approach. This inhibits their function maximisation (Imoru et al., 2017).

However, there is a great need for precisely calculated values of short circuit current because one needs to know the specifications of elements to use when designing and repairing power systems. Whenever there is a short circuit fault, one needs to have the root mean square (RMS) value of maximum short circuit current to determine the breaking capacity and temperature stress of the system equipment (Das, 2012). One also needs to have the first peak values of fault current to evaluate the design capacity of switching devices (Gao et al., 2015).

When there is little reliability of methods and all of them giving approximate values, one will have to look at new techniques to deal with the problem and obtain more precise global optimum solutions (Ashish, 2015). Evolutionary algorithms such as the genetic algorithm and the particle swarm optimisation are meta-heuristic tools that help to solve complex optimisation problems. They use the stochastic approach (the process of maximising or minimising the value of a mathematical or statistical function when one or more variables are subject to randomness) (Mishra et al., 2015). For every problem, they commence with a set of randomly populated solutions that under-go initialisation, selection, mutation and recombination (Zhu, 2015). They use the Pareto sense in prioritising the solutions (Yao et al., 2015). This whole procedure makes the least fit solutions to be eliminated by an abstract test of fitness and the strong ones reproduce to give a better solution set than the previous ones. Short circuit faults occur unexpectedly and it is very difficult to precisely predict their point of occurrence and magnitude (Sallam et al., 2011). Therefore one needs to use a method that has a wide range of operating conditions and henceforth, evolutionary computational methods could be applicable.

1.3 Research problems

The detection of asymmetrical three-phase short circuit faults in the real world is a complex problem. In the real world, there are a lot of uncertainties and adverse conditions (Malik et al., 2011). These negative factors interfere with any fault evaluation procedure (Das, 2017; Sheng et al., 2016). There is a strong need for deep research to seek and address the following problems in electrical power distribution sub-systems:

i. Conventional methods of detecting asymmetrical three-phase short circuit faults are not very precise and reliable. In their fault evaluation procedures, they depend on numerous estimations from Standard IEC 60909 and IEC 61313. These estimates (R/X values, R/Z values and voltage factors) do not sufficiently cater for all the nominal voltages (Das, 2016). This gives rise to investigating other alternative methodologies that can sufficiently cater for all the nominal voltages (Sallam et al., 2011).

ii. The precision of the conventional methods decreases with an increase in the network size. Their precision also decreases with an increase in the number of machines contributing to the fault current (Das, 2016). This gives rise to look into other optimisation techniques that can attain more precise results (Ashvini et al., 2015).

iii. The conventional methods of detecting asymmetrical three-phase short circuit faults from the point of inception are not very robust in dealing with noise and uncertainties e.g. simultaneously occurring faults or consecutive faults within a short time, they often need human intervention i.e. they lack autonomy (Tleis, 2008). This gives rise to using more advanced, precise and reliable fault evaluation techniques (Tan, 2015).

1.4 Research objectives

The main objective of this dissertation was to develop a methodology that can sufficiently detect asymmetrical three-phase short circuit faults for every nominal voltage of distribution sub-systems within 550kV. During fault detection, the methodology would use conscientiously modelled GA and PSO to stochastically determine R/Z and R/X values. These values play a key role in determining the upstream and fault point impedances. Precise R/Z and R/X values lead to precise fault current magnitudes. These values would be determined on a case-to-case basis for every optimisation case with regards to the parameters and unique specifications of the power system. The methodology would test the effects of including non-spinning loads during fault detection at various network levels. It would also test the effects of including upstream reactances when detecting faults at points that are far away from the sources. The methodology would check if the inclusion of the above-mentioned factors leads to obtaining more precise fault magnitudes.

1.4.1 PSO modelling objectives

PSO would be modelled and implemented with the following objectives:

- To check the effects of creating a lot of particle positions and giving the particles a wide exploration range with regards to ensuring that all the search space is fully exploited.
- To check the effects of influencing particle distribution within the swarm with regards to enhancing its manipulation.
- To check the effects of continuously influencing the regulation of particle velocity and direction with regards to eliminating partial optimism and premature stagnation.
- The check the effects of adding a minimisation function that commences when the algorithm terminates (Hybrid functions e.g. Pattern search and Fmincon).

1.4.2 GA modelling objectives

GA would be modelled and implemented with the following objectives:

- To check the effects of arranging expectation over the use of probabilities with regards to stalling and degenerate scenarios during optimisation.
- To check the effects of arranging scores over the use of probabilities with regards to survival rates of individuals.
- To check if it is possible to continuously influence the number of individuals that can be created at each evolution stage to ensure search efficiency until the end of optimisation.
- To check if it is possible to sufficiently replace genes and achieve population diversity throughout optimisation and maintain it.
- To check the effects of implementing advanced gene concatenation when combining the properties of parents through crossover to form a single gene for the child.
- The check the effects of adding a minimisation function that commences when the algorithm terminates (hybrid functions e.g. Pattern-search and Fmincon).

1.5 Research significance

The fault evaluation procedures given by Standard IEC 60909 and IEC 61313 do not sufficiently cater for all the nominal voltages (this is shown in Chapter 3.6). Moreover, the IEC fault evaluation procedures do not account for all the possible operating scenarios. They are limited to a small range. Nonetheless, there remains a need for precisely detecting fault magnitudes at all times. If the proposed methodology is implemented correctly, it can offer reliable and precise solutions for all the nominal voltages within 550kV. It can also cater for a

wider range of operating scenarios e.g. fault evaluation whilst considering many machines contributing to the fault current and simultaneously occurring faults. This helps in the designing, setting up and repairing of power systems sufficiently.

1.6 Delimitations (Scope of study)

i. This research only focuses on short circuit faults.
ii. Asymmetrical three-phase faults can be classified as single phase-to-earth faults, phase-to-phase faults and two phases-to-earth faults. Not all the fault types could be tested and analysed in depth because of the limited time duration of this research.
iii. Not all possible operating scenarios and uncertainties that come along with short circuit faults could be covered by this research.
iv. Only a limited number of network schematics could be optimised because of the limited time duration.

1.7 Outline of the dissertation

This dissertation is organised as follows;

- Chapter 1, 'Introduction', presents the research background, research motivations, research problems, research objectives, its scope and the outline of the dissertation.
- Chapter 2, 'Literature review', presents a detailed review of the current fault evaluation methods and their weaknesses. It also gives suggestions for the computational problem and a detailed overview of the GA and PSO.
- Chapter 3, 'Research methodology', gives the research approach and the details of the proposed modelling and modifications that were implemented on the GA and PSO. The algorithms are also tested on the Rastrigin and Rosenbrock benchmark functions.
- Chapter 4, 'Computational procedures', gives the short circuit fault benchmark functions, optimisation problem, fault detection procedures and the tables of results.
- Chapter 5, 'Research findings discussions', discusses the computed coefficients, computed impedances and the computed currents. It also evaluates the best and worst algorithms for the computational problem that was under investigation.
- Chapter 6, 'Conclusion', presents the conclusions, recommendations and the list of publications.

CHAPTER 2

LITERATURE REVIEW

2.1 Review of the short circuit fault characteristics

Short circuit faults can transpire in any part of the power system but faults within the distribution sub-systems have the most complexity (Juszczak et al., 1992). Electrical distribution can either be by radial systems, ring systems or meshed systems (Das, 2017). Regardless of being the most complex, most electricity distribution is by the meshed system because of its improved reliability (Sallam et al., 2011). Distribution sub-systems have a lot of components that maintain a continuous flow of current and bring stability to power systems e.g. backup generators, isolators, circuit breakers, relays, stabilisers, meters, earthing gears and other auxiliary supplies (Das, 2016). Some of the equipment have non-linear properties and presents transient behaviour e.g. capacitors. A short circuit fault may be generated within the system or outside the system and this makes it very difficult to predict when and where the fault will occur and compute its magnitude (Sarlak et al., 2011). It is difficult for one to detect simultaneously and consecutively occurring faults. Asymmetrical three-phase short circuit faults can be phase-to-phase faults, single phase-to-earth faults or two phases-to-earth faults (Tleis, 2008). Whenever a fault occurs it divides the power system into an upstream network and a downstream network. Figure 2.1 illustrates how a fault divides a network system (Das, 2017). In Figure 2.1(a), the short circuit fault is located far from the sources and in Figure 2.1(b); the fault is located at the generator terminals. For faults far away from the sources, the effects of the parameters of the sources as rotating machines can be ignored, but for faults located at the generator terminals, the effects of the generator parameters should be taken into account (Das, 2017).

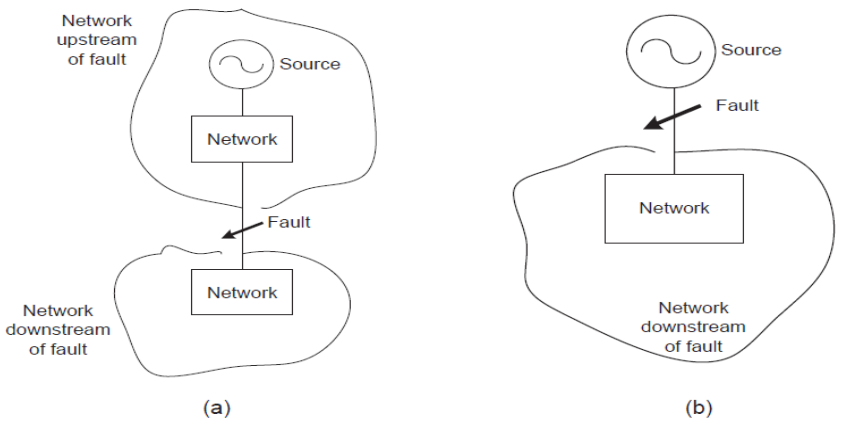

Figure 2.1 The characteristics of short circuit faults (Das, 2017)

When a short circuit fault occurs close enough to the terminals of a generator, the generator will produce four components of short circuit fault i.e. the aperiodic component, the sub-transient component, the transient component and the steady-state component (Sallam et al., 2011). Figure 2.2 is an illustration of the individual components. As seen in Figure 2.2, these components have different decay time constants. These decaying patterns are produced as a result of the non-instantaneous change in magnetic flux in machine windings (armature windings) (Ashish, 2015). The four components sum up to give the full short circuit spectrum shown in Figure 2.3.

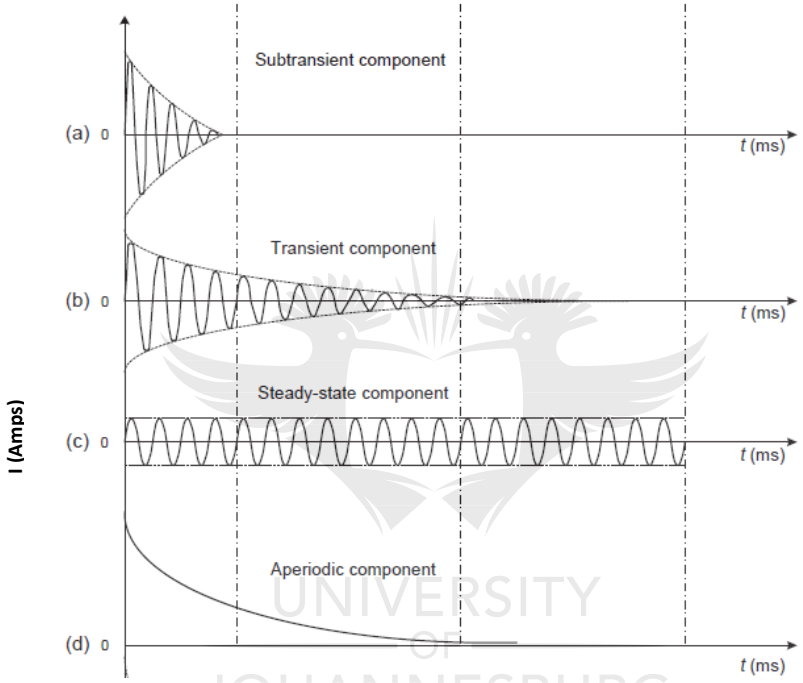

Figure 2.2 Short circuit sub-components (Sallam et al., 2011)

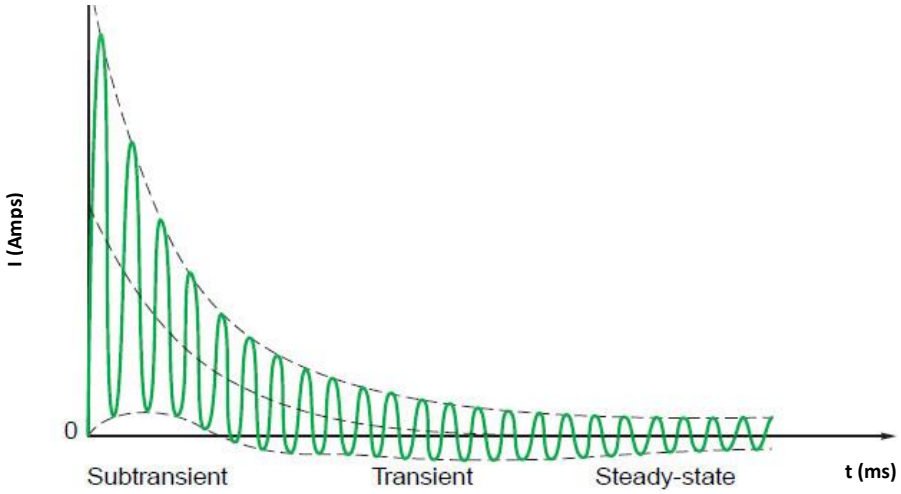

Figure 2.3 Full short circuit spectrum (Sallam et al., 2011)

Figure 2.4 shows the behaviour of short circuit faults from the point of inception (Malik et al., 2011). It can be seen that the fault current is the sum of a sinusoidal component and an exponential component. The sinusoidal component is the sinusoidal steady-state current resulting from the sinusoidal applied voltage (Costa et al., 2015). Figure 2.4 clearly shows that the fault current commences as an asymmetrical sinusoidal wave and becomes symmetrical as the transient exponential component dies away.

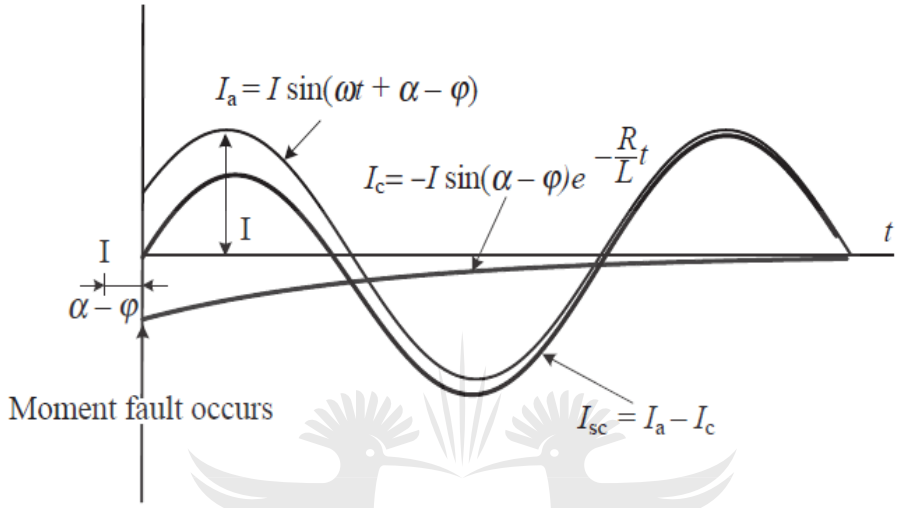

Figure 2.4 Short circuit faults from the moment of inception (Malik et al., 2011)

According to Standard IEC 60909 (IEC 60909-0, 2016; Das, 2017), when a short circuit fault occurs in a large network, with more than one device contributing to the fault, it is very difficult to compute the fault current magnitude because obtaining a Thevenin's equivalent circuit is complex (Costa et al., 2016). The process is data-intensive. Regardless of all that, there remains a strong need for precise fault magnitudes to calculate current flow into different elements of the power system during these abnormal operating conditions. The computed fault magnitudes are used in coordinating protection devices (Bakshi et al., 2012). They aid in defining the design specifications and repairs of the electric power system. The precise values also help to determine the temperature stress and breaking capacity of the system equipment and protective equipment (Ashish, 2015).

There are four main steps used in detecting fault currents and voltages. The steps remain almost the same regardless of the method, software or algorithm used. The steps are (Das, 2016; IEC 60909-0, 2001; IEC 60909-0, 2016):

i. Compute the various bus impedance matrices for the networks' sequences.
ii. Extract the Thevenin equivalent impedances for the faulted bus or buses.

iii. Use the sequence equivalent networks to calculate fault currents for individual sequences on faulted buses.

iv. Use the obtained sequence currents as the compensating currents to calculate the post-fault currents and voltages

2.2 Review of the current fault computational methods

2.2.1 Traditional methods

For the detection of asymmetrical three-phase short-circuit faults, symmetric components technique is the most commonly used method whereby any set of unbalanced phases is made to be represented by a set of balanced phases (Zhang et al., 2017). The system will be represented on a one-line diagram. After the representation, Kirchhoff's laws, Integral transformations or Laplace transformations can be used to calculate the fault magnitude (IEC 60909-0, 2016). One main weakness of this method is that a Thevenin equivalent voltage is used to represent all the sources before and at the fault point. A Thevenin impedance is used to obtain the fault current. A Thevenin equivalent circuit only accounts for the main sources and neglects the transient behaviour of some smaller components within the power system e.g. capacitors and inductors which store and discharge energy into the system (Tleis, 2008). This results in the obtained short circuit value being an approximate value and not the exact magnitude (Folarin et al., 2018). Another weakness is that in large networks, in trying to break down the system to compute 'Per-Unit' values, some important information which is supposed to be included is neglected i.e. Charging currents within the lines are totally neglected and load currents are considered to be negligible whilst the fault current is what is mainly considered in the fault evaluation processes (Ghaderi et al., 2015). This also decreases the precision of the obtained fault magnitudes. The network breakdown in large systems to obtain 'Per-Unit' values is a process that is difficult to implement and not easily tractable (Efe, 2015). Obtaining impedances could seem easy but in practice, it is very difficult because a lot of different voltage sources i.e. main power sources, sub-stations, transformers, rotating machines and loads are connected into a vast network by numerous cables (Ghaderi et al., 2015). Another weakness is that when an asymmetrical three-phase fault occurs in a supposedly balanced system, the fault location is considered to be the only point of interconnection for the sequence networks and the other parts of the network are neglected in

the fault detection procedures. This also decreases the precision of the obtained fault magnitudes (Chavali et al., 2011).

2.2.2 Computer applications

Some computers are programmed to perform a time-domain fault analysis or a quasi steady-state fault analysis (Das, 2017). These computer programs are mainly used for vast and complicated network systems.

2.2.2.1 Time-domain fault analysis

Time-domain fault analysis requires all the details of the system model and network components. In its detection of asymmetrical three-phase short-circuit faults, it uses current and voltage signals obtained during the steady states and transient states (IEC 60909-0, 2001). It detects faults through a time and phasor domain iterative analysis. At each sampling time, an estimate of the load dynamics is considered. Accuracy of the technique depends on the fault database of the bus distribution system in use (Sanseverino et al., 2012). A limited number of uncertainties with relation to the fault resistance, voltage magnitude at source, angle unbalance at source, fault type, power system frequency, power factor and load magnitude can be tested. Accuracy of the obtained results greatly depends on the time of data acquisition (Leva et al., 2005). The major weakness of this method is its sensitivity to parameters. Another weakness is the need for accurate sampling intervals and data acquisition times. An error in obtaining these values results in obtaining an approximate fault value and not the precise fault magnitudes (Costa et al., 2016).

2.2.2.2 Quasi Steady-State Fault Analysis

Quasi steady-state fault analysis does calculations by considering linear models and performing fault analysis at a steady-state (Varun et al., 2016). When a fault occurs, there will be a rise in current and transient behaviour for a certain time (Tleis, 2008). Quasi steady-state fault analysis detects a fault when one part of the system reacts differently to the other parts i.e. mainly changes in timescale (period and duration of wave cycles). Simplification of the time dependence of the faster-reacting parts (fault) of the system to the slower reacting parts (unfaulty) reduces the number of variables to be solved (Leva et al., 2005). The main

weakness of this method is in detecting very small faults and very large faults. This is because some of the faults do not present sufficient enough transient behaviour for the method to be able to detect (Sanseverino et al., 2012). Also, faults with a similar frequency to the main wave but with a difference in amplitude could be neglected by the method. In uncertain environments e.g. consecutive occurring faults, the method can confuse the fault state to the unfaulty state thereby producing imprecise results (Tleis, 2008).

The main weakness of the above-mentioned computer methods is that they are sensitive to the initial parameters, meaning that they do not offer conceptual simplicity (Das, 2012). Also, these computer methods employ static heuristics whereby they begin with a single solution whilst searching for a single solution. This means that these computer methods do not offer function maximisation. Another weakness is that in optimising functions in uncertain environments e.g. a network that has multiple components contributing to the fault, they struggle to determine the global optimum solutions and often need human intervention (lack autonomy) (Malik et al., 2011).

2.2.3 Recent software tools

ETAP software, Easy-Power software and Matlab software are power system analysis software tools which are also commonly used for short circuit fault analysis (Costa et al., 2016). These software tools have various toolboxes and libraries which assist in the prediction; calculation and plotting of short circuit faults. These software tools are very recent and they are constantly updated to try and keep up with the market trends and complexity of the real-world power systems.

2.2.3.1 ETAP software

ETAP (Electrical Transient Analysis Program) has key features which include ANSI/IEEE Standards C37 and UL49, IEC Standards 60909 and 61363 and GOST Standards R-52735 (Das, 2016). These standards are quite conservative in some cases which is positive for calculating symmetrical short circuit faults and less complex asymmetrical short circuit faults (Kim et al., 2016). For large and complicated networks, they do not give explicit details. This leaves the user to devise and formulate the most appropriate steps depending on the complexity of the situation (Das, 2017; Kim et al., 2016).

2.2.3.2 EasyPower software

EasyPower software is mainly based on ANSI/IEEE standard 141. It gives the steps and procedures for detecting fault currents (Das, 2017). It lays out the stage by stage processes and sub-divides large circuits on the schematic drawer. This makes the whole process data-intensive and difficult to implement (Han et al., 2016).

2.2.3.3 Matlab software

Matlab has toolboxes and libraries for power system and short circuit analysis which include Simulink and M-Script Files. Matlab can be used to create and analyse various network schematics. It can also be used to process bus-admittance and bus-impedance matrices of high dimensions (Dall'Anese et al., 2016). However, in simulating a network system in an environment with uncertainties, it does not give reasonable results e.g. if a network system has simultaneously occurring faults or consecutive faults within a short window, there might be signal attenuation within Matlab Simulink and all the values go to zero. This is not necessarily true for real world power systems (Tleis, 2008).

Easy-Power and ETAP do not support parallel computing which can give precise results quickly. Parallel computing gives options to filter starting points based on feasibility (Li et al., 2015). All the three software, just like the traditional methods, can only retain one minimum which could not be the global minimum (Samson et al., 2016). They rely on the user to balance the optimisation problem. On their own, they cannot reach a balance point. They are not robust in dealing with noise and uncertainties and they are not adaptive and cannot deal with dynamic environments (Sarlak et al., 2011). They are not suitable for odd-behaving functions i.e. non-linear, non-convex, non-differentiable and discontinuous functions (Li et al., 2015). They cannot offer function maximisation. They offer single-objective optimisation but cannot offer multi-objective optimisation (Prince et al., 2014).

2.3 Weaknesses of conventional methods and software

A method is expected to balance, schedule and prioritise an optimisation problem. A method is expected to provide reasonable and satisfactory results via a computational process that is fast, accurate, reliable and relatively simple (Tan, 2015). The conventional methods make

some assumptions during their fault evaluation procedures and neglect some important aspects of power systems (Das, 2016; Das, 2017; Tan, 2015):

- They consider all the sources to be balanced and to be of equal phase and magnitude.
- A Thevenin voltage is used to represent all sources at the fault point and prior to the fault.
- An infinite bus-bar is used to represent large size networks.
- Reactances are considered during fault detection whilst resistances are considered to be negligible.
- Fault currents are considered during fault detection whilst load currents are considered to be negligible.
- Charging currents within the lines are neglected during the calculation processes.
- Transformers are considered to be on a nominal tap position.
- All the three phases are assumed to have the same impedance and the lines of transmission are also considered to be fully transposed.

The assumptions listed above show that the conventional methods neglect and overlook some important aspects of the power system and its components. This reduces the precision of the obtained fault magnitude. This results in getting an approximate fault magnitude that greatly deviates from the exact value. Apart from the assumptions made in their fault evaluation processes, the various methods are not robust in dealing with uncertainties and non-linearity and this gives rise to the problems of convergence (Shou et al., 2015). The traditional methods and software tools employ static heuristics in their search for solutions. They begin with a single candidate solution and search iteratively for a single solution. They also do not offer conceptual simplicity (Nitin et al., 2015). In big network problems, they fail to perform autonomously and often need human intervention. They are not robust to dynamic changes. Even when the fitness function is defined they are still very sensitive to parameters (Sahoo et al., 2014). In these traditional methods and software, it is also very difficult to employ hybridization (Elmqvist et al., 2016; Gast et al., 2014).

2.4 Suggestions for the optimisation problem

When there is little reliability of methods and all of them just giving approximations, one will have to look at new optimisation techniques. The main issues that have to be addressed by an optimisation method include robustness to noise, non-linearity, local minima trapping, convergence, autonomy, conceptual simplicity, parameter sensitivity, hybridization,

tractability, data intensiveness, computational time, application of static or dynamic heuristics, single-objective or multi-objective optimisation and reliability when handling both large and small networks (Lim et al., 2014). Other factors which could also be considered might be in the method being a stochastic direct approach and/or the ability to use the Pareto sense in its optimisation processes (Zhang et al., 2014). Numerous existing approaches try to address these problems. However, they do not sufficiently do so (Smriti et al., 2014). With the various methods analysed in this paper, the genetic algorithm and the particle swarm optimisation have been suggested as optimisation techniques to be explored for this computational problem.

2.4.1 Detailed overview of the GA

The genetic algorithm commences by randomly creating an initial population. It goes on to create new populations by exploiting members of the present generation to create the subsequent populations. The procedures that are followed in creating the new populations are as follows (Sahoo et al., 2014; Yao et al., 2015):

- Computation of the fitness values of the current members (population) and assigning 'scores' with regards to the computed fitness levels.
- The raw fitness scores are 'scaled' so that they can be converted into an operable range of values.
- Members called parents are selected based on their fitness. These members are the only ones who can contribute their genes for making the next generations.
- A limited amount of individuals with lower fitness are also chosen and are allowed to pass into the next generation.
- The parents produce children through a process whereby some random changes are made to a parent in a process called 'mutation' or children are made by combining properties of parents through a process called 'crossover'.
- The children replace the current population thus giving rise to the subsequent generations.
- The procedures continue until a 'termination criterion' has been met.

However, the genetic algorithm has some weaknesses. One of its main weaknesses is premature convergence (Yao et al., 2015). The chief cause of this is the loss of diversity. If

population diversity can be achieved throughout the optimisation procedures, the search path will become much better (Ghamisi et al., 2015). Trapping into a suboptimal solution will also be avoided (Zhu, 2015). Perfect mutation and crossover help to avoid the loss of genetic material by ensuring and maintaining diversity (Zhang et al., 2014). A user can modify the genetic algorithm to suit their optimisation problem. This proves to be very effective as some weaknesses of the genetic algorithm can easily be supplemented by these procedures (Javaid et al., 2017; Sahoo et al., 2014). A flow chart of the genetic algorithm optimisation procedures is given in Figure 2.5.

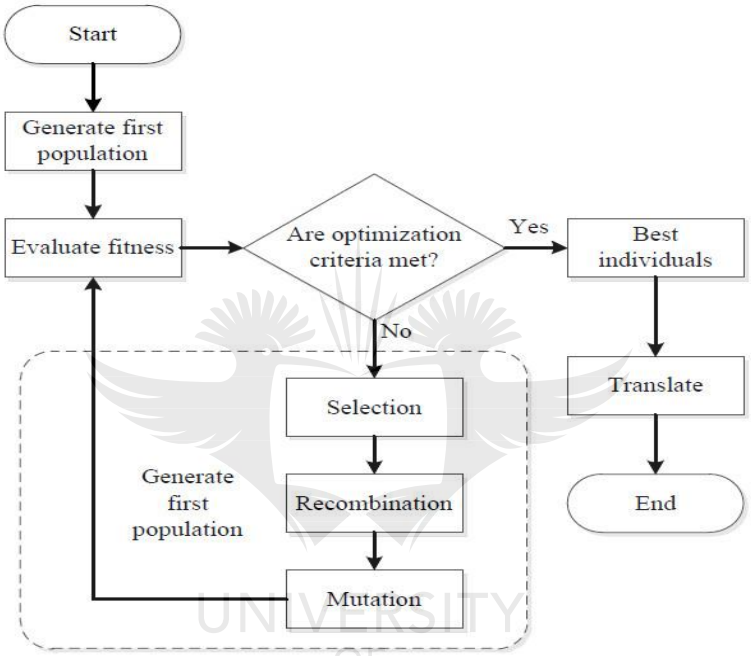

Figure 2.5 GA optimisation procedures (Zhu, 2015)

2.4.2 Detailed overview of the PSO

The algorithm commences by creating some initial particles whilst simultaneously giving them some initial velocities and positions (Carvalho et al., 2009). The objective function under optimisation is evaluated at every particle location. This process helps in determining the best locations and the best function values (Vitorino et al., 2015). The particles are then assigned new velocities again. This velocity is derived based on the current particle velocity, the best locations of an individual particle and its neighbours' best location (Zhang et al., 2014). The algorithm keeps on iteratively updating the particles' velocities and locations by the above-mentioned steps until a termination criterion has been reached. Termination criterion might be the maximum time, maximum stall time, an objective limit, maximum

iterations or any other custom made function with regards to the variables within the function under optimisation (Li et al., 2014; Shou et al., 2015). A flow chart of the PSO optimisation procedures is given in Figure 2.6.

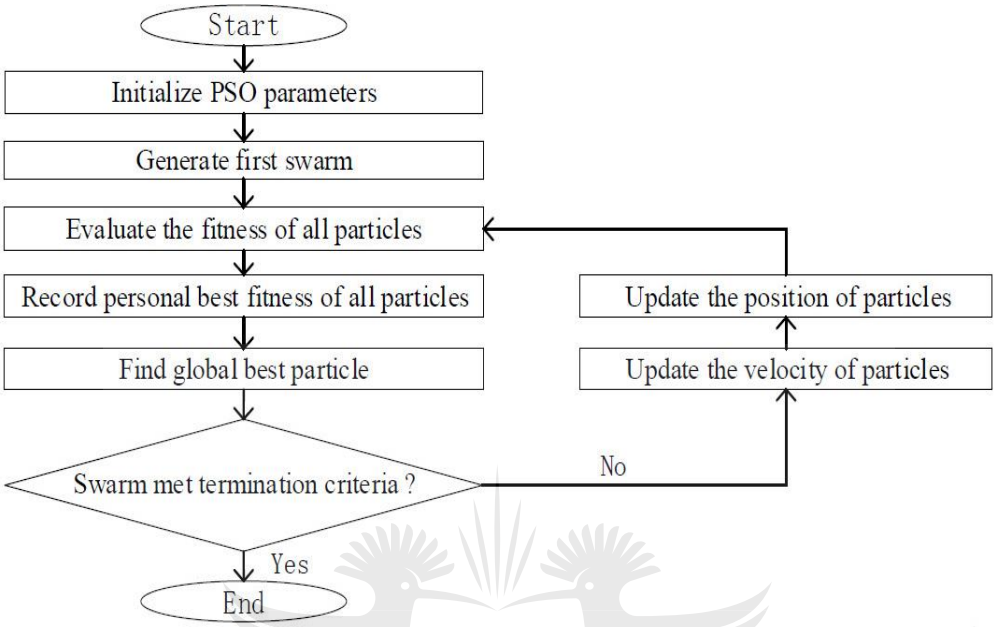

Figure 2.6 PSO optimisation procedures (Zhang et al., 2014)

The advantages of PSO are: the optimisation procedures and calculations are very simple; it is conceptually simple; it is easy to implement; it is derivative-free; and it has very few parameters and these parameters do not impact the solutions greatly as in other evolutionary algorithms (Ghamisi et al., 2015). The disadvantages of PSO are: it suffers from partial optimism which degrades the regulation of its velocity and direction (Vitorino et al., 2015); it can often converge to local minima and not the global minima (Zhu, 2015); and it can often experience premature convergence if the parameters are not chosen meticulously (Ababneh, 2015).

2.5 Literature review conclusion

The detection of asymmetrical three-phase short-circuit faults is a complex problem. In the real world, there are uncertain environments which adversely affect the current methods of asymmetrical three-phase fault evaluation (Tleis, 2008). Nonetheless, a power system must be able to provide reliable and continuous power flow to consumers during either normal or abnormal operating conditions (Das, 2017). This influences the selection of an optimisation

tool based on its qualities and properties. Table 2.1 presents a survey and an analysis of the various computational tools. The information in Table 2.1 is obtained from (Ashvini et al., 2015; Das, 2016; Malik et a., 2011; Rao et al., 2016; Sallam et al., 2011; Soroudi et al., 2016; Tleis, 2008; Yudong et al., 2014). For Table 2.1 below, 'poor' indicates the inapplicability or non-existence of a particular characteristic; 'good' indicates the existence and applicability of a particular property but with the computational approach often obtaining mediocre results; and 'excellent' indicates that a computational approach obtains precise results for a given characteristic.

Table 2.1: Computational methods and their properties

	Computational approach							
	Direct method	Easy-Power	ETAP	EAs	Per-Unit method	Symmetric components	Quasi analysis	Time domain analysis
Adaptivity	Ø	+	+	++	Ø	Ø	Ø	+
Autonomy	Ø	+	++	++	Ø	Ø	Ø	+
Convergence	+	+	+	++	+	+	+	+
Heuristics	S-H	S-H	S-H	D-H	S-H	S-H	S-H	S-H
Hybridization	Ø	Ø	+	++	Ø	Ø	Ø	Ø
Large networks	Ø	+	++	++	Ø	Ø	+	+
Speed	+	++	++	++	+	+	+	++
Objectivity	S-Obj	S-Obj	S-Obj	M-Obj	S-Obj	S-Obj	S-Obj	S-Obj
Tractability	Ø	+	+	++	Ø	Ø	Ø	+
odd-function evaluation	Ø	Ø	Ø	++	Ø	Ø	Ø	Ø
Conceptual simplicity	Ø	+	+	++	Ø	Ø	Ø	Ø
Robust to noise	Ø	+	+	++	Ø	Ø	Ø	+
Concurrent computing	Ø	Ø	Ø	++	Ø	Ø	Ø	Ø

Key:
D-H – Dynamic heuristics
S-Obj – Single objective
M-Obj – Multi-objective
S-H – Static heuristics
++ – Excellent
\+ – Good
Ø – Poor

CHAPTER 3

RESEARCH METHODOLOGY

3.1 Research approach

This study presents a detailed analytical modelling technique for detecting three-phase short circuit faults for distribution networks of power systems with nominal voltages less than 550kV using evolutionary algorithms (GA and PSO). For electric distribution sub-systems, the resistances (R) are normally much smaller than the reactances (X). The resistances and reactances make up the impedance (Z) (Sing et al., 2016). Standard IEC 60909 and IEC 61313 give the R/X and R/Z values for networks below 550kV nominal voltage. The R/Z ratios will always be a value between 0.1 and 0.3 (Sallam et al., 2011). The R/X ratios vary depending on the network configuration but they are generally in the range of 0.1 to 1 (Tleis, 2008). These values are derived based on the source voltage of a network (Sallam et al., 2011). Here, the modified evolutionary algorithms are used to stochastically determine the R/X and R/Z values during fault evaluation. The proposed methodology does not depend on the predefined estimated values from Standard IEC 60909 (alongside IEC 61363, IEC 60034 and IEC 60076) but computes these values on a case-to-case basis for every optimisation case. This method brings about the inclusion of non-spinning loads in fault detection at various network levels and also the inclusion of upstream reactances when detecting faults at points that are far away from the sources. This leads to obtaining much more precise fault magnitudes (Costa et al., 2015). Conventional short-circuit detection methods with the guide of Standard IEC 60909, IEC 61363, IEC 60034 and IEC 60076 are used to separately obtain fault values for use in comparison with the results obtained by the EAs. Three main tools were used to detect fault values for evaluations and analysis i.e.

1) Conventional methods i.e. Symmetric components technique and the Direct method.
2) The Genetic Algorithm (GA)
3) The Particle Swarm Optimisation (PSO)

The tools were implemented using Matlab R2017a software installed on an Acer Aspire with Intel(R) Celeron(R) processor at 1.80GHz and 4.00GB Ram with Windows 10 Pro operating system. Matlab can be utilized to perform fault analysis in an effective, well-organised and fast way (Costa et al., 2015). The goal of having several tools was to have a comparative

results analysis. The Matlab command window would initially assists in creating some fitness functions for evaluations. Matlab M-Script Files would also assist in the implementation of the conventional methods and the two evolutionary algorithms. Matlab and evolutionary algorithms can handle large systems which are not easily tractable using hand calculations. Codes on the command window can easily be edited therefore Matlab would be used to create and edit most of the functions.

3.2 The proposed GA modifications

The GA weaknesses mentioned in Chapter 2.4 led to the creation of modified custom mutation, selection, creation, crossover and fitness scaling functions. The details of the proposed modelling that was implemented in the custom functions are given below. Their accompanying motivations are also included.

3.2.1 Creation function

The genetic algorithm has two in-built creation options which are creation 'uniform' and creation 'linear-feasible'. These in-built functions do not give satisfactory and explicit options with regards to altering and making amendments to some parameters (Ghamisi et al., 2015). This proves to be a big limitation since they do not sufficiently address important factors. A custom creation function was developed to address two main defects that are not properly accounted for by the in-built functions i.e.

- To continuously influence the number of individuals that can be created at each evolution stage which ensures search efficiency until termination of the optimisation process.
- To create a sufficient initial population for linear-constrained cases and bound-constrained cases.

Since the genetic algorithm works as a multipath search algorithm, the above-mentioned changes would ensure search efficiency until termination of the optimisation processes (Parhi et al., 2019). This would greatly decrease the chances of local minima trapping (Zhu, 2015). This would also help the algorithm to effectively explore all the search spaces where the probability of finding optimum solutions is highest (Javaid et al., 2017).

For the first problem, subsequent individuals in the proposed creation function were created with regards to the total population and initial population provided. Two variables were created and added to help in making the adjustments when searching for optimum solutions. The proposed adjustments were implemented as follows:

$$\text{IndividualsToBeCreated} = ß * (\text{totalPopulation} - \Psi) \quad (3\text{-}1)$$
$$ß \in [0 \; ; \; \text{infinity}]$$
$$\Psi \in [0 \; ; \; \text{InitialPopulationProvided}]$$

For the second problem, adjustments to the range of values used in creating the initial populations when considering bounds and constraints would give the desired outcomes when creating the population arrays. The proposed adjustments were implemented as follows:

$$r = \phi * (\text{options.PopInitRange}) \quad (3\text{-}2)$$
$$\phi \in [0 \; ; \; \text{infinity}]$$
$$L = r(1,:) \quad (3\text{-}3)$$
$$sp = r(2,:) - L \quad (3\text{-}4)$$

$$\text{Population}(\text{initialPopulationProvided} + 1\text{:end},:) = \text{repelem}(L, \text{individualsToBeCreated}, 1) + \text{repelem}(sp, \text{individualsToBeCreated}, 1) * \text{rand}(\text{individualsToBeCreated}, \text{GenomeLength}) \quad (3\text{-}5)$$

where 'sp' is span, 'L' is the lowerbound and 'r' is the range.

The magnitude of ϕ directly affected the selection of ß and Ψ because the subscripted assignment dimensions of the IndividualsToBeCreated were not supposed to mismatch the Population arrays. Although ϕ, ß and Ψ were in the range: $[0; \text{infinity}]$, small integer values were tested due to the large population sizes that were being used in the experiments. By trial and error, the optimum values were: $\phi = 4$, $ß = 1$ and $\Psi = 0$.

3.2.2 Fitness scaling function

In the proposed fitness scaling function, the best candidates would be given the highest chances of survivals and influencing reproduction. We proposed the use of a variable (μ). The variable was created to control the relationship between scores, expectation and the number

of parents. μ would determine the amount of expectation with regards to the population size. By trial and error, an optimum value between 0 and 1 could be determined. This value would select the optimum number of scores for the parents at any particular stage during the evolution cycles. For the proposed scaling function, when ($\mu < 1$), then

$$\mu = \text{nearest}(\text{numel}(\text{scores}) * \mu * \text{rand}) \quad (3\text{-}6)$$

Another unique characteristic of the proposed custom fitness scaling function was the arrangement of scores in descending order so that the top scores would always be given priority in influencing expectation. This eliminated the use of probabilities that are commonly used by the in-built functions (Parhi et al., 2019). The scores were sorted as follows:

$$[\sim, \text{i}] = \text{sort}(\text{scores}, 'descend') \quad (3\text{-}7)$$

The biggest strength of the created custom fitness scaling function was that regardless of when raw scores were not in a good range, the best scores would still have precedence. Another advantage was that there would be no stalling during optimisation when there was a degenerate scenario i.e. when some of the scores had equal magnitudes. Stalling is a big problem for fitness scaling functions that use probabilities when assigning scores and arranging expectations (Ghamisi et al., 2015). Another advantage of the created function was that there were never any negative expectations because of $\mu \in [0; 1]$.

This made the proposed scaling function have much better qualities than the traditional in-built scaling functions e.g. shift-linear fitness scaling has problems with the survival rates of individuals, proportional and rank fitness scaling have problems when raw scores are not in a good range (Zhang et al., 2015). Top fitness scaling has problems in choosing the best quantity of scores for parents whilst it also does not have optimum default values for higher dimension instances (Javaid et al., 2017; Mishra et al., 2015).

3.2.3 Selection function

The proposed selection function would sort expectation in descending order by:

$$\text{expectation} = \text{sort}(\text{expectation}(:,1), 'descend')' \quad (3\text{-}8)$$

This made it easier for parents to be selected with regards to their expectations. The best parents would be given top priority and they would be selected for crossover and mutation. This also excluded the need for selection probabilities that exist in the traditional selection functions e.g. selection roulette, selection remainder and selection stochastic uniform (Zhang et al., 2014). After sorting expectation, the parents were integers randomly chosen using the number of parents and the new expectation and they were limited to the interval: $[1; \text{populationSize}]$.

By trial and error, this proposed custom selection function proved useful and better for the actual evolution of higher-performing individuals.

3.2.4 Mutation function

In the proposed mutation function, the genes that were mutated were equally spread throughout the genes' range. The probability of a genome being mutated was controlled with the aid of a variable (η) within the range: $[0; 1]$. By trial and error, values of η in the range: $[0.05: 0.20]$ proved to give optimum results after setting all the other optional parameters.

Secondly, a gene had to be replaced by a value randomly chosen from a guided range. The bigger the range implied more diversity since the probability of replacing a gene with a value (similar structure) that had already replaced another gene would be small (Zhang et al., 2015). Variable 'α' was created and used for implementing that. η in conjunction with α was used as follows:

$$\text{mutationPoints} = \text{nonzeros}(\text{rand}(1, \text{length}(\text{thisPopulation}(\text{parents}(i), :))) < \eta) \quad (3\text{-}9)$$

$$\text{range} = \alpha * \text{state.Generation} * (\text{options.PopInitRange}(:, \text{mutationPoints})) \quad (3\text{-}10)$$

$$\alpha \in [0 \ ; \ \text{infinity}]$$

The optimum value of α was 8, with bigger values increasing the optimisation time without showing any significant improvement in the results. Very large values of α were not tried because of the large population size that was being used for the GA. Based on (3-10), another variable 'γ' was created and it was used to control the mutation process in the creation of children by the following procedures:

$$A = \text{state.Generation} * \text{range}(1,:) \quad (3\text{-}11)$$

$$B = \text{state.Generation} * \text{range}(2,:) \quad (3\text{-}12)$$

$$\text{spread} = \gamma * \text{state.Generation} * (B - A) \quad (3\text{-}13)$$

$$\gamma \in [0 \; ; \; \text{infinity}]$$

The optimum value of γ was 4 with bigger values of γ not suitable since the optimisation procedures had specific bounds and domains as constraints. Equation (3-13) would go on to be used as follows:

$$\text{child}(\text{MutPts}) = \text{spread} .* [\frac{\text{abs}(\text{randn}(1,\text{numel}(\text{MutPts})))}{\text{length}(\text{thisPopulation})}] \quad (3\text{-}14)$$

$$\text{MutChildren}(i,:) = \text{child} * \text{GenomeLength} \quad (3\text{-}15)$$

Where 'MutPts' were the mutation points and 'MutChildren' were the mutated children

3.2.5 Crossover function

For this research, a five-point crossover was developed and used. The crossover function would start by creating a pointer which locates the two best parents. This was in coherence with the individuals with the best scores and best expectation in the selection and fitness scaling functions. The crossover function would then create the crossover points based on the length of either parent1 or parent2. For example, if Parent1 and Parent2 were the parents:

$$\text{Parent1} = [1, 2, 3, 4, 5, 6, 7, 8, 9, 10, 11, 12] \quad (3.16)$$

$$\text{Parent2} = [A, B, C, D, E, F, G, H, I, J, K, L] \quad (3.17)$$

In the crossover function, crossover would take place at intervals of:

$$\text{Cross\_Point} = 0.17 * \text{length}(\text{Parent1}) + \text{Cross\_Point} \quad (3.18)$$

Therefore, the crossover points on Parent1 would be 2, 4, 6, 8 and 10. The crossover function would concatenate the genes from the parents and return the following child:

$$\text{Child\_fivePoint} = [1\ 2\ C\ D\ 5\ 6\ G\ H\ 9\ 10\ K\ L] \quad (3.19)$$

3.2.6 Parameter settings of the GA

In this paper, the traditional genetic algorithm uses the reference GA; the genetic algorithm that has the proposed modifications to supplement some defects uses the reference MGA. For the optimisation problem within this research, hybrid functions that could be added since the optimisation procedures had bounds (as constraints) were pattern search and fmincon. These minimisation functions would run after the MGA terminates and retain a more accurate solution. MGA with the pattern search minimisation algorithm uses the reference MGAP. MGA with the fmincon minimisation algorithm uses the reference MGAF. Therefore, the four different genetic algorithms that were tested on the fitness functions evaluated within this research were GA, MGA, MGAF and MGAP. Table 3.1 gives the genetic algorithm parameters. Some parameters in Table 3.1 would be adjusted in various instances to suit the proposed modifications and hybrid functions.

Table 3.1: Parameters of the Genetic algorithms

Parameter	Setting
Creation function	Custom (modified)
Crossover function	Custom (modified)
Population size & Type	1000 ; Double Vector
Initial population range	[-10; 10]
Pareto fraction	0.4
Selection function	Custom (modified)
Penalty factor	100
Initial penalty	10
Migration fraction and interval	0.2 ; 20
Fitness scaling function	Custom (modified)
Migration direction	Both
Mutation function	Custom (modified)
Stall test	Geometric weighted
Stall time limit & Time limit	60 ; 60
Hybrid functions	Fmincon and Pattern-search
Non-linear constraint solver	Augmented Lagrangian

3.3 The proposed PSO modifications

The weaknesses mentioned in Chapter 2.4 led to the creation of a modified custom creation function. The details of the proposed modifications that were implemented and their motivations are given below.

The particle swarm algorithm has one in-built creation function called 'pswcreationuniform' which does not satisfactorily address the weaknesses of the algorithm (Cvetkovski et al., 2014). The proposed creation function was created to address three main defects that are not properly accounted for by 'pswcreationuniform'. The three changes below would greatly diminish the weaknesses of the particle swarm optimisation i.e.

- Creating the maximum number of initial positions. This would help the particles to avoid premature stagnation (Zhu, 2015). It would also give the particles a wide exploration range (Vitorino et al., 2015). A large number of initial positions would ensure that all the search space is exploited effectively (Zhang et al.,, 2014).
- To effectively influence how the particles were distributed within the swarm. This would greatly enhance its manipulation (Li et al., 2014).
- To create the remaining particles by randomly sampling a larger search space. This would ensure continuous diversity (Shou et al., 2015).

For the first problem, the number of positions during each cycle was being created with regards to the number of particles present and the initial/current set positions. Two variables were used for making the adjustments. The proposed adjustments were implemented as follows:

$$\text{numPositionsToCreate} = ß * (\text{numParticles} - \Psi) \quad (3\text{-}20)$$
$$ß \in [0 \; ; \; 10]$$
$$\Psi \in [0 \; ; \; \text{numInitialPositions}]$$

For the second and third problems, adjustments were made to the span (sp) that was used in creating the remaining particles. The proposed adjustments were implemented as follows:

$$sp = \phi * ub - \delta * lb \quad (3\text{-}21)$$
$$\phi, \delta \in [0 \; ; \; 10]$$

The created span would go on to be used as follows:

$$\text{swarm}(\text{numInitPositions} + 1{:}\,\text{end}, :) = \text{repelem}(\text{lb}, \text{numPositionsToCreate}, 1) + \text{repelem}(\text{sp}, \text{numPositionsToCreate}, 1) * \text{abs}(\text{randn}(\text{numPositionsToCreate}, \text{nvars})) \quad (3\text{-}22)$$

The magnitudes of ϕ and δ directly affected the selection of β and γ because the subscripted assignment dimensions were not supposed to mismatch i.e. the number of particles and the arrays of positions. By trial and error, the optimum values used in these experiments were: $\beta = 1, \gamma = 0$ and $\delta = \phi = 2$.

Instead of using: $\phi, \delta, ß \in [0 \ ; \ \text{infinity}]$, the upper limit was set to 10 which was reasonable with regards to the large swarm sizes that were being used in the parameter box given in Table 3.2. A lot of parameters could be altered in the custom creation function, but the proposed adjustments highlighted above proved to give the best results.

3.3.1 Parameter settings of the PSO

In this paper, the traditional particle swarm algorithm uses the reference PSO and the particle swarm optimisation that has the proposed modifications to supplement some defects uses the reference MPSO. For the optimisation problem in this research, hybrid functions that could be added since the optimisation procedures had bounds (as constraints) were pattern search and fmincon. These minimisation functions would run after the MPSO terminates and retain a more accurate solution. MPSO with the patternsearch minimisation algorithm uses the reference MPSOP. MPSO with the fmincon minimisation algorithm uses the reference MPSOF. Therefore, the four different particle swarm algorithms that were tested on the fitness functions evaluated within this research were PSO, MPSO, MPSOF and MPSOP.

Some parameters in Table 3.2 could be adjusted at various instances to suit the proposed modifications and hybrid functions. The acceleration constants were also varied adaptively during iterations to improve the quality of the solutions.

Table 3.2: Particle swarm algorithm parameters

Parameter	Setting
Creation function	Custom (modified)
Swarm size	1000
Initial swarm span	2000
Self-Adjustment weight	1.65
Social adjustment weight	1.55
Min-Neighbors Fraction	0.30
Inertia range	[0.1,1.1]
Max Stall time	60
Max Time limit	60
Hybrid functions	Fmincon and Pattern-search

3.4 Hybrid functions

The main aim of hybridization is to lessen or mitigate the limitations of an algorithm with diversification aspects of another algorithm. In this paper, a hybrid function is a minimisation function that runs after the genetic algorithms or the particle swarm algorithms terminate. When EAs terminate, the hybrid function takes the final point of the EAs as its initial point and returns a more accurate result (Lim et al., 2014). Four hybrid functions that could be chosen were ‘fminsearch’, ‘fminunc’, ‘fmincon’ and ‘pattern-search’. For this research, only fmincon and pattern search could be used since they allow constrained minimisation. They were added to the EAs without any modifications or the inclusion of extra derivatives.

3.5 Testing of the algorithms

The GA, MGA, MGAF, MGAP, PSO, MPSO, MPSOF and MPSOP were first tested on two standard benchmark functions. This was done to confirm their robustness and accuracy. The

tests would also show if the proposed modelling of the algorithms and the conscientious parameter selection were good. The Rastrigin function and the Rosenbrock function were used as the benchmark test functions. The details are given below.

3.5.1 The Rastrigin Function

The Rastrigin function is given below (Yao et al., 2015). All the algorithms were run 5 times and their results are presented in Tables 3.3 and 3.4.

$$f(x) = 20 + X_1^2 + X_2^2 - 10(\cos 2\pi X_1 + \cos 2\pi X_2) \quad (3.23)$$
$$Xi \in [-5.12, 5.12]$$

Table 3.3: Particle swarm results on the Rastrigin function

	First Run	Second Run	Third Run	Fourth Run	Fifth Run
	[X_1 ; X_2]	[X_1 ; X_2]	[X_1 ; X_2]	[X_1 ; X_2]	[X_1 ; X_2]
PSO	[0.0027 ; -0.0052]	[0 ; 0]	[0.068 ; -0.14]	[0 ; -0.995]	[0 ; 0]
MPSO	[0 ; 0]	[0.364 ; -0.221]	[0 ; 0]	[0 ; 0]	[0 ; 0]
MPSOF	[-2.985 ; 0]	[0 ; 0]	[0 ; 0]	[1.99 ; -0.995]	[0 ; 0]
MPSOP	[0 ; 0]	[0 ; 0]	[0 ; 0]	[0 ; 0]	[0.995 ; 0]

Table 3.4: Genetic algorithm results on the Rastrigin function

	First Run	Second Run	Third Run	Fourth Run	Fifth Run
	[X_1 ; X_2]	[X_1 ; X_2]	[X_1 ; X_2]	[X_1 ; X_2]	[X_1 ; X_2]
GA	[0 ; 0]	[0 ; 1.99]	[-2.43 ; 0.006]	[0 ; 0]	[0 ; -0.743]
MGA	[0.645 ; 0.0015]	[0.442 ; -0.351]	[0 ; 0]	[0 ; 0]	[0 ; 0]
MGAF	[0 ; 0]	[0.619 ; -1.1]	[0 ; 0]	[1.99 ; -0.995]	[0 ; 0]
MGAP	[0 ; 0]	[0 ; -0.995]	[0 ; 0]	[0 ; 0]	[0 ; 0]

3.5.2 The Rosenbrock Function

The Rosenbrock function is given below (Zhang et al., 2014). All the algorithms were run 5 times and their results are presented in Tables 3.5 and 3.6.

$$f(x) = 100 * (X_2 - X_1^2) + (1 - X_1)^2 \quad (3.24)$$
$$Xi \in [-10, 10]$$

Table 3.5: Particle swarm results on the Rosenbrock function

	First Run	Second Run	Third Run	Fourth Run	Fifth Run
	[X_1 ; X_2]	[X_1 ; X_2]	[X_1 ; X_2]	[X_1 ; X_2]	[X_1 ; X_2]
PSO	[1 ; 1]	[1 ; 1]	[1 ; 1]	[1 ; 1]	[1 ; 1]
MPSO	[1 ; 1]	[1 ; 1]	[1 ; 1]	[1 ; 1]	[1 ; 1]
MPSOF	[1 ; 1]	[1 ; 1]	[1 ; 1]	[1 ; 1]	[1 ; 1]
MPSOP	[1 ; 1]	[1 ; 1]	[1 ; 1]	[1 ; 1]	[1 ; 1]

Table 3.6: Genetic algorithm results on the Rosenbrock function

	First Run	Second Run	Third Run	Fourth Run	Fifth Run
	[X_1 ; X_2]	[X_1 ; X_2]	[X_1 ; X_2]	[X_1 ; X_2]	[X_1 ; X_2]
GA	[1 ; 1]	[1 ; 1]	[1 ; 1]	[1 ; 1]	[1 ; 1]
MGA	[1 ; 1]	[1 ; 1]	[1 ; 1]	[1 ; 1]	[1 ; 1]
MGAF	[1 ; 1]	[1 ; 1]	[1 ; 1]	[1 ; 1]	[1 ; 1]
MGAP	[1 ; 1]	[1 ; 1]	[1 ; 1]	[1 ; 1]	[1 ; 1]

3.5.3 Interpretation of the results

The Rastrigin function has a global minimum of $[0;\ 0]$ and the Rosenbrock function has a global minimum of $[1; 1]$. From Tables 3.3 and 3.4, it can be seen that PSO, GA and MGAF struggle with retaining the global minima. They sometimes converge to local minima. This makes them less reliable. For the Rosenbrock function which has results tabulated in Tables 3.5 and 3.6, all the algorithms managed to converge to the global minima because the function is less complicated as compared to the Rastrigin function.

One of the objectives of this research was to minimise the weaknesses of the genetic algorithm and the particle swarm optimisation. The proposed modelling in the created custom functions and the meticulous parameter selection proved to improve the algorithms significantly. The tests on the Rastrigin and Rosenbrock functions clearly show the improvement in the algorithms.

The top 6 algorithms, from Tables 3.3 – 3.6, were selected for use in the optimisation procedures for this research. The selected algorithms were MPSO, MPSOF, MPSOP, MGA, MGAF and MGAP. In optimisation cases, an algorithm that converges poorly and settles to local minima is regarded as inaccurate and unreliable (Zhang et al., 2014). That particular algorithm must not be given much priority with regards to optimising much more sophisticated problems (Yao et al., 2015). Henceforth GA and PSO were discarded and not used for the remainder of the experiments.

3.6 Implementation of the algorithms/methods

The details for detecting short circuit faults based on Standard IEC 60909 and Standard IEC 61363 are given below (Das, 2016; IEC 60909-0, 2001; IEC 60909-0, 2016; 2000; Sallam et al, 2011; Tleis, 2008):

When $\sum X$ is the sum of reactances and $\sum R$ is the sum of resistances, short circuit impedance Z_{sc} is given by:

$$(Z_{sc})^2 = (\sum R)^2 + (\sum X)^2 \qquad (3\text{-}25)$$

$$Z_{sc} = \sqrt{(\sum R)^2 + (\sum X)^2} \tag{3-26}$$

Here, we define: $X_{up-stream} =$ upstream reactance

$R_{up-stream} =$ upstream resistance

$Z_{up-stream} =$ upstream impedance

For high voltage systems, Standard IEC 60909 and Standard IEC 61313 deduce upstream impedances and resistances from the following estimates (ratios):

At 150 kV $\rightarrow$ $\frac{R_{up-stream}}{Z_{up-stream}} \approx 0.1$

$$R_{up-stream} \approx 0.1 * Z_{up-stream} \tag{3.27}$$

At 20 kV $\rightarrow$ $\frac{R_{up-stream}}{Z_{up-stream}} \approx 0.2$

$$R_{up-stream} \approx 0.2 * Z_{up-stream} \tag{3.28}$$

At 6 kV $\rightarrow$ $\frac{R_{up-stream}}{Z_{up-stream}} \approx 0.3$

$$R_{up-stream} \approx 0.3 * Z_{up-stream} \tag{3.29}$$

According to (Tleis, 2008), nominal voltages that are not explicitly given in the ranges above can be estimated accordingly.

Reactances can be obtained from (3-26) as follows:

$$X_{up-stream} = \sqrt{(Z_{up-stream})^2 - (R_{up-stream})^2} \tag{3-30}$$

The relationship between reactance and impedance can be further simplified to:

$$\frac{X_{up-stream}}{Z_{up-stream}} = \sqrt{1 - \left(\frac{R_{up-stream}}{Z_{up-stream}}\right)^2}$$

$$X_{up-stream} = \left[\sqrt{1 - \left(\frac{R_{up-stream}}{Z_{up-stream}}\right)^2}\right] * Z_{up-stream} \quad (3\text{-}31)$$

Standard IEC 60909, IEC 60034 and IEC 60076 also highlight the following two points (Das, 2016; IEC 60909-0, 2001; IEC 60909-0, 2016):

i. When R/X is small, in the order of 0.1 to 0.2 for low-voltage networks and 0.05 to 0.1 for medium-voltage networks, for synchronous machines, the reactance may be considered to be comparable to the impedance and the following estimates can be applied:

$$R_{Generators} \approx 0.1 * X_{Generators} \quad (3.32)$$

$$R_{Motors} \approx 0.2 * X_{Motors} \quad (3.33)$$

ii. In general, the transformer reactances are much greater than the resistances and the following estimates can be applied where $X_{Transformer}$ is the transformer reactance, $R_{Transformer}$ is the transformer resistance and $Z_{Transformer}$ is the transformer impedance:

$$X_{Transformers} \gg\gg\gg R_{Transformers}$$

$$X_{Transformers} \approx Z_{Transformers} \quad (3.34)$$

$$R_{Transformers} \approx 0.2 * X_{Transformers} \quad (3.35)$$

3.6.1 The computation process

An overview of the fault detection procedures at various network levels is given in Figure 3.1. It should be noted from Figure 3.1 that the total impedance at any fault point constitutes of:

- Up-stream resistances and reactances
- The resistances and the reactances of all the other components at that particular fault point i.e. cables, breakers and bus-bars.

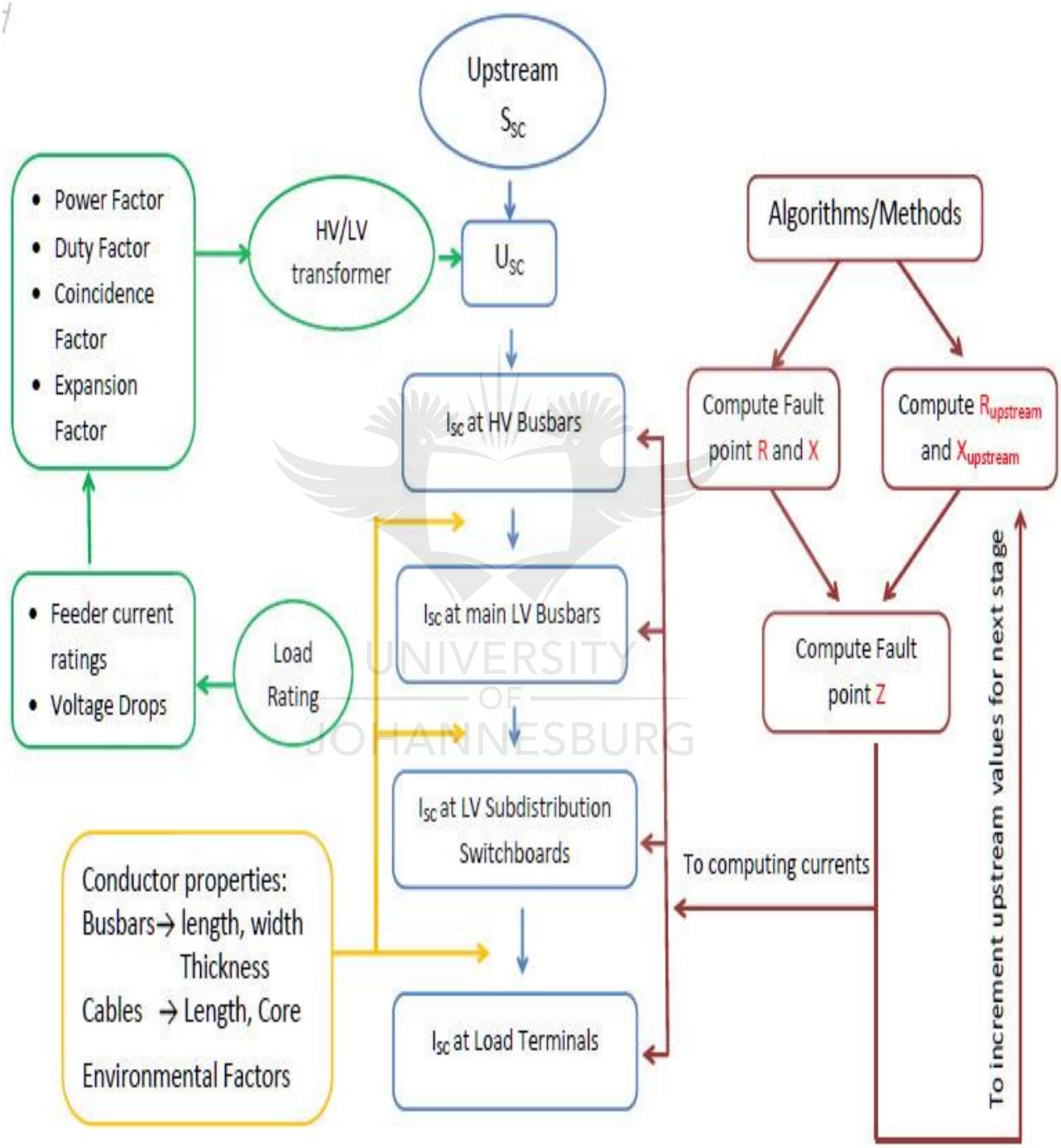

Figure 3.1 Overview of the fault detection process

3.6.1.1 Conventional methods

The first fault detection methodology was the use of conventional methods i.e. the Symmetric components technique and the Direct-Method. The conventional methods detected fault magnitudes entirely based on Standard IEC 60909 and IEC 61313 (alongside IEC 60034 and IEC 60076). The ratios of resistance to impedance that were substituted into (3-31) were obtained from the approximations given in (3-27) to (3-29) by Standard IEC 60909. There was a need for proper application of correct voltage factors and impedance correction factors since the proper implementation of these factors increases simplicity and technical accuracy during the fault evaluation processes of the conventional methods (Ashvini et al., 2015).

3.6.1.2 Evolutionary algorithms (GA and PSO)

The second fault detection methodology was the use of EAs i.e. the modified genetic algorithms and the modified particle swarm optimisation. From the IEC coefficients given in (3-27) and (3-28), there are some nominal voltages that are not properly accounted for, e.g. if a power system is of 85kV nominal voltage, it is difficult for a designer to choose either equation (3-27) or (3-28). Also, for nominal voltages that are over 200kV, there are no precise IEC values that a user can depend on. This greatly affects the precision of the computed fault impedances and currents for these nominal voltages. This influenced the development of the proposed fault detection approach that was used by the EAs.

The evolutionary algorithms (EAs) detected fault values by recalculating impedances at each fault location taking into account the fault point impedances and the up-stream reactances. They also considered non-spinning loads and the effects of sources for fault points far away from the sources. They detected fault values based on (3.26). The coefficient values that can be seen in (3.27) to (3.35) were determined stochastically with regards to the parameters and unique specifications of the optimised network. The EAs obtained their coefficients independently and did not use the IEC estimate values. Their stochastically determined coefficients were further used to obtain the fault point impedances and currents. Comparisons between CMs and EAs results would help in determining if EAs and the proposed methodology could be further used to cater for voltage regions that are not sufficiently accounted for by Standard IEC and the conventional methods. To supplement Figure 3.1, Figure 4.11 in Chapter 4 gives more explicit details of the EAs fault evaluation procedures.

CHAPTER 4

COMPUTATIONAL PROCEDURES

4.1 Background equations, benchmarks and their derivatives

The functions that are analysed in this section are given by (Das, 2016; Das, 2017; IEC 60909-0, 2001; IEC 60909-0, 2016; 2000; Malik et al., 2011; Sallam et al, 2011; Tleis, 2008). These equations supplement Standard IEC 60909 and IEC 61313 equations that are given in Section 3.5 i.e. equations (3.26) to (3.35). From these well-known benchmark functions, new functions for optimisation within this research could be derived.

The periodic component is the AC component, non-periodic component is the decaying DC component and first cycle values are the RMS of max I_{fault} and the initial peak magnitude of the transient period. The system impedance seen at the fault point characterises the amplitude and time of decay of fault current. The sub-components of short circuit current are given by:

Steady-state current component ($I_{steady\text{-}state}$) is given by:

$$I_{steady-state}(t) = \frac{V_{max}}{X}\cos(wt + \alpha) \quad (4.1)$$

Sub-transient current component ($I_{sub\text{-}transient}$) is given by:

$$I_{sub-transient}(t) = V_{max}[\frac{1}{X''} - \frac{1}{X'}] * e^{-t/T''}\cos(wt + \alpha) \quad (4.2)$$

Transient current component ($I_{transient}$) is given by:

$$I_{transient}(t) = V_{max}[\frac{1}{X'} - \frac{1}{X}] * e^{-t/T'}\cos(wt + \alpha)] \quad (4.3)$$

Aperiodic current component ($I_{aperiodic}$) is given by:

$$I_{aperiodic}(t) = \frac{V_{max}}{X''}e^{-t/T}\cos(\alpha) \quad (4.4)$$

When $\alpha = 0$ or when $wt = \pi(2k + 1)$, whereby k is an integer, peak fault current occurs:

$$I_{peak} = [V_{max}[\frac{1}{X} + \left(\frac{1}{X'} - \frac{1}{X}\right) * e^{-\frac{t}{T'}} + \left(\frac{1}{X''} - \frac{1}{X'}\right) * e^{-t/T''}] + \frac{V_{max}}{X''}e^{-t/T} \quad (4.5)$$

$$I_{peak} = I_{fault} * \sqrt{2} * (1.02 + 0.98e^{-\frac{3R}{X}}) \quad (4.6)$$

X'' is the sub-transient reactance, X' is the transient reactance, X is the synchronous reactance, T'' is the sub-transient time constant, T' is the transient time constant, T is the aperiodic time constant, V_{max} is the maximum phase voltage at the source terminals, I_{fault} is the normal fault current and α is the switching angle.

4.1.1 One line-to-earth fault

Considering Figure 4.1 where a fault is assumed to have happened at node K which results in a single phase-to-earth fault through impedance;

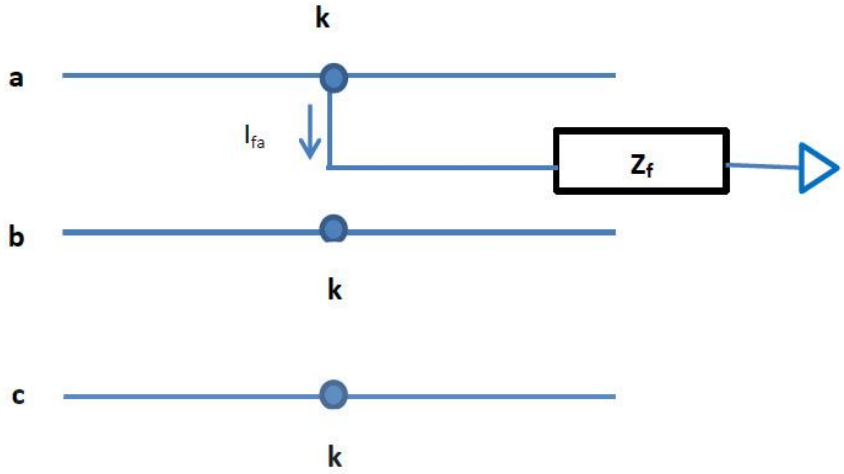

Figure 4.1 Asymmetrical one line-to-earth fault diagram

Before the occurrence of a fault, the system is unloaded and no current flows in lines b and c

$$I_{fb} = I_{fc} = 0 \quad (4.7)$$

At the fault point, phase voltage is given by:

$$V_{ka} = I_{fa} * Z_f \quad (4.8)$$

Based on (4.7) and (4.8), the matrix equation for a line to earth fault will be (Das, 2016):

$$I_{fa}012 = \frac{1}{3} * \begin{bmatrix} I_{fa} \\ 0 \\ 0 \end{bmatrix} * \begin{bmatrix} 1 & 1 & 1 \\ 1 & a & a^2 \\ 1 & a^2 & a \end{bmatrix} \quad (4.9)$$

A Thevenin equivalent diagram of a single line-to-earth fault is given in Figure 4.2.

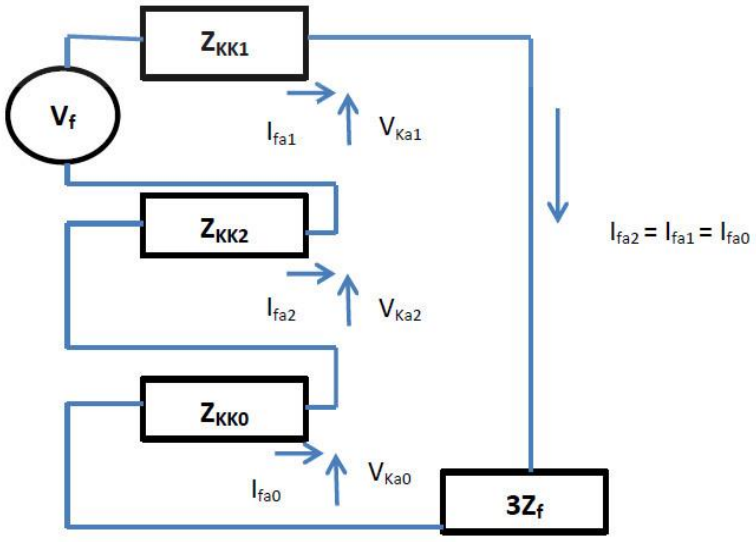

Figure 4.2 A Thevenin equivalent circuit of the line-to-earth fault (Tleis, 2008)

It can be derived from Figure 4.2 that the currents for the three sequences during a one line-to-earth fault are in series.

From (4.9) the following equation can be obtained (Das, 2016):

$$I_{fa2} = \ I_{fa1} = \ I_{fa0} = \frac{I_{fa}}{3} \tag{4.10}$$

From Figure 4.2 it can be derived that:

$$V_{ka0} = -I_{fa0} * Z_{kk0} \tag{4.11}$$

$$V_{ka1} = V_f - (I_{fa1} * Z_{kk1}) \tag{4.12}$$

$$V_{ka2} = -I_{fa2} * Z_{kk2}$$

Equations (4.10) to (4.12) assist in deriving the following:

$$V_{ka} = \ V_{ka2} + \ V_{ka1} + \ V_{ka0}$$
$$= \ V_f - (I_{fa1} * (Z_{kk2} + Z_{kk1} \ + Z_{kk0})) \tag{4.13}$$

$$V_{ka2} = I_{fa} * Z_f = Z_f(I_{fa2} + I_{fa1} + I_{fa0}) = \ 3 * I_{fa0} * Z_f$$

Therefore, in accordance with Kirchhoff's laws the one line-to-earth fault current is given by:

$$I_{fa0} = \frac{V_f}{Z_{kk1}+Z_{kk0}+ 3Z_f+ Z_{kk2}} \tag{4.14}$$

Figure 4.3 is an illustration from Matlab Simulink of the single line-to-earth fault.

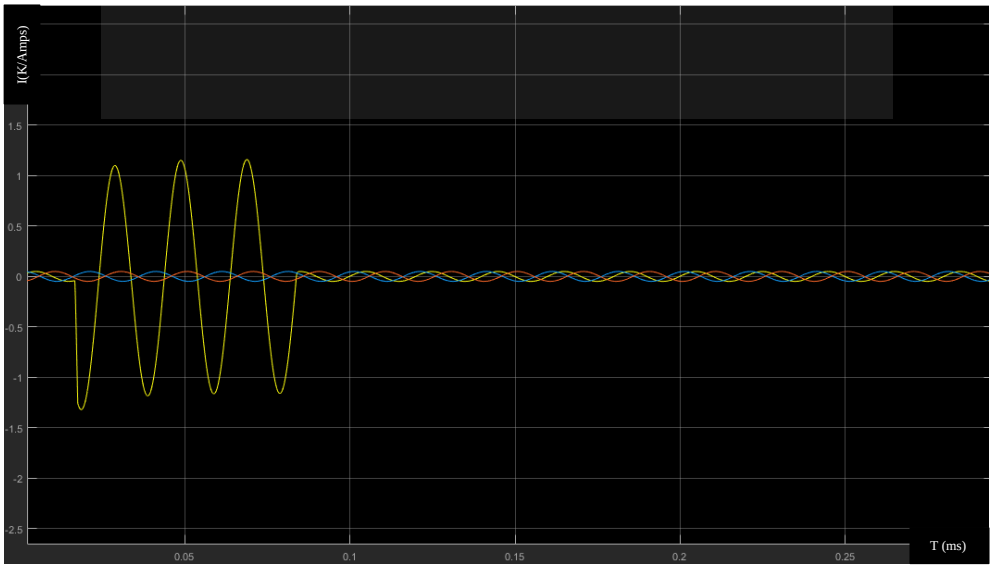

Figure 4.3 A Matlab illustration of the Line-to-Earth fault

4.1.2 Line-to-line fault

Considering Figure 4.4 where a fault is assumed to have happened at node K which results in a line-to-line fault between lines b and c;

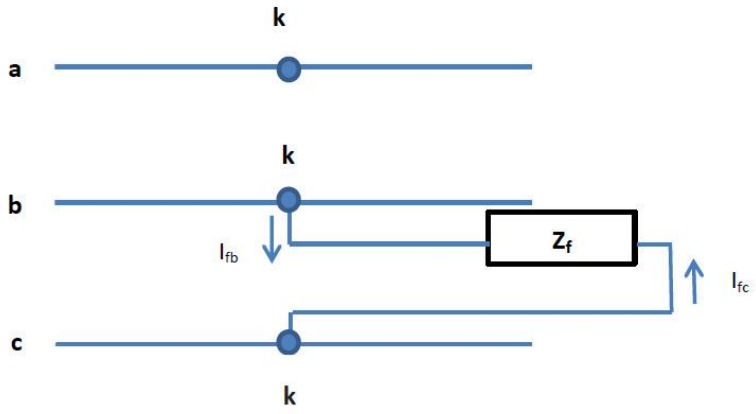

Figure 4.4 Asymmetrical Line-to-line fault diagram

Before the occurrence of a fault, the system is unloaded and no current flows in line a:

$$I_{fa} = 0 \quad (4.15)$$

From the shorted phases b and c, one can derive that:

$$I_{fb} = -I_{fc} \quad (4.16)$$

Based on (4.15) and (4.16), the matrix equation for a line-to-line fault will be (Das, 2016):

$$I_{fa}012 = D\begin{bmatrix} 0 \\ I_{fb} \\ -I_{fb} \end{bmatrix} = \frac{1}{3}\begin{bmatrix} 0 \\ I_{fb}(a - a^2) \\ I_{fb}(a^2 - a) \end{bmatrix} \quad (4.17)$$

Taking corresponding elements, it can be derived that:

$$I_{fa0} = 0$$

$$-I_{fa1} = I_{fa2} \quad (4\text{-}18)$$

It can be noted that no current from the zero-sequence (line a) gets into node K. Henceforth, for a line-to-line fault, the zero-sequence can be considered to be a dead network. Negative and positive sequences (line b and line c) are negative/opposite to each other.

Using equation (4.17) and Figure 4.4 and Figure 4.5, the voltage at the fault point is given by:

$$V_{kb} - V_{kc} = I_{fb} * Z_f \quad (4.19)$$

$$V_{kb} - V_{kc} = V_{ka1}(a^2 - a) + V_{ka2}(a - a^2) \quad (4.20)$$
$$= (a^2 - a) * (V_{ka1} - V_{ka2})$$

From (4.17), (4.19) and (4.20) it can be noted that: $-I_{fa1} = I_{fb2}$ and $I_{fb0} = 0 = I_{fa0}$

$$I_{fb2} + I_{fb1} = I_{fb} = I_{fa1} * a^2 + I_{fb2} * a = I_{fa1} * (a^2 - a) \quad (4.21)$$

$$V_{ka1} - V_{ka2} = I_{fa1} * Z_f \quad (4.22)$$

From (4.19) to (4.22), it can be derived that the negative sequence and the positive sequence are in parallel as illustrated in Figure 4.5 (Tleis, 2008):

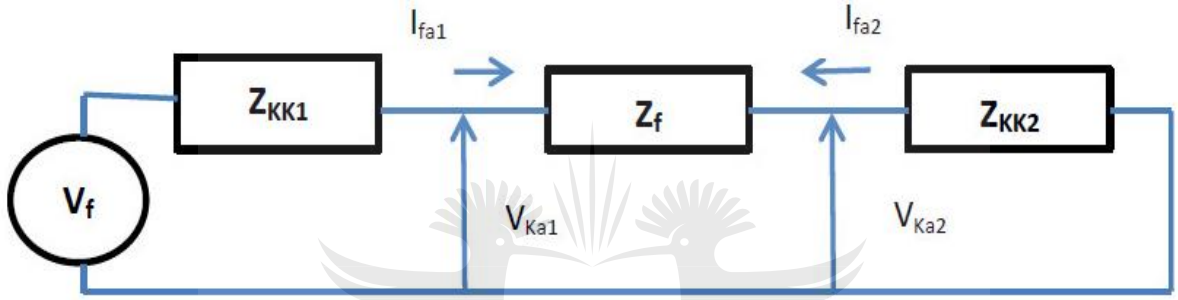

Figure 4.5 A Thevenin equivalent circuit of the line-to-line fault (Tleis, 2008)

Therefore, in accordance with Kirchhoff's laws, the line-to-line fault current is given by:

$$-I_{fa2} = I_{fa1} = \frac{V_f}{Z_{kk1} + Z_f + Z_{kk2}} \quad (4.23)$$

Figure 4.6 is an illustration from Matlab Simulink of the line-to-line fault.

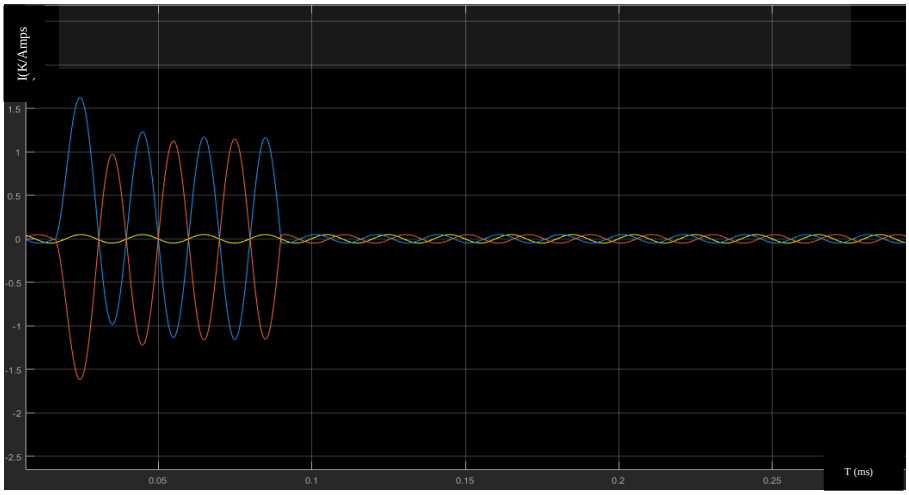

Figure 4.6 A Matlab illustration of the Line-to-Line fault

4.1.3 Two lines-to-earth fault

Considering Figure 4.7 where a fault is assumed to have happened at node K resulting in a two lines-to-earth fault between lines c and b through impedance.

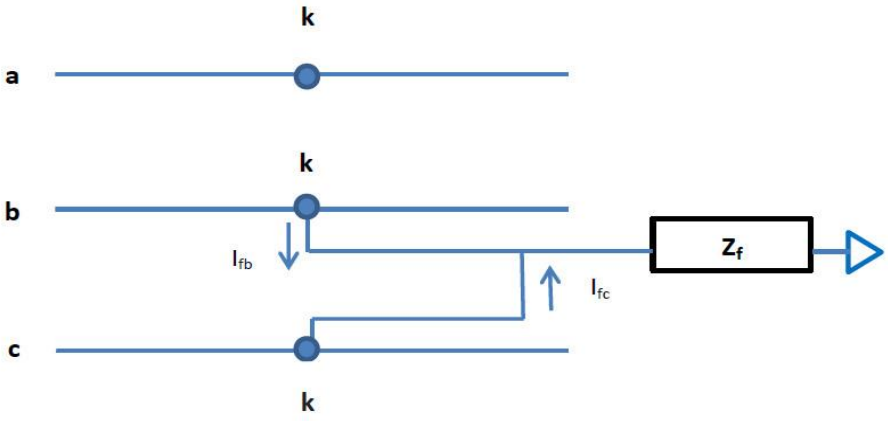

Figure 4.7 Asymmetrical two-lines-earth fault

Before occurrence of the fault, the system is unloaded, therefore:

$$I_{fa0} = \frac{1}{3}\,(I_{fb} + I_{fa} + I_{fc}) = \frac{1}{3}(I_{fc} + I_{fb}) \tag{4.24}$$

Phase voltages for lines b and c are:

$$V_{kc} = V_{kb} = (I_c + I_b) * Z_f = I_{fao} * Z_f * 3 \tag{4.25}$$

Based on (4.24) and (4.25), the matrix equation for a two lines-to-earth fault will be:

$$V_{ka}012 = D\begin{bmatrix} V_{ka} \\ V_{kb} \\ V_{kc} \end{bmatrix} = \frac{1}{3}\begin{bmatrix} 2V_{kb} + V_{ka} \\ V_{kb}(a + a^2) + V_{ka} \\ V_{kb}(a^2 + a) + V_{ka} \end{bmatrix} \tag{4.26}$$

The following two equations can be obtained from (4.26);

$$V_{ka2} = V_{ka1} \tag{4.27}$$

$$V_{ka1} + V_{ka2} + V_{ka0} + 2V_{kb} = V_{ka} + 2V_{kb} = 3V_{ka0} \tag{4.28}$$

By substituting (4.27) and (4.25) into (4.28) and grouping like terms:

$$V_{ka1} = V_{ka2} = V_{ka0} - (I_{fao} * Z_f * 3) \tag{4.29}$$

Because $I_{fa} = 0$, then

$$I_{fao} + I_{fa1} + I_{fa2} = 0 \quad (4.30)$$

A Thevenin equivalent circuit of the two lines-to-earth fault is given in Figure 4.8.

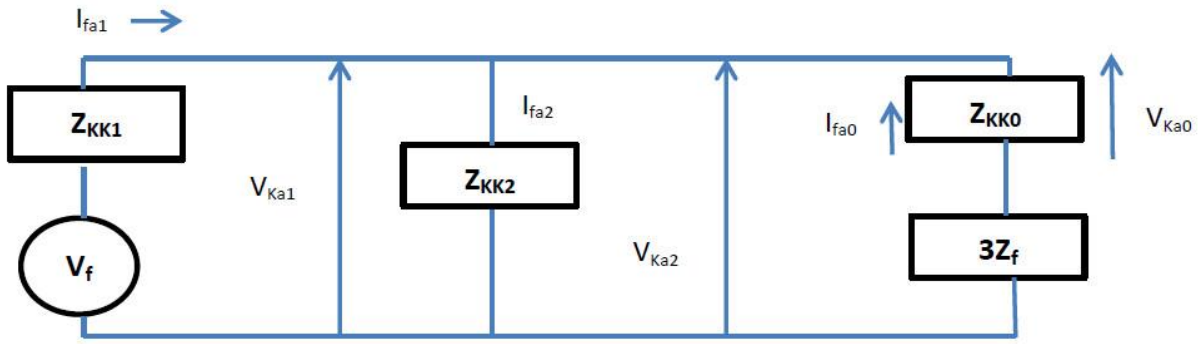

Figure 4.8 A Thevenin equivalent circuit of the two lines-to-earth fault (Tleis, 2008)

From Figure 4.8, a new equation can be derived (Das, 2016):

$$I_{fao} = \frac{V_f}{Z_{kk1} + Z_{kk2} || (Z_{kk0} + 3Z_f)} = \frac{V_f}{Z_{kk1} + \frac{Z_{kk2} * (Z_{kk0} + 3Z_f)}{Z_{kk2} + (Z_{kk0} + 3Z_f)}} \quad (4.31)$$

Using current divider principles, the negative and zero sequences will be (Das, 2016):

$$I_{fa0} = -I_{fa1} \frac{Z_{kk2}}{Z_{kk2} + (Z_{kk0} + 3Z_f)} \quad (4.32)$$

$$I_{fa2} = -I_{fa1} \frac{(Z_{kk0} + 3Z_f)}{Z_{kk2} + (Z_{kk0} + 3Z_f)} \quad (4.33)$$

Figure 4.9 is an illustration from Matlab Simulink of the two lines-to-earth fault.

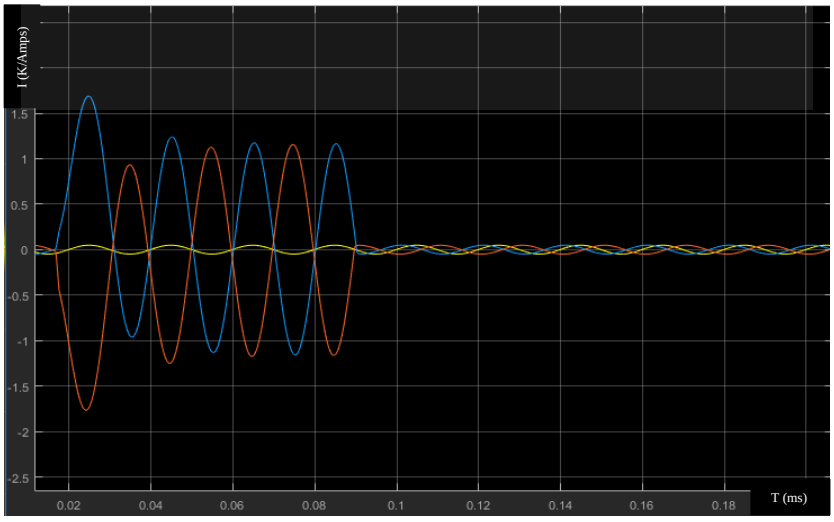

Figure 4.9 A Matlab illustration of the two lines-to-earth fault

4.2 Main optimisation problem

4.2.1 Optimisation model

The model of the network used in this work was created based on (Folarin et al., 2018; Prince et al., 2014; Sing et al., 2016). The model is shown in Figure 4.10. The model resembles a real-world system. It has all the basic components of a power system as well as some protection devices i.e. the main power supply, backup sources, transformers, synchronous machines, isolators, circuit breakers, relays, switches, earthing gears and loads. The algorithms/methods highlighted in Section 3 were all tested on the model for their robustness on the research problems highlighted in Section 1.3. The equations in Section 4.1 assisted in creating the fitness functions for evaluation.

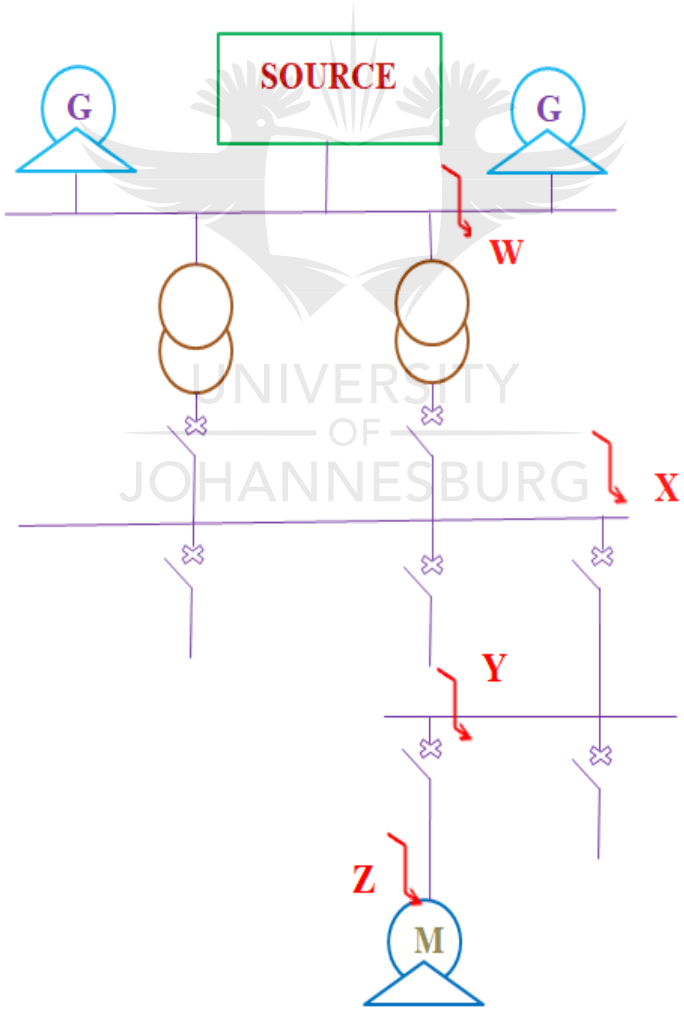

Figure 4.10 Line diagram for optimised network

The network above has an 18kV source supplying a high-voltage/low-voltage substation using a 1km overhead cable. Two 2000 kVA generators also supply as back-up power to the main source. The generators supply the substation busbars in parallel to the main source. Parallel-connected transformers of equal magnitude 1250kVA supply the LV busbars. The LV busbars supply feeders which go to 10 motors rated 100kW each. When the fault occurs, all the motors are running. All the connection cables are identical. Symmetrical three-phase short circuit current and asymmetrical three-phase line-to-line fault clear of the earth must be computed at:

- Point W i.e. at the HV bus-bars.
- Point X i.e. 15 meters from the transformer on the LV bus-bars.
- Point Y i.e. on the LV sub-distribution board bus-bars.
- Point Z i.e. at the motor terminals.
- The reverse currents from the motors should also be computed at all the bus-bars.

4.2.1.1 Detailed parameters of the network

Generators	2000kVA, $X_{subtransient}$ =20%
Transformers	1250kVA, U_{sc} =5.5%, secondary winding 250/410V
Motors	100kW, X=20%, cosØ=0.85, efficiency=0.9
Source Up-stream network	U=18kV, S_{sc}=500MVA
Overhead cables	1 km, 100mm^2
Main LV	3 bars, 15 meters, 400mm^2/ph
Circuit breakers	X = 0.15mΩ
Sub-distribution	100 meters, 3 single-core cables, 400mm^2
Feeder cables to motors	50 meters, 3 single-core cables, and 50mm^2

Up-stream impedance is given by: $Z_{up-stream} = \frac{U^2}{S_{sc}}$

Symmetrical three-phase fault: $I_{3-phase} = \frac{U/\sqrt{3}}{Z_{sc}}$

Asymmetrical line-to-line fault clear of earth: $I_{line-line} = \frac{U}{2*Z_{sc}}$

$$= \frac{\sqrt{3}}{2} * I_{3-phase}$$

$$\approx 0.866 * I_{3-phase}$$

4.2.2 Optimisation procedures

The short-circuit arc that occurs amongst bus-bars or conductors can reduce prospective fault current by a factor of 0.2 up to 0.5 (Tleis, 2008). When nominal voltages of the system are below 440 volts, the fault current can be decreased by a factor of more than 0.5. When computing fault values for use in determining the withstand capacity of equipment, the arc fault phenomenon may not be considered, but when computing minimum fault current, it can be taken into account (Das, 2017). In the above-mentioned problem, this phenomenon was considered at point X by all the computational methods. A magnitude factor of around 0.5 was considered since the transformer had a secondary winding of 250/410V. The current magnitudes based on the arc fault phenomenon are tabulated in Section 4.3.

4.2.2.1 Conventional methods

The conventional methods calculated fault current values entirely based on the steps and procedures from Standard IEC 60909. Equations (3.26) to (3.35) used in this section are found in Chapter 3 of this paper.

The network has an 18 kV source and therefore it could be derived from (3.28) that the ratio of resistance to impedance would be 0.2. Therefore;

$$R_{up-stream} = 0.2 * Z_{up-stream} \quad (4.34)$$

Substituting 0.2 into (3.31) gives:

$$X_{up-stream} = 0.98 * Z_{up-stream} \quad (4.35)$$

Therefore, from (4.34) and (4.35), it could be derived that:

$$R_{up-stream} \approx 0.2 * Z_{up-stream} \quad 0.2 * X_{up-stream} \quad (4.36)$$

Equations (4.34) to (4.36) assisted the conventional methods in obtaining the fault point reactances, resistances and impedances. For fault at point W, the source voltage would be divided by the obtained impedances to get the fault current. Points X, Y and Z were on the

low-voltage side of the transformers. The stepped-down voltages were used when calculating the fault currents (Das, 2017).

4.2.2.2 Evolutionary algorithms (GA and PSO)

The EAs had to stochastically determine the coefficient values that are given by Standard IEC 60909. These values would be determined with regards to the parameters and unique specifications of the power system in Section 4.2.

A Parameter Settings

To eliminate stochastic discrepancies, all the EAs were repeated 20 times at each fault point. The R/X and R/Z ratios for the nominal voltage that was being investigated had values that were between 0.1 and 1 as seen in equations (3.27) to (4.36). Therefore, all the search bounds of the EAs used in this experiment were varied adaptively within the range of lower-bound = -1 and upper-bound = 1. Given the 'quadratic nature' of most of the fitness functions that were being evaluated, these bounds would result in all the values that the EAs would obtain having a final 'absolute value' that is greater than 0 but less than or equal to 1.

The other parameter details have been provided in Tables 3.1 and 3.2 in Chapter 3.

B Optimisation procedure for EAs (GA and PSO)

(i) At point W:

There was a need to obtain the value of $X_{up\text{-}stream}$ from the value of $Z_{up\text{-}stream.}$ The value of $Z_{up\text{-}stream}$ was obtained using the given parameters of U and S_{sc}. After obtaining the value of $Z_{up\text{-}stream}$, the EAs would not go on to use either of the Standard IEC 60909 coefficients that were given in (4.35) to obtain the value of $X_{up\text{-}stream.}$ Instead, the coefficient was left as an unknown value within the objective function and it was determined stochastically using the procedures in Figure 4.11. The next step was to obtain $R_{up\text{-}stream}$ from the computed values of $X_{up\text{-}stream}$ and $Z_{up\text{-}stream.}$ EAs used (4.34) whereby they had to stochastically obtain the coefficient value. There was also a need to obtain the value of $R_{Generators}$ from the value of $X_{Generators}$. The value of $X_{Generators}$ was obtained from the given parameters about the power system. To obtain the

value of $R_{Generators}$, the EAs did not go on to use the R/X coefficient given in (3.32) but it was also determined stochastically using the procedures in Figure 4.11.

(ii) At points X, Y, Z:

For faults at points X, Y and Z, the reactances and the resistances were cumulative values i.e. they were comprised of the fault point values and the upstream values as illustrated by Figure 3.2 in Chapter 3. However, at point X, there was a need to obtain the value of $X_{Transformers}$ from the value of $Z_{Transformers}$. The obtained value of $X_{Transformers}$ would be further used to get the value of $R_{Transformers}$. The above-mentioned steps, based on Figure 4.11, were done to (3.34) and (3.35) i.e. the given R/X value in (3.35) was determined stochastically when computing the value of $R_{Transformers}$.

The procedures highlighted above show that EAs had to determine coefficient values at fault points W and X only. At point W, the EAs were determining the coefficients that were in (3.32), (4.34) and (4.35). At point X, they were determining the coefficient that was in (3.35). However, the reactances and the resistances they computed at point W were used as upstream values for point X. The reactances and the resistances from point X were used as upstream values for point Y and finally, the reactances and the resistances from point Y were used as the upstream values for point Z.

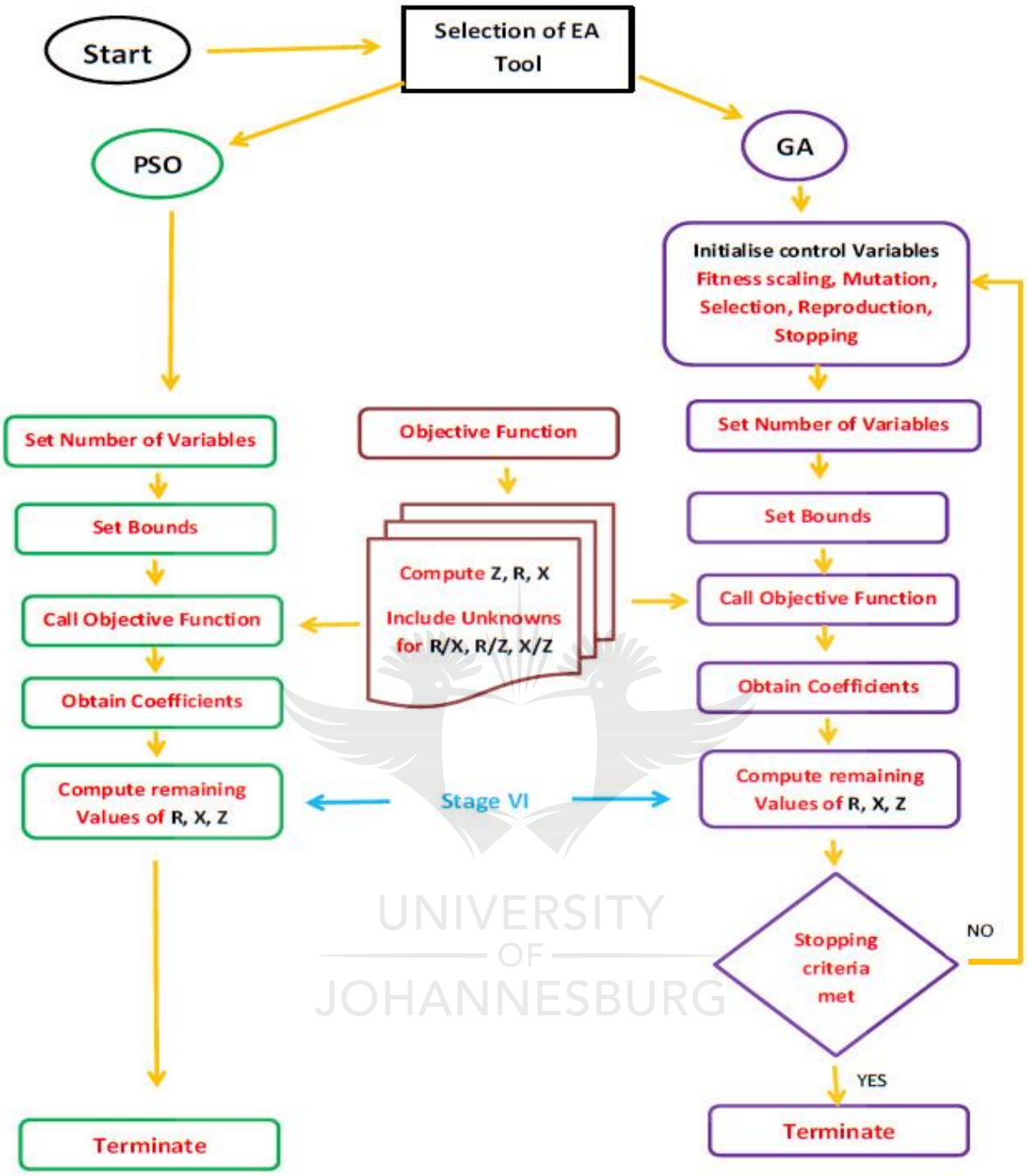

Figure 4.11 Evolutionary algorithms optimisation procedures

4.2.3 Fault simulation

4.2.3.1 Fault at point W

$$Z_{up-stream} = \frac{U^2}{S_{sc}}$$

$$X = \sqrt{Z^2 + R^2}$$

$$\frac{X_{up-stream}}{Z_{up-stream}} = \sqrt{1 - (\frac{R_{up-stream}}{Z_{up-stream}})^2}$$

From Eq. (3.28) at 18kV $\frac{X_{up-stream}}{Z_{up-stream}} = \sqrt{1-(0.2)^2} = 0.980$

Therefore $X_{up-stream} = 0.98 * Z_{up-stream}$

The resistivity of copper at 20^0C is 0.01851Ωmm^2/m (Das, 2016; Tleis, 2008).

For low-voltage lines reactance is 0.3Ω/km, for high-voltage it is 0.4Ω/km (Das, 2016; Tleis, 2008).

(i) Solution using conventional methods

$$Z_{up-stream} = \frac{U^2}{S_{sc}} = \frac{18000^2}{500 * 10^6} = 0.648\Omega$$

$X_{up\text{-}stream} = 0.98 * Z_{up\text{-}stream} = 0.98 * 0.648 = 0.63504\Omega$

$R_{up\text{-}stream} = 0.2 * Z_{up\text{-}stream} = 0.2 * 0.648 = 0.1296\Omega$

$X_{copper\text{-}cable} = 0.4\Omega/km * 1km = 0.4\Omega$

$R_{copper\text{-}cable} = 0.01851 * \frac{1000}{100} = 0.1851\Omega$

$X_w = 0.63504 + 0.4 = 1.03504\ \Omega$

$R_w = 0.1296 + 0.1851 = 0.3147\ \Omega$

$Z_w = \sqrt{X_w^2 + R_w^2} = \sqrt{0.3147^2 + 1.03504^2} = 1.0818\Omega$

Three phase steady-state short circuit current $I_w = \frac{18\,000}{1.0818 * \sqrt{3}} = 9.606kA$

Asymmetrical line-to-line fault with no earth $I_{line\text{-}line} = \frac{U}{2 * Z_{sc}}$

$$= \frac{\sqrt{3}}{2} * I_{3-phase}$$

$$= 0.866 * 9.606 = 8.319kA$$

$$I_{peak} = I_{fault} * \sqrt{2} * (1.02 + 0.98 * e^{-\frac{3R}{X}})$$

$$R/X = \frac{0.3147}{1.03504} = 0.304$$

Peak current = $\sqrt{2} * \left(1.02 + 0.98 * e^{-3*\frac{R}{X}}\right) * 9.606$

Symmetrical three-phase peak current $= 19.2053$ kA

Asymmetrical line-to-line peak current $= 0.866 * 19.2053$

$= 16.6318$kA

(ii) Solution using MGA

Let C1 be the coefficient in (4-35), C2 be the coefficient in (4-36) and C3 be the coefficient in (3-32). These coefficients were determined stochastically by use of the MGA. Table 4.1 below gives the magnitudes of the coefficient values that were obtained in 20 runs.

Table 4.1: The coefficient values obtained by MGA for point W

	MGA coefficient values for 20 runs		
	Min value	Max value	Average value for 20 runs
C1	0.73	1	0.995
C2	0.039	0.64	0.219
C3	0.001	0.24	0.107

The obtained average values were now used alongside the parameters of the power system to obtain the fault values.

$X_{Generators} = \frac{U^2}{2MVA} * 20\% = \frac{18000^2}{2*10^6} = 32.4\Omega$

$X_{up\text{-}stream} = C1*Z_{up\text{-}stream} = 0.995* Z_{up\text{-}stream} = 0.995 * 0.648 = 0.64476\Omega$

$R_{up\text{-}stream} = C2* Z_{up\text{-}stream} = 0.219* Z_{up\text{-}stream} = 0.219 * 0.648 = 0.141912\Omega$

$R_{Generators} = C3* X_{Generators} = 0.107* X_{Generators} = 0.107 * 32.4 = 3.4668\Omega$

$X_{copper\text{-}cable} = 0.4\Omega/km * 1km = 0.4\Omega$

$R_{copper\text{-}cable} = 0.1851\Omega$

$X_w = 0.64476 + 0.4 = 1.04476\ \Omega$

$R_w = 0.141912 + 0.1851 = 0.327012\ \Omega$

$Z_w = \sqrt{X_w^{\,2} + R_w^{\,2}} = \sqrt{0.327012^2 + 1.04476^2} = 1.095\Omega$

Three phase steady-state short circuit current $I_w = \frac{18\,000}{1.095*\sqrt{3}} = 9.491\text{kA}$

Asymmetrical line-to-line fault with no earth $I_{\text{line-line}} = \frac{U}{2*Z_{sc}}$

$= 0.866 * 9.491 = 8.219\text{kA}$

$R/_X = \frac{0.327012}{1.04476} = 0.313$

Peak current $= \sqrt{2} * \left(1.02 + 0.98 * e^{-3*\frac{R}{X}}\right) * 9.491\text{kA}$

Symmetrical three-phase peak current $= 18.834\text{kA}$

Asymmetrical line-to-line peak current $= 0.866 * 18.834\text{kA}$

$= 16.311\text{kA}$

(iii) Solution using MGAP

Let C1 be the coefficient in (4-35), C2 be the coefficient in (4-36) and C3 be the coefficient in (3-32). These coefficients were determined stochastically by the MGAP. Table 4.2 below gives the magnitudes of the coefficient values that were obtained in 20 runs.

Table 4.2: The coefficient values obtained by MGAP for point W

	MGAP coefficient values for 20 runs		
	Min value	Max value	Average value for 20 runs
C1	0.91	1	0.968
C2	0.063	0.48	0.194
C3	0.0081	0.19	0.0965

$X_{\text{up-stream}} = C1 * Z_{\text{up-stream}} = 0.968 * Z_{\text{up-stream}} = 0.968 * 0.648 = 0.627264\Omega$

$R_{\text{up-stream}} = C2 * Z_{\text{up-stream}} = 0.194 * Z_{\text{up-stream}} = 0.194 * 0.648 = 0.125712\Omega$

$R_{\text{Generators}} = C3 * X_{\text{Generators}} = 0.0965 * X_{\text{Generators}} = 0.0965 * 32.4 = 3.1266\Omega$

$X_{\text{copper-cable}} = 0.4\Omega/\text{km} * 1\text{km} = 0.4\Omega$

$R_{\text{copper-cable}} = 0.1851\Omega$

$X_w = 0.627264 + 0.4 = 1.027264\ \Omega$

$R_w = 0.125712 + 0.1851 = 0.310812\ \Omega$

$Z_w = \sqrt{X_w^{\,2} + R_w^{\,2}} = \sqrt{0.310812^2 + 1.027264^2} = 1.07325\Omega = 1.073\ \Omega$

Three phase steady-state short circuit current $I_w = \frac{18\,000}{1.073 * \sqrt{3}} = 9.685\text{kA}$

Asymmetrical line-to-line fault with no earth $I_{\text{line-line}} = \frac{U}{2 * Z_{sc}}$

$= 0.866 * 9.685 = 8.388\text{kA}$

$R/_X = \frac{0.310812}{1.027264} = 0.3026$

Peak current $= \sqrt{2} * \left(1.02 + 0.98 * e^{-3 * \frac{R}{X}}\right) * 9.685\text{kA}$

Symmetrical three-phase peak current $= 19.385\text{kA}$

Asymmetrical line-to-line peak current $= 0.866 * 19.385\text{kA}$

$= 16.788\text{kA}$

(iv) Solution using MGAF

Let C1 be the coefficient in (4-35), C2 be the coefficient in (4-36) and C3 be the coefficient in (3-32). These coefficients were determined stochastically by the MGAF. Table 4.3 below gives the magnitudes of the coefficient values that were obtained in 20 runs.

Table 4.3: The coefficient values obtained by MGAF for point W

	MGAF coefficient values for 20 runs		
	Min value	Max value	Average value for 20 runs
C1	0.65	1	0.89
C2	0.0294	0.301	0.163
C3	0.0014	0.247	0.086

$X_{\text{up-stream}} = C1 * Z_{\text{up-stream}} = 0.89 * Z_{\text{up-stream}} = 0.89 * 0.648 = 0.57672\Omega$

$R_{\text{up-stream}} = C2 * Z_{\text{up-stream}} = 0.163 * Z_{\text{up-stream}} = 0.163 * 0.648 = 0.105624\Omega$

$R_{\text{Generators}} = C3 * X_{\text{Generators}} = 0.086 * X_{\text{Generators}} = 0.086 * 32.4 = 2.7864\Omega$

$X_{\text{copper-cable}} = 0.4\Omega/\text{km} * 1\text{km} = 0.4\Omega$

$R_{\text{copper-cable}} = 0.1851\Omega$

$X_w = 0.57672 + 0.4 = 0.97672\ \Omega$

$R_w = 0.105624 + 0.1851 = 0.290724\ \Omega$

$Z_w=\sqrt{X_w{}^2 + R_w{}^2} = \sqrt{0.290724^2 + 0.97672^2} = 1.01907\Omega = 1.019\,\Omega$

Three phase steady-state short circuit current $I_w = \frac{18\,000}{1.019*\sqrt{3}} = 10.198\text{kA}$

Asymmetrical line-to-line fault with no earth $I_{\text{line-line}} = \frac{U}{2*Z_{sc}}$

$= 0.866 * 10.198 = 8.832\text{kA}$

$R/_X = \frac{0.290724}{0.97672} = 0.2977$

Peak current = $\sqrt{2} * \left(1.02 + 0.98 * e^{-3*\frac{R}{X}}\right) * 10.198\text{kA}$

Symmetrical three-phase peak current $= 20.497\text{kA}$

Asymmetrical line-to-line peak current $= 0.866 * 20.497\text{kA}$

$= 17.751\text{kA}$

(v) Solution using MPSO

Let the number of variables be equal to 3. Let Var1 be the coefficient in (4-35), Var2 be the coefficient in (4-36) and Var3 be the coefficient in (3-32). These coefficients were determined stochastically by use of the MPSO within Matlab software. Table 4.4 below gives the magnitudes of the coefficient values that were obtained in 20 runs.

Table 4.4: The coefficient values obtained by MPSO for point W

	MPSO coefficient values for 20 runs		
	Min value	Max value	Average value for 20 runs
Var1	0.963	1	1
Var2	0.006	0.433	0.194
Var3	0.0004	0.139	0.098

$X_{\text{Generators}} = \frac{U^2}{2\text{MVA}} * 20\% = \frac{18000^2}{2*10^6} = 32.4\Omega$

$X_{\text{up-stream}} = \text{Var1}*Z_{\text{up-stream}} = 1* Z_{\text{up-stream}} = 1 * 0.648 = 0.648\Omega$

$R_{\text{up-stream}} = \text{Var2}* Z_{\text{up-stream}} = 0.194* Z_{\text{up-stream}} = 0.194 * 0.648 = 0.125712\Omega$

$R_{\text{Generators}} = \text{Var3}* X_{\text{Generators}} = 0.098* X_{\text{Generators}} = 0.098 * 32.4 = 3.1752\Omega$

$X_{\text{copper-cable}} = 0.4\Omega/\text{km} * 1\text{km} = 0.4\Omega$

$R_{\text{copper-cable}} = 0.1851\Omega$

$X_w = 0.648 + 0.4 = 1.048\,\Omega$

$R_w = 0.125712 + 0.1851 = 0.310812\,\Omega$

$Z_w = \sqrt{X_w^{\,2} + R_w^{\,2}} = \sqrt{0.310812^2 + 1.048^2} = 1.093\,\Omega$

Three phase steady-state short circuit current $I_w = \frac{18\,000}{1.093 * \sqrt{3}} = 9.508\text{kA}$

Asymmetrical line-to-line fault with no earth $I_{\text{line-line}} = \frac{U}{2 * Z_{sc}}$

$= 0.866 * 9.508 = 8.234\text{kA}$

$R/X = \frac{0.310812}{1.048} = 0.2966$

Peak current = $\sqrt{2} * \left(1.02 + 0.98 * e^{-3*\frac{R}{X}}\right) * 9.508\text{kA}$

Symmetrical three-phase peak current $= 19.128\text{kA}$

Asymmetrical line-to-line peak current $= 0.866 * 19.128\text{kA}$

$= 16.565\text{kA}$

(vi) Solution using MPSOP

Let the number of variables be equal to 3. Let Var1 be the coefficient in (4-35), Var2 be the coefficient in (4-36) and Var3 be the coefficient in (3-32). These coefficients were determined stochastically by use of the MPSOP within Matlab software. Table 4.5 below gives the magnitudes of the coefficient values that were obtained in 20 runs.

Table 4.5: The coefficient values obtained by MPSOP for point W

	MPSOP coefficient values for 20 runs		
	Min value	Max value	Average value for 20 runs
Var1	1	1	1
Var2	0.0424	0.343	0.198
Var3	0.0001	0.176	0.099

$X_{\text{up-stream}} = \text{Var1} * Z_{\text{up-stream}} = 1 * Z_{\text{up-stream}} = 1 * 0.648 = 0.648\Omega$

$R_{\text{up-stream}} = \text{Var2} * Z_{\text{up-stream}} = 0.198 * Z_{\text{up-stream}} = 0.198 * 0.648 = 0.128304\Omega$

$R_{\text{Generators}} = \text{Var3} * X_{\text{Generators}} = 0.099 * X_{\text{Generators}} = 0.099 * 32.4 = 3.2076\Omega$

$X_{copper\text{-}cable} = 0.4\Omega/km * 1km = 0.4\Omega$

$R_{copper\text{-}cable} = 0.1851\Omega$

$X_w = 0.648 + 0.4 = 1.048\,\Omega$

$R_w = 0.128304 + 0.1851 = 0.313404\,\Omega$

$Z_w = \sqrt{X_w^{\,2} + R_w^{\,2}} = \sqrt{0.313404^2 + 1.048^2} = 1.094\,\Omega$

Three phase steady-state short circuit current $I_w = \frac{18\,000}{1.094*\sqrt{3}} = 9.499kA$

Asymmetrical line-to-line fault with no earth $I_{line\text{-}line} = \frac{U}{2*Z_{sc}}$

$= 0.866 * 9.499 = 8.227kA$

$R/_X = \frac{0.313404}{1.048} = 0.299$

Peak current $= \sqrt{2} * \left(1.02 + 0.98 * e^{-3*\frac{R}{X}}\right) * 9.499kA$

Symmetrical three-phase peak current $= 19.071kA$

Asymmetrical line-to-line peak current $= 0.866 * 19.071kA$

$= 16.516kA$

(vii) Solution using MPSOF

Let the number of variables be equal to 3. Let Var1 be the coefficient in (4-35), Var2 be the coefficient in (4-36) and Var3 be the coefficient in (3-32). These coefficients were determined stochastically by use of the MPSOF within Matlab software. Table 4.6 below gives the magnitudes of the coefficient values that were obtained in 20 runs.

Table 4.6: The coefficient values obtained by MPSOF for point W

	MPSOF coefficient values for 20 runs		
	Min value	Max value	Average value for 20 runs
Var1	0.989	1	1
Var2	0.0019	0.442	0.188
Var3	0.0074	0.204	0.105

$X_{up\text{-}stream} = Var1 * Z_{up\text{-}stream} = 1 * Z_{up\text{-}stream} = 1 * 0.648 = 0.648\Omega$

$R_{up\text{-}stream} = Var2 * Z_{up\text{-}stream} = 0.188 * Z_{up\text{-}stream} = 0.188 * 0.648 = 0.121824\Omega$

$R_{Generators} = Var3^{*}\ X_{Generators} = 0.105^{*}\ X_{Generators} = 0.105 * 32.4 = 3.402\Omega$

$X_{copper\text{-}cable} = 0.4\Omega/km * 1km = 0.4\Omega$

$R_{copper\text{-}cable} = 0.01851^{*}\frac{1000}{100} = 0.1851\Omega$

$X_w = 0.648 + 0.4 = 1.048\ \Omega$

$R_w = 0.121864 + 0.1851 = 0.306924\ \Omega$

$Z_w = \sqrt{X_w^{\ 2} + R_w^{\ 2}} = \sqrt{0.306924^2 + 1.048^2} = 1.092\ \Omega$

Three phase steady-state short circuit current $I_w = \frac{18\,000}{1.092 * \sqrt{3}} = 9.517kA$

Asymmetrical line-to-line fault with no earth $I_{line\text{-}line} = \frac{U}{2 * Z_{sc}}$

$= 0.866 * 9.517 = 8.242kA$

$R/_X = \frac{0.306924}{1.048} = 0.2929$

Peak current = $\sqrt{2} * \left(1.02 + 0.98 * e^{-3*\frac{R}{X}}\right) * 9.517kA$

Symmetrical three-phase peak current $= 19.206kA$

Asymmetrical line-to-line peak current $= 0.866 * 19.206kA$

$= 16.633kA$

4.2.3.2 Fault at point X

Point X is at the busbars for the main LV switchboard. The reactances and resistances of the high-voltage side should be recalculated for the low-voltage network (Tleis, 2008).

$\frac{410}{18\,000} * \frac{410}{18\,000} = 0.5 * 10^{-3}$

Transformer impedance on LV side $Z_T = \frac{1}{2} * \frac{5.5}{100} * \frac{410^2}{10^6} = 4.6 * 10^{-3}\Omega$

$X_T \approx Z_T \approx 4.6 * 10^{-3}\ \Omega$

Circuit breaker $X_{CB} = 0.15 * 10^{-3}\ \Omega$

Busbars $X_{BB} = 0.15 * 15 = 2.25 * 10^{-3}\ \Omega$

$R_{BB} = 0.023 * 10/400 = 0.575\ m\Omega$

(i) Solution using conventional methods

$R_T \approx 0.2 * X_T \approx 0.92 * 10^{-3}\ \Omega$

$X_x = [(X_w * 0.5) + 4.6 + 0.15 + 2.25] * 10^{-3}$

$= 7.79\text{m}\ \Omega$

$R_x = [(R_w * 0.5) + 0.92 + 0.575] * 10^{-3}$

$= 1.93\text{m}\Omega$

$Z_x = \sqrt{X_x^{\,2} + R_x^{\,2}}$

$Z_X = \sqrt{7.79^2 + 1.93^2} = 8.01\text{m}\Omega$

Three phase steady-state short circuit current $I_x = \frac{410}{8.01 * \sqrt{3}} = 29.552\text{kA}$

Asymmetrical line-to-line fault with no earth $I_{\text{line-line}} = \frac{U}{2 * Z_{sc}}$

$= 0.866 * 29.552 = 25.592\text{kA}$

$R/_X = \frac{1.93}{7.79} = 0.24775$

Peak current $= \sqrt{2} * \left(1.02 + 0.98 * e^{-3 * \frac{R}{X}}\right) * 29.552\text{kA}$

Symmetrical three-phase peak current $= 62.1065\text{kA}$

Asymmetrical line-to-line peak current $= 0.866 * 62.1065\text{kA}$

$= 53.7842\ \text{kA}$

(ii) Solution using MGA

Let C1 be the coefficient in (3-35). The coefficient was determined stochastically by use of the MGA. Table 4.7 below gives the magnitudes of the coefficient values that were obtained in 20 runs.

Table 4.7: The coefficient values obtained by MGA for point X

	MGA coefficient values for 20 runs		
	Min value	Max value	Average value for 20 runs
C1	0.186	0.192	0.192

$R_T = 4.6 * 0.192 = 0.8832\Omega$

$X_x = [(1.04476 * 0.5) + 4.6 + 0.15 + 2.25] * 10^{-3}$

$= 7.522\text{m}\,\Omega$

$R_x = [(0.327012 * 0.5) + 0.8832 + 0.575] * 10^{-3}$

$= 1.6217\text{m}\,\Omega$

$Z_x = \sqrt{X_x^{\,2} + R_x^{\,2}}$

$Z_X = \sqrt{7.522^2 + 1.6217^2} = 7.695\text{m}\Omega$

Three phase steady-state short circuit current $I_x = \frac{410}{7.695 * \sqrt{3}} = 30.762\text{kA}$

Asymmetrical line-to-line fault with no earth $I_{\text{line-line}} = \frac{U}{2 * Z_{sc}}$

$= 0.866 * 30.762 = 26.641\text{kA}$

$R/_X = \frac{1.6217}{7.522} = 0.2156$

Peak current $= \sqrt{2} * \left(1.02 + 0.98 * e^{-3 * \frac{R}{X}}\right) * 30.762\text{kA}$

Symmetrical three-phase peak current $= 66.702\text{kA}$

Asymmetrical line-to-line peak current $= 0.866 * 67.702\text{kA}$

$= 57.766\text{ kA}$

(iii) Solution using MGAP

Let C1 be the coefficient in (3-35). The coefficient was determined stochastically by use of the MGAP. Table 4.8 below gives the magnitudes of the coefficient values that were obtained in 20 runs.

Table 4.8: The coefficient values obtained by MGAP for point X

	MGAP coefficient values for 20 runs		
	Min value	Max value	Average value for 20 runs
C1	0.192	0.192	0.192

$R_T = 4.6 * 0.192 = 0.8832\Omega$

$X_x = [(1.027264 * 0.5) + 4.6 + 0.15 + 2.25] * 10^{-3}$

$= 7.514\text{m}\,\Omega$

$R_x = [(0.310812 * 0.5) + 0.8832 + 0.575] * 10^{-3}$

$= 1.614\text{m}\Omega$

$Z_x=\sqrt{X_x{}^2 + R_x{}^2}$

$Z_X = \sqrt{7.514^2 + 1.614^2} = 7.685\text{m}\Omega$

Three phase steady-state short circuit current $I_x= \frac{410}{7.685*\sqrt{3}} = 30.802\text{kA}$

Asymmetrical line-to-line fault with no earth $I_{\text{line-line}} = \frac{U}{2*Z_{sc}}$

$= 0.866 * 30.802 = 26.675\text{kA}$

$R/_X = \frac{1.614}{7.514} = 0.2148$

Peak current = $\sqrt{2} * \left(1.02 + 0.98 * e^{-3*\frac{R}{X}}\right) * 30.802\text{kA}$

Symmetrical three-phase peak current $= 66.843\text{kA}$

Asymmetrical line-to-line peak current $= 0.866 * 66.843\text{kA}$

$= 57.888\text{ kA}$

(iv) Solution using MGAF

Let C1 be the coefficient in (3-35). The coefficient was determined stochastically by use of the MGAF. Table 4.9 below gives the magnitudes of the coefficient values that were obtained in 20 runs.

Table 4.9: The coefficient values obtained by MGAF for point X

	MGAF coefficient values for 20 runs		
	Min value	Max value	Average value for 20 runs
C1	0.192	0.192	0.192

$R_T = 4.6 * 0.192 = 0.8832\Omega$

$X_x = [(0.97672 * 0.5) + 4.6 + 0.15 + 2.25] * 10^{-3}$

$= 7.488\text{m}\ \Omega$

$R_x = [(0.2977 * 0.5) + 0.8832 + 0.575] * 10^{-3}$

$= 1.607\text{m}\,\Omega$

$Z_x = \sqrt{X_x^{\,2} + R_x^{\,2}}$

$Z_X = \sqrt{7.488^2 + 1.607^2} = 7.659\text{m}\Omega$

Three phase steady-state short circuit current $I_x = \frac{410}{7.659 * \sqrt{3}} = 30.907\text{kA}$

Asymmetrical line-to-line fault with no earth $I_{\text{line-line}} = \frac{U}{2 * Z_{sc}}$

$= 0.866 * 30.907 = 26.766\text{kA}$

$R/_X = \frac{1.607}{7.488} = 0.2146$

Peak current $= \sqrt{2} * \left(1.02 + 0.98 * e^{-3 * \frac{R}{X}}\right) * 30.907\text{kA}$

Symmetrical three-phase peak current $= 67.084\text{kA}$

Asymmetrical line-to-line peak current $= 0.866 * 67.084\text{kA}$

$= 58.097\text{ kA}$

(v) Solution using MPSO

Let Var1 be the coefficient in (3-35). Table 4.10 below gives the magnitudes of the coefficient values that were obtained in 20 runs.

Table 4.10: The coefficient values obtained by MPSO for point X

	MPSO coefficient values for 20 runs		
	Min value	Max value	Average value for 20 runs
Var1	0.192	0.193	0.192

$R_T = 4.6 * 0.192 = 0.8832\Omega$

$X_x = [(1.048 * 0.5) + 4.6 + 0.15 + 2.25] * 10^{-3}$

$= 7.524\text{m}\,\Omega$

$R_x = [(0.310812 * 0.5) + 0.8832 + 0.575] * 10^{-3}$

$= 1.614\text{m}\,\Omega$

$Z_x = \sqrt{X_x^{\,2} + R_x^{\,2}}$

$Z_X = \sqrt{7.524^2 + 1.614^2} = 7.696\text{m}\Omega$

Three phase steady-state short circuit current $I_x = \frac{410}{7.696*\sqrt{3}} = 30.758\text{kA}$

Asymmetrical line-to-line fault with no earth $I_{\text{line-line}} = \frac{U}{2*Z_{sc}}$

$= 0.866 * 30.758 = 26.637\text{kA}$

$R/_X = \frac{1.614}{7.524} = 0.2145$

Peak current $= \sqrt{2} * \left(1.02 + 0.98 * e^{-3*\frac{R}{X}}\right) * 30.758\text{kA}$

Symmetrical three-phase peak current $= 66.767\text{kA}$

Asymmetrical line-to-line peak current $= 0.866 * 66.767\text{kA}$

$= 57.822\text{ kA}$

(vi) Solution using MPSOP

Let Var1 be the coefficient in (3-35). Table 4.11 below gives the magnitudes of the coefficient values that were obtained in 20 runs.

Table 4.11: The coefficient values obtained by MPSOP for point X

	MPSOP coefficient values for 20 runs		
	Min value	Max value	Average value for 20 runs
Var1	0.192	0.193	0.192

$R_T = 4.6 * 0.192 = 0.8832\Omega$

$X_x = [(1.048 * 0.5) + 4.6 + 0.15 + 2.25] * 10^{-3}$

$= 7.524\text{m}\,\Omega$

$R_x = [(0.313404 * 0.5) + 0.8832 + 0.575] * 10^{-3}$

$= 1.615\text{m}\,\Omega$

$Z_x = \sqrt{X_x^{\,2} + R_x^{\,2}}$

$Z_X = \sqrt{7.524^2 + 1.615^2} = 7.695\text{m}\Omega$

Three phase steady-state short circuit current $I_x = \frac{410}{7.695*\sqrt{3}} = 30.762\text{kA}$

Asymmetrical line-to-line fault with no earth $I_{\text{line-line}} = \frac{U}{2*Z_{sc}}$

$= 0.866 * 30.762 = 26.641\text{kA}$

$R/_X = \frac{1.615}{7.524} = 0.2146$

Peak current = $\sqrt{2} * \left(1.02 + 0.98 * e^{-3*\frac{R}{X}}\right) * 30.762\text{kA}$

Symmetrical three-phase peak current $= 66.769\text{kA}$

Asymmetrical line-to-line peak current $= 0.866 * 66.769\text{kA}$

$= 57.824$ kA

(vii) Solution using MPSOF

Let Var1 be the coefficient in (3-35). Table 4.12 below gives the magnitudes of the coefficient values that were obtained in 20 runs.

Table 4.12: The coefficient values obtained by MPSOF for point X

	MPSOF coefficient values for 20 runs		
	Min value	Max value	Average value for 20 runs
Var1	0.192	0.193	0.192

$R_T = 4.6 * 0.192 = 0.8832\Omega$

$X_x = [(1.048 * 0.5) + 4.6 + 0.15 + 2.25] * 10^{-3}$

$= 7.524\text{m}\,\Omega$

$R_x = [(0.306924 * 0.5) + 0.8832 + 0.575] * 10^{-3}$

$= 1.612\text{m}\,\Omega$

$Z_x = \sqrt{X_x^2 + R_x^2}$

$Z_X = \sqrt{7.524^2 + 1.612^2} = 7.6947 = 7.695\text{m}\Omega$

Three phase steady-state short circuit current $I_x = \frac{410}{7.695*\sqrt{3}} = 30.762\text{kA}$

Asymmetrical line-to-line fault with no earth $I_{line\text{-}line} = \frac{U}{2*Z_{sc}}$

$= 0.866 * 30.762 = 26.641\text{kA}$

$R/_X = \frac{1.612}{7.524} = 0.2146$

Peak current = $\sqrt{2} * \left(1.02 + 0.98 * e^{-3*\frac{R}{X}}\right) * 30.762\text{kA}$

Symmetrical three-phase peak current $= 66.769\text{kA}$

Asymmetrical line-to-line peak current $= 0.866 * 66.769\text{kA}$

$= 57.824\text{ kA}$

4.2.3.3 Fault at point Y

For fault at point Y, the reactances and resistances for the 400mm^2 cables and circuit-breakers must be added to X_y and R_y.

Cable

$X_{cable} = 0.15 * 100 = 15\text{ m }\Omega$

$R_{cable} = 0.036 * 100/400 = 9\text{ m }\Omega$

(i) Solution using conventional methods

$X_y = [Xx + 0.15 + 15] * 10^{-3}$

$= 22.94\text{m }\Omega$

$R_y = [Rx + 9] * 10^{-3}$

$= 10.93\text{m }\Omega$

$Z_y = \sqrt{X_y^2 + R_y^2}$

$Z_y = \sqrt{10.93^2 + 22.94^2} = 25.4108\text{m}\Omega$

Three phase steady-state short circuit current $I_y = \frac{410}{25.4*\sqrt{3}} = 9.319\text{kA}$

Asymmetrical line-to-line fault $= 0.866 * 9.319 = 8.070\text{kA}$

$R/_X = \frac{10.93}{22.94} = 0.4765$

Peak current = $\sqrt{2} * \left(1.02 + 0.98 * e^{-3*\frac{R}{X}}\right) * 9.319\text{kA}$

Symmetrical three-phase peak current $= 16.5347\text{kA}$

Asymmetrical line-to-line peak current $= 0.866 * 16.5347 = 14.3191\text{kA}$

(ii) Solution using MGA

The values of X_X and R_X used are the values that were obtained by MGA at point X.

$X_y = [7.522 + 0.15 + 15] * 10^{-3}$

$= 22.672\text{m}\,\Omega$

$R_y = [1.6217 + 9] * 10^{-3}$

$= 10.6217\text{m}\,\Omega$

$Z_y = \sqrt{X_y^{\,2} + R_y^{\,2}}$

$Z_y = \sqrt{10.6217^2 + 22.672^2} = 25.037\text{m}\Omega$

Three phase steady-state short circuit current $I_y = \frac{410}{25.037 * \sqrt{3}} = 9.455\text{kA}$

Asymmetrical line-to-line fault $= 0.866 * 9.455 = 8.188\text{kA}$

$R/_X = \frac{10.6217}{22.672} = 0.4685$

Peak current $= \sqrt{2} * \left(1.02 + 0.98 * e^{-3*\frac{R}{X}}\right) * 9.455\text{kA}$

Symmetrical three-phase peak current $= 16.852\text{ kA}$

Asymmetrical line-to-line peak current $= 0.866 * 16.852\text{kA}$

$= 14.595\text{ kA}$

(iii) Solution using MGAP

The values of X_X and R_X used are the values that were obtained by MGAP at point X.

$X_y = [7.514 + 0.15 + 15] * 10^{-3}$

$= 22.664\text{m}\,\Omega$

$R_y = [1.614 + 9] * 10^{-3}$

$= 10.614\text{m}\,\Omega$

$Z_y = \sqrt{X_y^{\,2} + R_y^{\,2}}$

$Z_y = \sqrt{10.614^2 + 22.664^2} = 25.026\text{m}\Omega$

Three phase steady-state short circuit current $I_y = \frac{410}{25.026*\sqrt{3}} = 9.459\text{kA}$

Asymmetrical line-to-line fault $= 0.866 * 9.459 = 8.191\text{kA}$

$R/X = \frac{10.614}{22.664} = 0.4683$

Peak current = $\sqrt{2} * \left(1.02 + 0.98 * e^{-3*\frac{R}{X}}\right) * 9.459\text{kA}$

Symmetrical three-phase peak current $= 16.862$ kA

Asymmetrical line-to-line peak current $= 0.866 * 16.862\text{kA}$

$= 14.603$ kA

(iv) Solution using MGAF

The values of X_X and R_X used are the values that were obtained by MGAF at point X.

$X_y = [7.488 + 0.15 + 15] * 10^{-3}$

$= 22.638\text{m}\ \Omega$

$R_y = [1.607 + 9] * 10^{-3}$

$= 10.607\text{m}\ \Omega$

$Z_y = \sqrt{X_y^2 + R_y^2}$

$Z_y = \sqrt{10.607^2 + 22.638^2} = 25\text{m}\Omega$

Three phase steady-state short circuit current $I_y = \frac{410}{25*\sqrt{3}} = 9.469\text{kA}$

Asymmetrical line-to-line fault $= 0.866 * 9.469 = 8.2\text{kA}$

$R/X = \frac{10.607}{22.638} = 0.4686$

Peak current = $\sqrt{2} * \left(1.02 + 0.98 * e^{-3*\frac{R}{X}}\right) * 9.469\text{kA}$

Symmetrical three-phase peak current $= 16.876$ kA

Asymmetrical line-to-line peak current $= 0.866 * 16.876\text{kA}$

$= 14.615$ kA

(v) Solution using MPSO

The values of X_X and R_X used are the values that were obtained by MPSO at point X

$X_y = [7.524 + 0.15 + 15] * 10^{-3}$

$= 22.674\text{m}\,\Omega$

$R_y = [1.614 + 9] * 10^{-3}$

$= 10.614\text{m}\,\Omega$

$Z_y = \sqrt{X_y^2 + R_y^2}$

$Z_y = \sqrt{10.614^2 + 22.674^2} = 25.035\text{m}\Omega$

Three phase steady-state short circuit current $I_y = \frac{410}{25.035 * \sqrt{3}} = 9.455\text{kA}$

Asymmetrical line-to-line fault $= 0.866 * 9.455 = 8.189\text{kA}$

$R/X = \frac{10.614}{22.674} = 0.4681$

Peak current = $\sqrt{2} * \left(1.02 + 0.98 * e^{-3*\frac{R}{X}}\right) * 9.455\text{kA}$

Symmetrical three-phase peak current $= 16.856\text{kA}$

Asymmetrical line-to-line peak current $= 0.866 * 16.856\text{kA}$

$= 14.598\text{ kA}$

(vi) Solution using MPSOP

The values of X_X and R_X used are the values that were obtained by MPSOP at point X

$X_y = [7.524 + 0.15 + 15] * 10^{-3}$

$= 22.674\text{m}\,\Omega$

$R_y = [1.615 + 9] * 10^{-3}$

$= 10.615\text{m}\,\Omega$

$Z_y = \sqrt{X_y^2 + R_y^2}$

$Z_y = \sqrt{10.615^2 + 22.674^2} = 25.036\text{m}\Omega$

Three phase steady-state short circuit current $I_y = \frac{410}{25.036 * \sqrt{3}} = 9.455\text{kA}$

Asymmetrical line-to-line fault $= 0.866 * 9.455 = 8.188\text{kA}$

$R/_X = \frac{10.615}{22.674} = 0.4682$

Peak current = $\sqrt{2} * \left(1.02 + 0.98 * e^{-3*\frac{R}{X}}\right) * 9.455\text{kA}$

Symmetrical three-phase peak current $= 16.855\text{kA}$

Asymmetrical line-to-line peak current $= 0.866 * 16.855\text{kA}$

$= 14.597\text{ kA}$

(vii) Solution using MPSOF

The values of X_X and R_X used are the values that were obtained by MPSOF at point X

$X_y = [7.524 + 0.15 + 15] * 10^{-3}$

$= 22.674\text{m}\,\Omega$

$R_y = [1.612 + 9] * 10^{-3}$

$= 10.612\text{m}\,\Omega$

$Z_y = \sqrt{X_y^{\,2} + R_y^{\,2}}$

$Z_y = \sqrt{10.612^2 + 22.674^2} = 25.034\text{m}\Omega$

Three phase steady-state short circuit current $I_y = \frac{410}{25.034 * \sqrt{3}} = 9.456\text{kA}$

Asymmetrical line-to-line fault $= 0.866 * 9.456 = 8.189\text{kA}$

$R/_X = \frac{10.612}{22.674} = 0.4680$

Peak current = $\sqrt{2} * \left(1.02 + 0.98 * e^{-3*\frac{R}{X}}\right) * 9.456\text{kA}$

Symmetrical three-phase peak current $= 16.859\text{kA}$

Asymmetrical line-to-line peak current $= 0.866 * 16.859\text{kA}$

$= 14.600\text{ kA}$

4.2.3.4 Fault at point Z

For fault at Z, the reactances and resistances for the 35mm^2 cables and circuit-breakers must be added to X_z and R_z.

Cable $X_{cable} = 0.9 * 50 = 4.5\ m\Omega$

$R_{cable} = 0.023 * 50/35 = 32.86\ m\Omega$

(i) Solution using conventional methods

$X_z = [Xy + 0.15 + 4.5] * 10^{-3}$

$= 27.59m\Omega$

$R_z = [Ry + 32.86] * 10^{-3}$

$= 43.79m\Omega$

$Z_z = \sqrt{X_z^2 + R_z^2}$

$Z_z = \sqrt{27.59^2 + 43.79^2} = 51.76m\Omega$

Three phase steady-state short circuit current $I_z = \frac{410}{51.76*\sqrt{3}} = 4.573kA$

Asymmetrical line-to-line fault $= 0.866 * 4.573 = 3.960kA$

$R/X = \frac{43.79}{27.59} = 1.5872$

Peak current = $\sqrt{2} * \left(1.02 + 0.98 * e^{-3*\frac{R}{X}}\right) * 4.573kA$

Symmetrical three-phase peak current $= 6.651kA$

Asymmetrical line-to-line peak current $= 0.866 * 6.651kA$

$= 5.7597\ kA$

(ii) Solution using MGA

The values of X_Y and R_Y that are used are the values that were obtained by MGA at point Y.

$X_z = [22.672 + 0.15 + 4.5] * 10^{-3}$

$= 27.322\text{m}\,\Omega$

$R_z = [10.6217 + 32.86] * 10^{-3}$

$= 43.4817\text{m}\,\Omega$

$Z_z = \sqrt{X_z^{\,2} + R_z^{\,2}}$

$Z_z = \sqrt{27.322^2 + 43.4817^2} = 51.353\text{m}\Omega$

Three phase steady-state short circuit current $I_z = \frac{410}{51.353 * \sqrt{3}} = 4.610\text{kA}$

Asymmetrical line-to-line fault $= 0.866 * 4.610 = 3.992\text{kA}$

$R/X = \frac{43.4817}{27.322} = 1.5915$

Peak current = $\sqrt{2} * \left(1.02 + 0.98 * e^{-3 * \frac{R}{X}}\right) * 4.610\text{kA}$

Symmetrical three-phase peak current $= 6.704\text{kA}$

Asymmetrical line-to-line peak current $= 0.866 * 6.704\text{kA}$

$= 5.806\text{kA}$

(iii) Solution using MGAP

The values of X_Y and R_Y that are used are the values that were obtained by MGAP at point Y.

$X_z = [22.664 + 0.15 + 4.5] * 10^{-3}$

$= 27.314\text{m}\,\Omega$

$R_z = [10.614 + 32.86] * 10^{-3}$

$= 43.474\text{m}\,\Omega$

$Z_z = \sqrt{X_z^{\,2} + R_z^{\,2}}$

$Z_z = \sqrt{27.314^2 + 43.474^2} = 51.342\text{m}\Omega$

Three phase steady-state short circuit current $I_z = \frac{410}{51.342 * \sqrt{3}} = 4.611\text{kA}$

Asymmetrical line-to-line fault $= 0.866 * 4.611 = 3.993\text{kA}$

$$R/X = \frac{43.474}{27.314} = 1.5916$$

Peak current = $\sqrt{2} * \left(1.02 + 0.98 * e^{-3*\frac{R}{X}}\right) * 4.611\text{kA}$

Symmetrical three-phase peak current $= 6.705\text{kA}$

Asymmetrical line-to-line peak current $= 0.866 * 6.705\text{kA}$

$= 5.807\text{kA}$

(iv) Solution using MGAF

The values of X_Y and R_Y that are used are the values that MGAF obtained at point Y.

$X_z = [22.638 + 0.15 + 4.5] * 10^{-3}$

$= 27.288\text{m}\,\Omega$

$R_z = [10.607 + 32.86] * 10^{-3}$

$= 43.467\text{m}\,\Omega$

$Z_z = \sqrt{X_z^{\,2} + R_z^{\,2}}$

$Z_z = \sqrt{27.288^2 + 43.467^2} = 51.323\text{m}\Omega$

Three phase steady-state short circuit current $I_z = \frac{410}{51.323*\sqrt{3}} = 4.612\text{kA}$

Asymmetrical line-to-line fault $= 0.866 * 4.612 = 3.994\text{kA}$

$$R/X = \frac{43.467}{27.288} = 1.5929$$

Peak current = $\sqrt{2} * \left(1.02 + 0.98 * e^{-3*\frac{R}{X}}\right) * 4.612\text{kA}$

Symmetrical three-phase peak current $= 6.707\text{kA}$

Asymmetrical line-to-line peak current $= 0.866 * 6.707\text{kA}$

$= 5.808\text{kA}$

(v) Solution using MPSO

The values of X_Y and R_Y used are the values that MPSO obtained at point Y.

$X_z = [22.674 + 0.15 + 4.5] * 10^{-3}$

$= 27.324\text{m}\,\Omega$

$R_z = [10.614 + 32.86] * 10^{-3}$

$= 43.474\text{m}\,\Omega$

$Z_z = \sqrt{X_z^2 + R_z^2}$

$Z_z = \sqrt{27.324^2 + 43.474^2} = 51.345\text{m}\Omega$

Three phase steady-state short circuit current $I_z = \frac{410}{51.345 * \sqrt{3}} = 4.610\text{kA}$

Asymmetrical line-to-line fault $= 0.866 * 4.610 = 3.993\text{kA}$

$R/X = \frac{43.474}{27.324} = 1.5912$

Peak current = $\sqrt{2} * \left(1.02 + 0.98 * e^{-3*\frac{R}{X}}\right) * 4.610\text{kA}$

Symmetrical three-phase peak current $= 6.704\text{kA}$

Asymmetrical line-to-line peak current $= 0.866 * 6.704\text{kA}$

$= 5.806\text{ kA}$

(vi) Solution using MPSOP

The values of X_Y and R_Y used are the values that MPSOP obtained at point Y.

$X_z = [22.674 + 0.15 + 4.5] * 10^{-3}$

$= 27.324\text{m}\,\Omega$

$R_z = [10.615 + 32.86] * 10^{-3}$

$= 43.475\text{m}\,\Omega$

$Z_z = \sqrt{X_z^2 + R_z^2}$

$Z_z = \sqrt{27.324^2 + 43.475^2} = 51.349\text{m}\Omega$

Three phase steady-state short circuit current $I_z = \frac{410}{51.349 * \sqrt{3}} = 4.610\text{kA}$

Asymmetrical line-to-line fault $= 0.866 * 4.610 = 3.992\text{kA}$

$$R/X = \frac{43.475}{27.324} = 1.5911$$

Peak current = $\sqrt{2} * \left(1.02 + 0.98 * e^{-3*\frac{R}{X}}\right) * 4.610\text{kA}$

Symmetrical three-phase peak current $= 6.704\text{kA}$

Asymmetrical line-to-line peak current $= 0.866 * 6.704\text{kA}$

$= 5.806\text{ kA}$

(vii) Solution using MPSOF

The values of X_Y and R_Y used are the values that MPSOF obtained at point Y.

$X_z = [(22.674 + 0.15 + 4.5] * 10^{-3}$

$= 27.324\text{m}\,\Omega$

$R_z = [(10.612 + 32.86] * 10^{-3}$

$= 43.472\text{m}\,\Omega$

$Z_z = \sqrt{X_z^2 + R_z^2}$

$Z_z = \sqrt{27.324^2 + 43.472^2} = 51.346\text{m}\Omega$

Three phase steady-state short circuit current $I_z = \frac{410}{51.346 * \sqrt{3}} = 4.610\text{kA}$

Asymmetrical line-to-line fault $= 0.866 * 4.610 = 3.992\text{kA}$

$$R/X = \frac{43.472}{27.324} = 1.5910$$

Peak current = $\sqrt{2} * \left(1.02 + 0.98 * e^{-3*\frac{R}{X}}\right) * 4.610\text{kA}$

Symmetrical three-phase peak current $= 6.704\text{kA}$

Asymmetrical line-to-line peak current $= 0.866 * 6.704\text{kA}$

$= 5.806\text{ kA}$

4.2.4 Reverse motor currents

This section computes the reverse motor currents at the various network levels highlighted in figure 4.10. The motor currents were added to the fault currents computed in Section 4.2.3 and the total fault current is tabulated in Section 4.3

4.2.4.1 Fault at point Z

The motors can be considered as 'generators' that are supplying the fault points with a reverse current that is superimposed on the network fault current.

Impedance considered is $\frac{1}{10} * Z_M$ for the 10 parallel motors plus cable impedance (because all the motors have separate feeders).

Cable 35mm^2

$X_{cable} = 0.9 * 50 = 4.5\ m\Omega$

$R_{cable} = 0.023 * 50/35 = 32.86\ m\Omega$

Motor at 100kW

$X = \frac{20}{100} * \frac{410^2}{100000/(0.9*0.85)} = 257.2\ m\Omega$

$R = 0.2 * X = 51.44\ m\Omega$

$X_m = [(257.2/10) + 4.5] * 10^{-3}$

$= 30.22m\Omega$

$R_m = [(51.44/10) + 32.86] * 10^{-3}$

$= 38m\Omega$

$Z_m = \sqrt{X_m^{\ 2} + R_m^{\ 2}}$

$Z_m = \sqrt{30.22^2 + 38^2} = 48.55m\Omega$

Steady-state short circuit current $I_z = \frac{410}{48.55*\sqrt{3}} = 4.876kA$

That is the current expected from any of the motors onto the low-voltage busbar.

4.2.4.2 Fault at point Y

Cable 35mm^2

$X_{cable} = 0.9 * 50 = 4.5m\Omega$

$R_{cable} = 0.023 * 50/35 = 32.86m\Omega$

$X_m = [257.2 + 4.5] * 10^{-3}$

$= 261.7m\ \Omega$

$R_m = [51.44 + 32.86] * 10^{-3}$

$= 84.3\text{m}\,\Omega$

$Z_m = \sqrt{84.3^2 + 261.7^2} = 274.9\text{m}\Omega$

Steady-state short circuit current $I_m = \frac{410}{274.9*\sqrt{3}} = 861.1\text{A}$

For 10 motors $= 8.611\text{kA}$

The total short circuit current on the sub-distribution board increases.

4.2.4.3 Fault at point X

Cable 400mm^2

$X_{cable} = 0.15 * 100 = 15\ \text{m}\Omega$

$R_{cable} = 0.036 * \frac{100}{400} = 9\ \text{m}\Omega$

Cable 35mm^2

$X_{cable} = 0.9 * 50 = 4.5\ \text{m}\Omega$

$R_{cable} = 0.023 * 50/35 = 32.86\text{m}\Omega$

$X_m = [257.2 + 4.5 + 15] * 10^{-3}$

$=276.7\text{m}\,\Omega$

$R_m = [51.44 + 32.86 + 9] * 10^{-3}$

$=93.3\text{m}\,\Omega$

$Z_m = \sqrt{93.3^2 + 276.7^2} = 292\text{m}\Omega$

Steady-state short circuit current $I_m = \frac{410}{292*\sqrt{3}} = 810.7A$

For 10 motors $= 8.107\text{kA}$

The short-circuit current on the main low-voltage switchboard busbars also increases.

4.2.4.4 Fault at point W

When the low-voltage/high-voltage transformation value is multiplied by point X values, the fault current induced by the load on the high-voltage side of the source can be obtained (Sallam et al., 2011; Tleis, 2008).

$8107 * 410/18000 = 184.66\text{A}$

4.3 Tables of results

All the findings from the tables of results are discussed in Chapter 5. The abbreviation 'AF' used in this section stands for Arc Fault hazard.

Table 4.13: The coefficients obtained by MGA compared to the IEC coefficients

Equation with coefficient	MGA coefficient values for 20 runs			IEC value	Percentage deviation
	Min value	Max value	Average for 20 runs		
(3-32)	0.0006	0.24	0.107	0.1	7%
(3-35)	0.186	0.192	0.192	0.2	4%
(4-35)	0.73	1	0.995	0.98	1.5%
(4-36)	0.039	0.64	0.219	0.2	9.5%

Table 4.14: The coefficients obtained by MGAP compared to the IEC coefficients

Equation with coefficient	MGAP coefficient values for 20 runs			IEC value	Percentage deviation
	Min value	Max value	Average for 20 runs		
(3-32)	0.0081	0.19	0.0965	0.1	3.5%
(3-35)	0.192	0.192	0.192	0.2	4%
(4-35)	0.91	1	0.968	0.98	1.22%
(4-36)	0.063	0.48	0.194	0.2	3%

Table 4.15: The coefficients obtained by MGAF compared to the IEC coefficients

Equation with coefficient	MGAF coefficient values for 20 runs			IEC value	Percentage deviation
	Min value	Max value	Average for 20 runs		
(3-32)	0.0014	0.247	0.086	0.1	14%
(3-35)	0.006	0.192	0.192	0.2	4%
(4-35)	0.65	1	0.89	0.98	9.18%
(4-36)	0.0294	0.301	0.163	0.2	18.5%

Table 4.16: The coefficients obtained by MPSO compared to the IEC coefficients

Equation with coefficient	MPSO coefficient values for 20 runs			IEC value	Percentage deviation
	Min value	Max value	Average for 20 runs		
(3-32)	0.0004	0.139	0.098	0.1	2%
(3-35)	0.186	0.193	0.192	0.2	4%
(4-35)	0.963	1	1	0.98	2%
(4-36)	0.006	0.433	0.194	0.2	3%

Table 4.17: The coefficients obtained by MPSOP compared to the IEC coefficients

Equation with coefficient	MPSOP coefficient values for 20 runs			IEC value	Percentage deviation
	Min value	Max value	Average for 20 runs		
(3-32)	0.001	0.176	0.099	0.1	1%
(3-35)	0.192	0.192	0.192	0.2	4%
(4-35)	1	1	1	0.98	2%
(4-36)	0.0424	0.343	0.198	0.2	1%

Table 4.18: The coefficients obtained by MPSOF compared to the IEC coefficients

Equation with coefficient	MPSOF coefficient values for 20 runs			IEC value	Percentage deviation
	Min value	Max value	Average for 20 runs		
(3-32)	0.0074	0.204	0.105	0.1	5%
(3-35)	0.192	0.192	0.192	0.2	4%
(4-35)	0.989	1	1	0.98	2%
(4-36)	0.0019	0.442	0.188	0.2	6%

Table 4.19: Comparison between the MGA and CM impedances

	MGA value	CM value	Difference	Percentage deviation
Fault Point	Z	Z	Z	
W	1.095 Ω	1.082 Ω	0.013 Ω	1.2%
X	7.695 mΩ	8.010 mΩ	0.315 mΩ	3.93%
Y	25.037mΩ	25.411 mΩ	0.374 mΩ	1.47%
Z	51.353mΩ	51.757 mΩ	0.404 mΩ	0.78%

Table 4.20: Comparison between the MGAP and CM impedances

	MGAP value	CM value	Difference	Percentage deviation
Fault Point	Z	Z	Z	
W	1.073 Ω	1.082 Ω	0.009Ω	0.83%
X	7.685 mΩ	8.010 mΩ	0.325mΩ	4.06%
Y	25.026mΩ	25.411 mΩ	0.385mΩ	1.52%
Z	51.342mΩ	51.757 mΩ	0.415mΩ	0.80%

Table 4.21: Comparison between the MGAF and CM impedances

	MGAF value	CM value	Difference	Percentage deviation
Fault Point	Z	Z	Z	
W	1.019 Ω	1.082 Ω	0.063 Ω	5.82%
X	7.659 mΩ	8.010 mΩ	0.351mΩ	4.38%
Y	25mΩ	25.411 mΩ	0.411mΩ	1.62%
Z	51.323mΩ	51.757 mΩ	0.434mΩ	0.83%

Table 4.22: Comparison between the MPSO and CM impedances

	MPSO value	CM value	Difference	Percentage deviation
Fault Point	Z	Z	Z	
W	1.093 Ω	1.082 Ω	0.011Ω	1.02%
X	7.696 mΩ	8.010mΩ	0.314mΩ	3.92%
Y	25.035mΩ	25.411mΩ	0.376mΩ	1.48%
Z	51.345mΩ	51.757mΩ	0.412mΩ	0.80%

Table 4.23: Comparison between the MPSOP and CM impedances

	MPSOP value	CM value	Difference	Percentage deviation
Fault Point	Z	Z	Z	
W	1.094 Ω	1.082 Ω	0.012Ω	1.11%
X	7.695mΩ	8.010 mΩ	0.315mΩ	3.93%
Y	25.036mΩ	25.411 mΩ	0.375mΩ	1.48%
Z	51.349mΩ	51.757 mΩ	0.408mΩ	0.79%

Table 4.24: Comparison between the obtained MPSOF and CM impedances

	MPSOF value	CM value	Difference	Percentage deviation
Fault Point	Z	Z	Z	
W	1.092Ω	1.082 Ω	0.010Ω	0.92%
X	7.695mΩ	8.010 mΩ	0.315mΩ	3.93%
Y	25.034mΩ	25.411 mΩ	0.377mΩ	1.48%
Z	51.346mΩ	51.757 mΩ	0.411mΩ	0.79%

Table 4.25: Genetic algorithms fault currents without reverse motor currents in kA

	FAULT POINT **W**		FAULT POINT **X**				FAULT POINT **Y**		FAULT POINT **Z**	
	I_{3P}	**I_{LL}**	**I_{3P}**	**I_{LL}**	**I_{3P}** AF	**I_{LL}** AF	**I_{3P}**	**I_{LL}**	**I_{3P}**	**I_{LL}**
CM	9.606	8.319	29.552	25.592	15	13	9.319	8.070	4.573	3.960
MGA	9.491	8.219	30.762	26.641	15	13	9.455	8.188	4.610	3.992
MGAP	9.685	8.388	30.802	26.675	15	13	9.459	8.191	4.611	3.993
MGAF	10.198	8.832	30.907	26.766	15	13	9.469	8.200	4.612	3.994

Table 4.26: Genetic algorithms fault currents with reverse motor currents in kA

	FAULT POINT **W**		FAULT POINT **X**				FAULT POINT **Y**		FAULT POINT **Z**	
	I_{3P}	**I_{LL}**	**I_{3P}**	**I_{LL}**	**I_{3P}** AF	**I_{LL}** AF	**I_{3P}**	**I_{LL}**	**I_{3P}**	**I_{LL}**
RMC	0.185		8.107				8.611		4.876	
CM	9.791	8.504	37.659	33.699	20	18	17.930	16.681	9.449	8.836
MGA	9.676	8.404	38.869	34.748	20	18	18.066	16.799	9.486	8.868
MGAP	9.870	8.573	38.909	34.782	20	18	18.070	16.802	9.487	8.869
MGAF	10.383	9.017	39.014	34.873	20	18	18.080	16.811	9.488	8.870

Table 4.27: Particle Swarm fault currents without reverse motor currents in kA

	FAULT POINT **W**		FAULT POINT **X**				FAULT POINT **Y**		FAULT POINT **Z**	
	I_{3P}	I_{LL}	I_{3P}	I_{LL}	I_{3P} AF	I_{LL} AF	I_{3P}	I_{LL}	I_{3P}	I_{LL}
CM	9.606	8.319	29.552	25.592	15	13	9.319	8.070	4.573	3.960
MPSO	9.508	8.234	30.758	26.637	15	13	9.455	8.188	4.610	3.993
MPSOP	9.499	8.227	30.762	26.641	15	13	9.455	8.188	4.610	3.992
MPSOF	9.517	8.242	30.762	26.641	15	13	9.456	8.189	4.610	3.992

Table 4.28: Particle Swarm fault currents with reverse motor currents in kA

	FAULT POINT **W**		FAULT POINT **X**				FAULT POINT **Y**		FAULT POINT **Z**	
	I_{3P}	I_{LL}	I_{3P}	I_{LL}	I_{3P} AF	I_{LL} AF	I_{3P}	I_{LL}	I_{3P}	I_{LL}
RMC	0.185		8.107				8.611		4.876	
CM	9.791	8.504	37.659	33.699	20	18	17.930	16.681	9.449	8.836
MPSO	9.693	8.419	38.865	34.744	20	18	18.066	16.799	9.486	8.869
MPSOP	9.684	8.412	38.869	34.748	20	18	18.066	16.799	9.486	8.868
MPSOF	9.702	8.427	38.869	34.748	20	18	18.067	16.800	9.486	8.868

Table 4.29: Genetic algorithms peak fault currents in kA

	FAULT POINT **W**		FAULT POINT **X**				FAULT POINT **Y**		FAULT POINT **Z**	
	I_{3P}	I_{LL}	I_{3P}	I_{LL}	I_{3P} AF	I_{LL} AF	I_{3P}	I_{LL}	I_{3P}	I_{LL}
CM	19.205	16.632	62.107	53.784	35.00	30.00	16.535	14.319	6.651	5.760
MGA	18.834	16.311	66.702	57.766	35.00	30.00	16.852	14.595	6.704	5.806
MGAP	19.385	16.788	66.843	57.888	35.00	30.00	16.862	14.603	6.705	5.807
MGAF	20.497	17.751	67.084	58.097	35.00	30.00	16.876	14.615	6.707	5.808

Table 4.30: Particle Swarm algorithms peak fault currents in kA

	FAULT POINT **W**		FAULT POINT **X**				FAULT POINT **Y**		FAULT POINT **Z**	
	I_{3P}	I_{LL}	I_{3P}	I_{LL}	I_{3P} AF	I_{LL} AF	I_{3P}	I_{LL}	I_{3P}	I_{LL}
CM	19.205	16.632	62.107	53.784	35.00	30.00	16.535	14.319	6.651	5.760
MPSO	19.128	16.565	66.767	57.822	35.00	30.00	16.856	14.598	6.704	5.806
MPSOP	19.071	16.516	66.769	57.824	35.00	30.00	16.855	14.597	6.704	5.806
MPSOF	19.206	16.633	66.796	58.824	35.00	30.00	16.859	14.600	6.704	5.806

CHAPTER 5

RESEARCH FINDINGS DISCUSSION

5.1 The computed coefficients

Tables 4.13 to 4.18 give the coefficient values that were obtained by all the evolutionary algorithms (EAs). The values in the tables are an average of 20 runs. A column of the predefined Standard IEC values is also included in the tables for comparison. From the tables, when all the EA coefficients are rounded off to one decimal place, they will be equal to the IEC coefficient values. This makes all the tested evolutionary algorithms capable of handling the computational problem that was being investigated. An analysis is made below as to which ones are the most suitable.

The coefficient values that were obtained by the MGAP, MPSO, MPSOP and MPSOF are within an approximate range. There is a less than 7% deviation amongst them. This is because the convergence points of these algorithms were almost the same. The MGAF and MGA coefficient values deviate a lot more from those obtained by the other algorithms indicating that they struggled with convergence to the global minima.

However, the coefficients obtained by the EAs are slightly different from the values given by Standard IEC 60909 and IEC 61363. The MGAP, MPSO and MPSOP coefficients deviate from the IEC values by not more than 4% whilst the MPSOF coefficients deviate by up to 6%. This makes the former three to be the much better EA options for the computational problem. The MGA and MGAF values deviate from the IEC values by up to 9.5% and 18.5% respectively. This makes them not suitable enough for the computational problem of detecting short circuit faults. Figure 5.1 is a plot of the optimisation tools against their maximum percentage deviation from the predefined IEC values. The trends in Figure 5.1 explicitly show the best and worst algorithms when computing coefficient values.

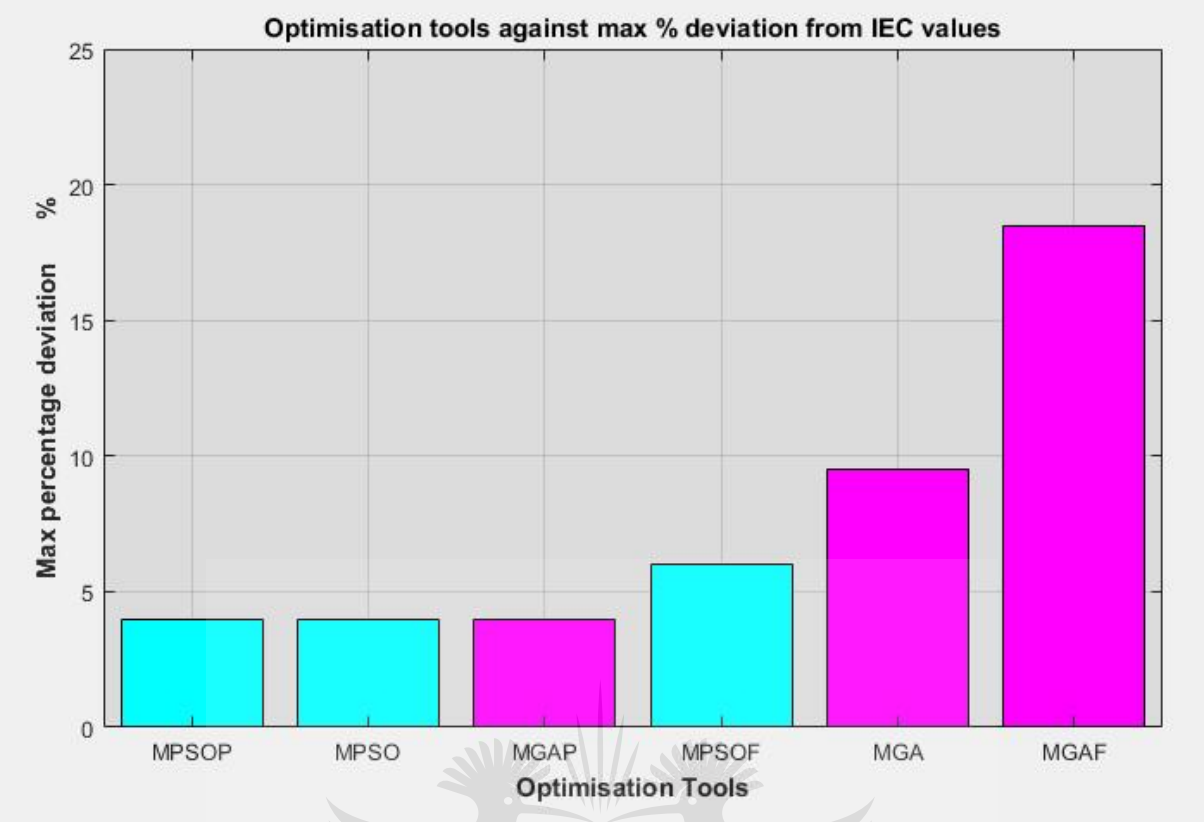

Figure 5.1 Optimisation tools plotted against their maximum percentage deviations

When running the algorithms to obtain the coefficient values, the average time per run was noted and it has been plotted in Figure 5.2. The MGAP, MPSO and MPSOP converged at a lesser number of iterations, thus their computational time was short. Computational time is a key element used when evaluating an algorithm.

Moreover, when doing the runs, 18 or more times, the MGAP, MPSO and MPSOP algorithms would obtain a value that is almost equal or equal to the IEC given values. This gives the three algorithms a 'confidence interval' greater than 90% when searching for coefficients. This makes the three algorithms to be more reliable since they quickly attain stable and precise results and go on to consistently converge at the same point. This cements the three as the best performing and most suitable algorithms for the computational problem that was being investigated.

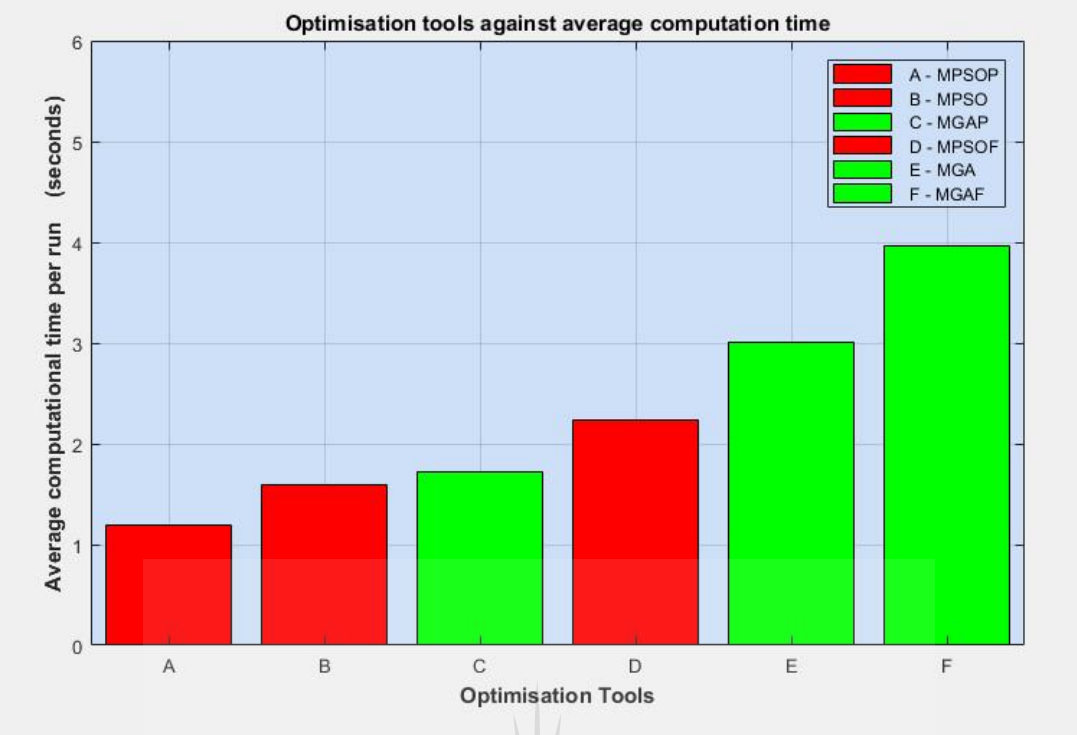

Figure 5.2 Optimisation tools plotted against their average computational time

5.2 The computed impedances

Tables 4.19 to 4.24 give the fault point impedances that were obtained by all the EAs and conventional methods (CMs). The impedances that were obtained using the EAs computed coefficients were almost equal to the impedances that the CMs obtained using IEC coefficients. This is because the coefficients that were used by the EAs and CMs were within an approximate range.

Based on Tables 4.19 to 4.24, disregarding MGAF which has the most abnormal deviations stated in Section 5.1, for faults at the source terminals and faults at the load terminals i.e. at points W and Z in Figure 4.10, there was a small difference in the values of impedance obtained by the CMs and EAs. The percentage deviation between EAs and CMs impedance values are not more than 1.2% and 0.83% at points W and Z respectively. For faults on the low-voltage busbars and low-voltage subdistribution boards i.e. at points X and Y, the differences in the obtained values are significant. The percentage deviation between EAs and CMs values at point X is around 4% and at point Y it is around 1.5%. CMs give much larger impedance values as compared to the EAs.

Based on the trends mentioned above, it can be noted that at the beginning of the power line i.e. at the main source terminals (point W at 0km in Figure 4.10) and the end of the power line i.e. at the motor terminals (point Z at 1km in Figure 4.10), there are slight differences in the impedance values. For points X and Y that are in the middle of the power system and distant enough from the rotating machines, CMs give much larger impedance values as compared to the EAs.

A large impedance value means that when that impedance value is substituted into Kirchhoff's voltage and current laws, a small value of short circuit current will be obtained. This means that for faults on busbars and subdistribution boards, CMs tend to understate the magnitude of short circuit current. This is dangerous, especially in the setting of protection devices. Figure 5.3 is the plot of the asymmetrical three-phase line-to-line currents (without the arc fault hazard) that were computed using the impedances from the genetic algorithms and CMs. Figure 5.4 is the plot of the asymmetrical three-phase line-to-line currents (without the arc fault hazard) that were computed using the impedances from the particle swarm algorithms and CMs. Figure 5.5 is the plot of the asymmetrical three-phase line-to-line currents (without the arc fault hazard) that were computed by all the methods. Peak fault currents and the symmetrical three-phase fault currents also give a similar trend to the asymmetrical three-phase line-to-line currents that have been plotted below. The only difference will be on the current magnitudes.

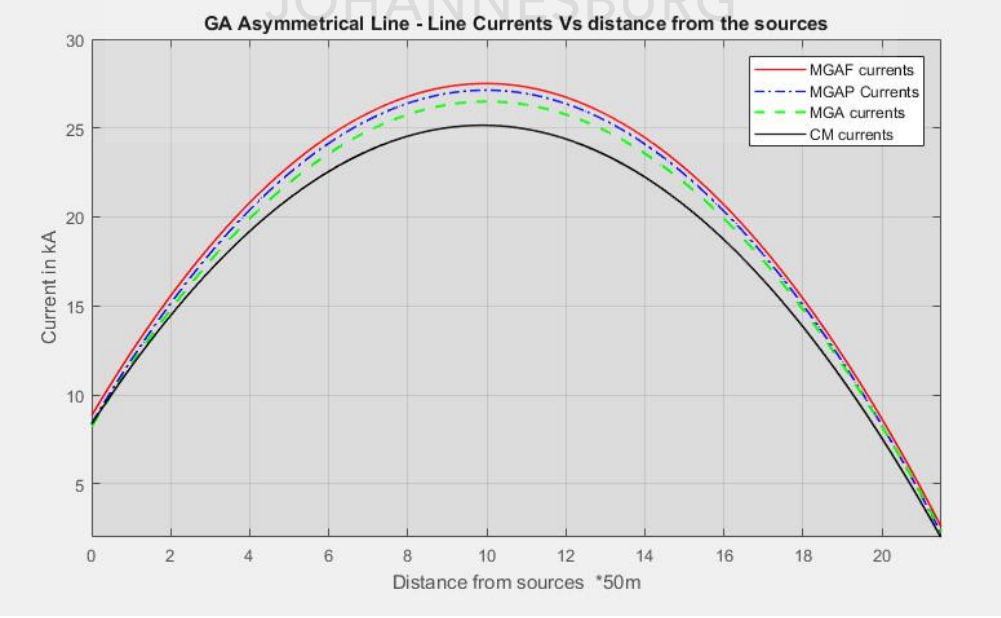

Figure 5.3 GA and CM asymmetrical fault currents against distance from the rotating machines

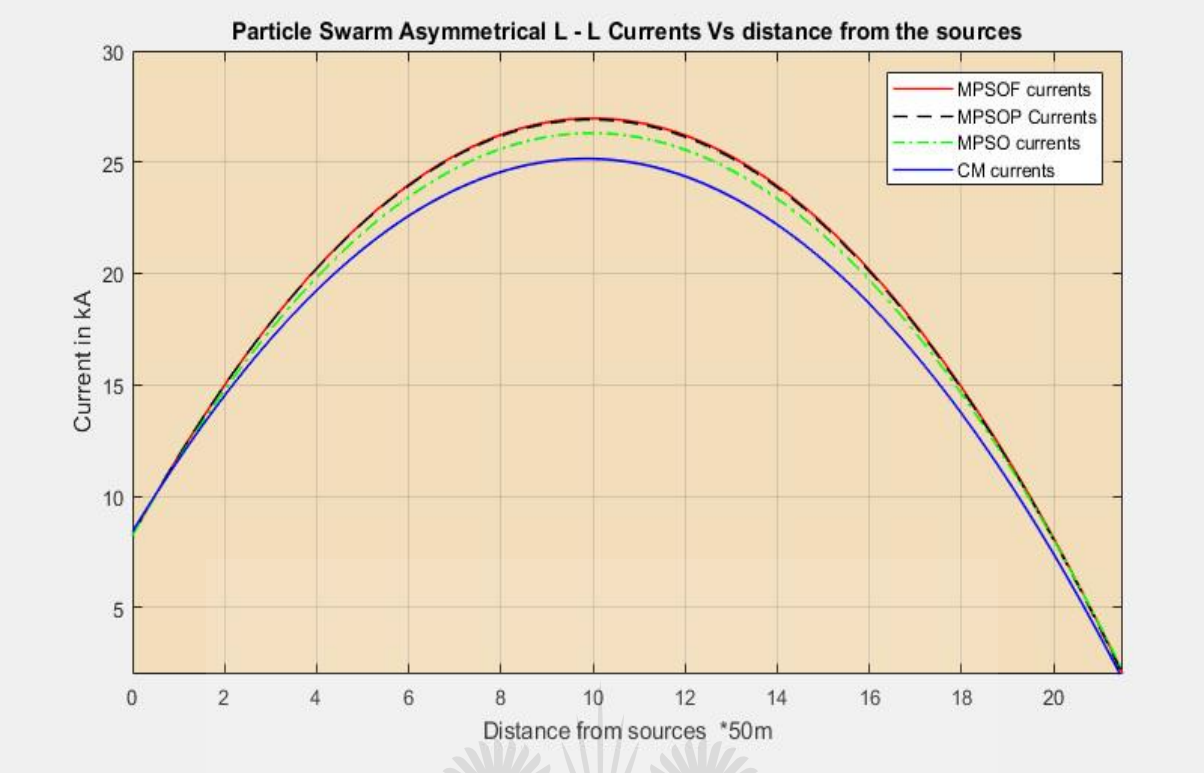

Figure 5.4 PSO and CM asymmetrical fault currents against distance from the rotating machines

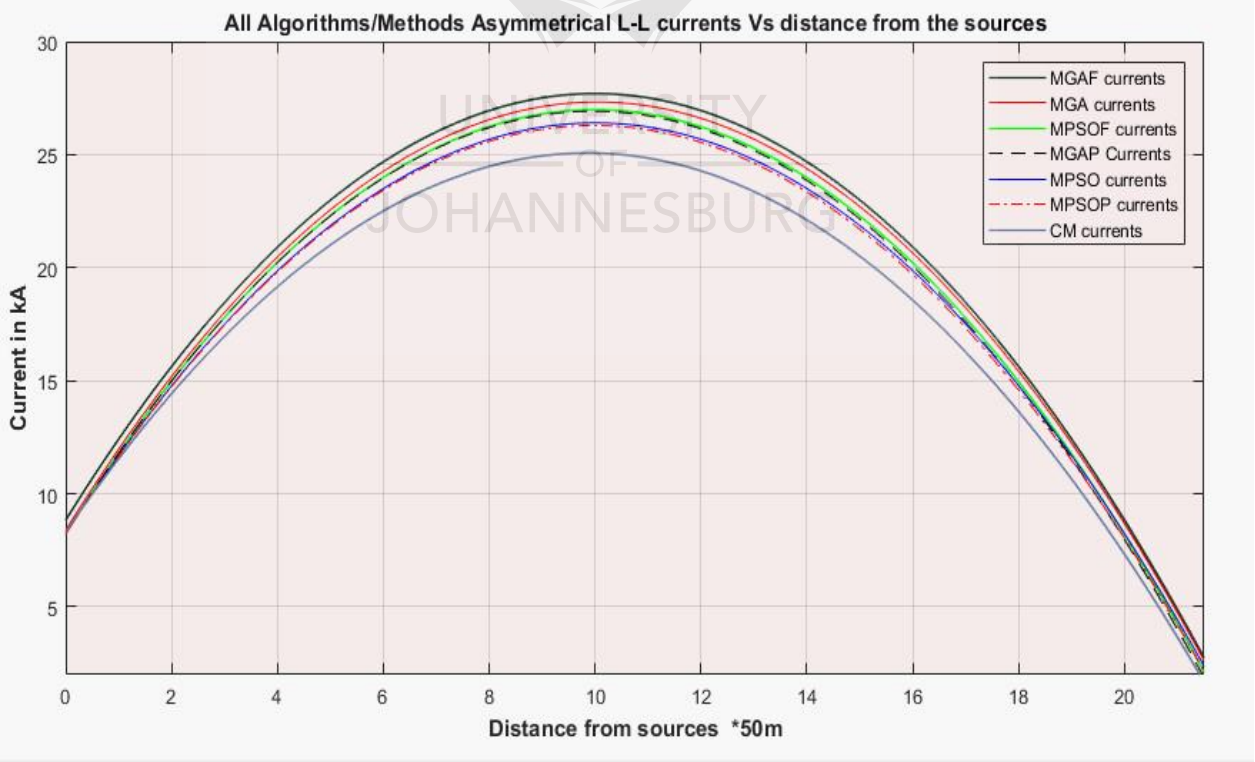

Figure 5.5 EAs and CM asymmetrical fault currents against distance from the rotating machines

Figures 5.3 to 5.5 clearly show the sections of the power system that the CMs do not properly account for. At the terminals of the rotating machines, all the algorithms/methods give similar fault magnitudes but along the power system i.e. at the bus-bars and subdistribution boards, there are large variations with the CMs under-stating the fault current magnitudes.

Standard IEC 60909 tries to rectify this problem but fails to do so sufficiently. Standard IEC 60909 states that for faults at points far away from the sources where there is a considerable effect of spinning loads e.g. a motor:

- It is easier for conventional methods to 'estimate conservatively' the fault currents than to calculate the equivalent impedances (Das, 2016; IEC 60909-0, 2016). This is because the fault evaluation procedures of CMs are not very precise and reliable.
- Currents by motors at these points can be calculated using the 'motor + cable' total impedance or the current can be estimated using the starting motor current (I_{start}) and the rated current of a generator (I_r) (IEC 60909-0,2001; Malik et al., 2011):

$$\frac{I_{start}}{I_r} * \text{rated motor current} \quad (5\text{-}1)$$

The estimates used by the CMs, from Standard IEC 60909, provide conservative protection current values. Nonetheless, these fault values will not be the precise fault magnitudes such as the ones that can be obtained by EAs at any network level.

5.3 The computed currents

The optimisation results for the computed short circuit currents are given in Tables 4.25 to 4.30. In this research, two fault conditions were computed i.e. symmetrical three-phase faults and asymmetrical three-phase line-to-line faults. The symmetrical three-phase fault was computed because it is generally considered that symmetrical three-phase faults induce the highest fault currents (Sallam et al., 2011). Therefore its investigation was necessary because it plays a key role in equipment selection (equipment with the highest electrodynamic and current withstand capability). The asymmetrical three-phase line-to-line fault was computed to check if the proposed methodology applied to asymmetrical three-phase short circuit faults, which was one of the main objectives of this research.

Based on Tables 4.25 to 4.30, for faults at busbars which have a possibility of arc hazards (fault point X from Figure 4.10), the fault magnitudes that were obtained by all the methods were the same when taking the arc hazard phenomenon into account (with a magnitude factor of around 0.5). However, for faults at the remaining parts of the network (points W, Y and Z), there are some slight differences between the EAs results and the CMs results. This is mainly because the R/X and R/Z values used by the EAs are slightly different from the values used by the CMs. CMs strictly used values given by Standard IEC 60909, IEC 61313, IEC 60034 and IEC 60076 whereas EAs stochastically computed these values. The trends presented in Sections 5.1 and 5.2 show the various impacts and the need for precise R/X and R/Z magnitudes at all instances for all the nominal voltages. Peak fault currents were obtained using normal fault currents. Therefore, precise values of normal fault current lead to precise values of peak fault current.

Nonetheless, the results obtained from the proposed methodology of using EAs and the results from the CMs based on the Standard IEC 60909 (alongside IEC 61313, IEC 60076 and IEC 60034) are very similar and within an approximate range. Therefore, protection units that can be defined using values obtained from either of the methods would be the same (Das, 2017). This means that the proposed methodology can be successfully used for the computation and evaluation of three-phase short circuit faults. The successful evaluation of a practical network example demonstrated in Chapter 4 highlights the strength and diverse applicability of EAs to power system computational problems.

The strengths of the EAs during the optimisation procedures included:

- Optimisation bounds that a user can specify.
- Adjustments to the evolutionary algorithms and flexible parameter selection which leads to effective optimisation processes.
- A population that a user can define in search for solutions with regards to the precision level desired and complexity of the optimisation problem.

Unlike CMs and the IEC procedures (in some instances), the use of EAs for detecting short circuit faults does not:

- Ignore the effects of the sources when detecting faults far away from the sources.

- Ignore and neglect some components e.g. non-spinning loads and protection devices.
- Use general estimates during fault evaluations but optimises power systems with regards to their unique specifications (does not rely on the IEC estimated coefficients or the use of equation (5-1)).

During fault detection, taking into consideration the above-mentioned factors leads to obtaining more precise values of short circuit fault current. Moreover, the procedures presented in Chapter 4 showed that EAs can be reliably used for the evaluation of any nominal voltage. The procedures also show that, unlike CMs, EAs offer a much wider operating capacity as they are not limited by a lot of estimations and approximations from Standard IEC. Their fault evaluation procedures also show that the proposed methodology can be used to detect much more precise fault magnitudes at various network levels. This makes EAs and their fault evaluation procedures to be more dependable than the CMs. This is because a more general rule is less reliable than a more specific one.

5.4 The failure of MGAF

Of all the algorithms, MGA and MGAF gave the least precise results but MGAF was the worst on computational time and the percentage deviation of its coefficient values from the IEC values. This led to the algorithm obtaining wayward fault point impedances which led to imprecise fault current magnitudes. The major reason for its failure was that, when using fmincon as a minimisation function, in some instances, it needs the specifications of a Hessian or a Jacobian or any other analytical gradients for it to function well. These help it to converge much easily to a feasible point (Costa et al., 2016). In this research, none of the above was added to the function and this probably impacted its convergence. MPSOF which also had the fmincon minimisation function did not suffer from such defects and proved to function very well regardless of not having these optional extra derivatives included.

CHAPTER 6

CONCLUSIONS AND RECOMMENDATIONS

6.1 Conclusions

Standard IEC 61313 and IEC 60909 lay out all the asymmetrical three-phase short circuit fault evaluation procedures. However, in their methodologies, they use a lot of estimates. The commonly used estimates are R/X and R/Z ratios. During fault evaluation, these ratios play a key role in determining the upstream and fault point impedances. Standard IEC lays out these ratios over a wide range that does not sufficiently cater for every nominal voltage within 550kV. When the need arises, the user has to estimate these values accordingly.

In this dissertation, GA and PSO were proposed as optimisation techniques. These algorithms were used to stochastically determine R/X and R/Z values during fault computation. One of the objectives of this research was to minimise the weaknesses of the genetic algorithm and the particle swarm optimisation before using them for fault evaluation. Some innovative coding adjustments were made to the traditional GA and PSO to reduce premature convergence, loss of population diversity and trapping into suboptimal solutions. Meticulous parameter selection was also implemented and Fmincon and Pattern-search minimisation functions were added to improve the algorithms. This resulted in the development of 6 algorithms i.e. MGA, MGAF, MGAP, MPSO, MPSOF and MPSOP.

The 6 algorithms were initially tested on benchmark functions i.e. the Rastrigin and Rosenbrock functions. The proposed modelling of the algorithms and conscientious parameter selection proved to improve the algorithms significantly. The tests on the benchmark functions clearly showed the improvement of the algorithms. The obtained results on the benchmark test functions showed that the proposed algorithms were much more robust, fast, efficient, reliable and accurate as compared to the traditional GA and PSO.

A model of a power system with nominal voltages within a range that is well catered for by Standard IEC 60909 and IEC 61313 was developed and optimised. Using the proposed experimental procedures in Chapter 4, the EAs managed to obtain coefficient values that were within an approximate range to the IEC values. MGAP, MPSO, MPSOF and MPSOP

coefficients deviated by not more than 6% from the IEC values. This resulted in their impedances deviating by less than 4% from the CMs impedances. Moreover, in determining R/X and R/Z values, the MGAP, MPSO, MPSOF and MPSOP runs had a 'confidence interval' greater than 90%. The three-phase fault currents that the EAs obtained were similar to the fault currents that were obtained by the CMs; with the EAs results arguably much better because of their efficacious and dependable fault evaluation procedures. The proposed methodology was also tested for its precision and reliability when there is an increase in the number of machines contributing to the fault current. Regardless of these uncertainties, the EAs still produced results within an approximate range to those produced by CMs.

This implies that if the methodology could give comparable results to CMs within the well-defined ranges, the proposed methodology can still go on to sufficiently satisfy nominal voltage regions that are not well catered for by CMs and Standard IEC. EAs can sufficiently sustain any nominal voltage because the proposed methodology optimises power systems on a case-to-case basis with regards to the parameters and unique specifications of a power system. The R/X and R/Z values that are used by EAs during fault evaluation, in all instances, are determined stochastically based on the properties of the power system. This leads to obtaining precise fault values in all instances. The proposed methodology can also be used to detect much more precise fault magnitudes at various network levels thereby designing, setting up and repairing power systems sufficiently.

The successful optimisation of the network in Chapter 4 shows that EAs can support both small and large networks of the radial distribution sub-systems. This means that EAs can also support the ring and the meshed distribution sub-systems since they are derivatives of the radial distribution sub-system. Henceforth, EAs can be successfully used for the complex problem of detecting three-phase short circuit faults for any nominal voltage within 550kV.

By using evolutionary algorithms for three-phase fault evaluation, the following procedures (for any nominal voltage) can be executed much more swiftly and conveniently i.e.

- Obtaining minimum and maximum fault currents.
- Setting-up power systems equipment effectively, efficiently and adequately.
- Determining the time requirements for the operation of various discrimination devices.
- Obtaining a much-informed guide on touch voltages and over-current protection.

6.2 Recommendations

There remains a need for more research on the depth and further applicability of evolutionary algorithms to the problem of computing short-circuit faults. One of the delimitations to this research was that not all possible operating scenarios associated with modern power systems could be tested. Therefore more research still needs to be done to determine the extensiveness of the applicability of evolutionary algorithms to this computational problem. Also, much research still needs to be done on finding other suitable hybrid functions to merge with the evolutionary algorithms. There also remains a need for further investigating how different network structures and sizes affect the results of EAs

6.3 Publications

I. Published Conference paper at ISCMI 2019 6th Intl. Conference on Soft Computing & Machine Intelligence. Title of the article is 'A Survey on the Recent Development of Asymmetrical Three Phase Short Circuit Faults Computation in Power Systems'.
II. Submitted Journal Paper to the International Journal of Computing. Title of the article is 'A Genetic Algorithm-based approach for three-phase fault evaluation in a Distribution Network'.

Acceptance Notification of Full Paper

2019 6th Intl. Conference on Soft Computing & Machine Intelligence
November 19-20, 2019, Johannesburg, South Africa
http://www.iscmi.us/index.html

Organized by | Technically Sponsored by

Paper ID#: MI003
Title of full Paper: A Survey on Recent development of Asymmetrical Three Phase Short Circuit Faults Computation in Power Systems

Dear Chikomborero Shambare, Yanxia Sun and Odunayo Imoru,

Congratulations! We're pleased to inform you that your full paper above has passed the blind review of the conference technical committees and has been accepted for both publication and oral presentation at the conference 2019 6th Intl. Conference on Soft Computing & Machine Intelligence (ISCMI 2019), Johannesburg, South Africa during November 19-20, 2019.

Your paper will be published in the **ISCMI 2019 Conference Proceedings** which are expected to be included in IEEE Xplore and indexed by EI Compendex, Scopus, etc.

References

Ababneh, J. (2015). Greedy particle swarm and biogeography-based optimization algorithm, International Journal of Intelligent Computing and Cybernetics, Vol. 8 Issue: 1, pp.28-49, https://doi.org/10.1108/IJICC-01-2014-0003

Ashish, K. N. (2015). Transmission line fault location based on distributed parameter line model. International Journal of Advanced Research in Electrical, Electronics and Instrumentation Engineering, Vol 4, pp.69-77.

Ashvini, B., Nagdewate, Swapnil, C. & Saurabh, M. (2015). Transmission fault analysis by Matlab simulation. IJESRT, Vol 2, pp. 330-333.

Bakshi, A. & Kulkarni, S.V. (2012). Towards short-circuit proof design of power transformers, COMPEL - The international journal of computation and mathematics in electrical and electronic engineering, Vol. 31, Issue: 2, pp.692-702, https://doi.org/10.1108/03321641211200662

Cai, B., Zhao, Y., Liu, H. & Xie, M. (2017). A data-driven fault diagnosis methodology in three phase inverters for PMSM drives systems. IEEE Trans Power Electronics, Vol 16, pp. 5590-5600.

Cai, C., Jiang, B. & Deng, L. (2015). General dynamic equivalent modelling of microgrid based on physical background. Energies, Vol 1, pp. 12929-12948.

Campoccia, A., Sanseverino, E.R. & Zizzo, G. (2007). A mathematical approach for studying interconnected earthing systems inside MV networks, COMPEL - The international journal of computation and mathematics in electrical and electronic engineering, Vol. 26 Issue: 5, pp.1364-1391, https://doi.org/10.1108/03321640710823064

Campos, M., Krohling, R. A. & Enriquez, I. (2014). Bare bones particle swarm optimization with scale matrix adaptation. IEEE Transactions on Cybernetics, Vol 44, pp. 1567-1578.

Carvalho, D.F.D. & Bastos-Filho, C.J.A. (2009). Clan particle swarm optimization, International Journal of Intelligent Computing and Cybernetics, Vol. 2 Issue: 2, pp.197-227, https://doi.org/10.1108/17563780910959875

Chavali, P., Yang, P. & Nehorai, A. (2014). A Distributed Algorithm for Home Energy Management System. IEEE Trans Smart Grid, Vol 4, pp. 282-290.

Costa, F. B. et al., (2015). Real-time detection of transients induced by high-impedance faults based on boundary wavelet transform. IEEE Trans. Industry Applications, Vol 51, pp. 5312-5323.

Cvetkovski, G., Petkovska, L. & Lefley, P. (2014). Optimal design of single phase permanent magnet brushless DC motor using particle swarm optimisation, COMPEL: The International Journal of Computation and Mathematics in Electrical and Electronic Engineering, Vol. 33 Issue: 6, pp.1863-1876, https://doi.org/10.1108/COMPEL-11-2013-0379

Dall'Anese, E. & Dhlope, S. V. (2016). Photovoltaic Inverter Controllers Seeking AC Optimal Power Flow Solutions. IEEE Transactions on power systems, Vol 31, pp. 2809-2823.

Das, J. C. (2017). Short-Circuit in AC and DC Systems ANSI, IEEE and IEC Standards. First edition. Boca Raton: CRC Press, Georgia.

Das, J. C. (2016). Power System Analysis - Short-Circuit Load Flow and Harmonics. Second edition. Boca Raton: CRC Press, Georgia.

Das, J.C. (2012), Power System Analysis Short-Circuit Load Flow and Harmonics. Second edition. Boca Raton: CRC Press, Georgia.

Dębowski, K. & Pasko, M. (2009). Symmetrization of asymmetrical nonlinear three-phase load supplied from non-ideal sinusoidal voltage source, COMPEL - The international journal of computation and mathematics in electrical and electronic engineering, Vol. 28 Issue: 3, pp.512-522, https://doi.org/10.1108/03321640910940819

Efe, S. B. (2015). Analysis and elimination of harmonics by using passive filters. BEU Journal of Science and Technology, Vol 5, pp. 48-51.

Elmqvist, H. & Mattsson, S. (2016). Exploiting model graph analysis for simplifies modelling and improved diagnostics. 7th International Workshop on Equation-Based Object Oriented Modelling Languages and Tools, pp. 7-14.

Folarin, A. et al., (2018). Modelling and simulation of loads into existing distribution network system using Matlab/Simulink. International organisation of scientific research-Journal of Electrical and Electronics Engineers (IOSR-JEEE), Vol 1, pp. 57-65.

Gast , N., Tomozei, D. C. & Le Boudec, J. (2014). Optimal generation and storage scheduling in the presence of renewable forecast uncertainties. IEEE Trans Smart Grid, Vol 4, pp.1328-1339.

Gao, Z., Cecati, C. & Ding, S. X. (2015). A survey of fault diagnosis and fault tolerant techniques-part 1: Fault diagnosis with model-based and signal based approaches. IEEE Trans Industrial Electronics, Vol 9, pp. 3757-3767.

Ghaderi, A., Mohammadpour, H. A., Ginn, H. L. & Shin, Y. J. (2015). High-impedance fault detection in distribution network using the time-frequency-based algorithm. IEEE Trans. Power Development, Vol 30, pp. 1260-1268

Ghamisi, P. & Benediktsson, J. A. (2015). Feature selection based on hybridization of genetic algorithm and particle swarm optimization. IEEE Geoscience and Remote Sensing Letters, Vol 12, pp. 303-313.

Han, R. & Zhou, Q. (2016). Data driven solutions for power systems fault analysis and novelty detection. The 11th International Conference on Computer Science and Education. pp. 86-91.

IEC 60909-0, (2016). Short-circuit currents in three-phase ac systems. Calculation of currents International Standard.

IEC 60909-0. (2001). Short-Circuit Currents in Three-Phase a.c. Systems - Calculation of Currents (1 ed.).

IEC 909-4. (2000). Short-Circuit Currents in Three-Phase a.c. Systems-Examples for the Calculation of Short-Circuit Currents (1 ed.).

Imoru, O., Bhaskar, M. A., Jimoh, A. A.G. & Haman, Y. (2017). Diagnosis of stator shorted-turn faults in induction machines using discrete wavelet transform. African Journal of Science, Technology, Innovation and Development. Vol 1, pp. 108-116. https://doi.org/10.1080/20421338.2017.1327933

Javaid, N. et al., (2017). A new meta-heuristic optimization algorithm inspired from strawberry plant for demand side management in smart grid. International Conference on Intelligent Networking and Collaborative Systems, pp. 143-154.

Juszczak, E. N. & Michał, (1992). The FEM Analysis of Non-symmetrical Short Circuit Forces And Fields In The Window Of Convertor Transformer, COMPEL - The international journal of computation and mathematics in electrical and electronic engineering, Vol. 11 Issue: 1, pp.213-216, https://doi.org/10.1108/eb051790

Kim, S. & Overby, T. (2015). Optimal subinterval selection approach for power system transient stability simulation. Energies, Vol 3, pp. 11871-11882.

Kono, T. & Katsura, S. (2016). Clarification of fundamental motion using hierachichal clustering and graph theory. IEEE Trans Industry Applications, Vol 9, pp.108-116.

Leva, S. & Morando, A.P. (2005). Lossy three-phase transmission line transient analysis by Park approach, COMPEL - The international journal of computation and mathematics in electrical and electronic engineering, Vol. 24, Issue: 3, pp.1041-1060, https://doi.org/10.1108/03321640510571237

Li, P. & Xiao, H. (2014). An improved quantum-behaved particle swarm optimization. The international journal of Applied intelligence, Vol 40, pp. 479-496.

Li, Y., He, H., Wang, Y., Xu, X. & Jiao, L. (2015). An improved multi-objective estimation of distributed algorithm for environmental economic dispatch of hydrothermal power systems. The international journal of Applied Soft Computing, Vol 14, pp.559-568.

Lim, H. W. & Isa, N. A. M. (2014). Particle swarm optimization with increasing topology connectivity. The international journal of Engineering Applications of Artificial Intelligence, Vol 27, pp. 80-102.

Malik, O. P., & Sallam, A.A (2011). Electric Distribution Systems. New Jersey: John Wiley & Sons.

Mathur, A., Pant, V. & Das, B. (2015). Unsymmetrical short-circuit analysis for distribution system considering loads. International Journal of Electrical Power and Energy Systems, Vol 70, pp. 27-38.

Mishra, M. et al., (2015). A Study on the Limitations of Evolutionary Computation and other Bio-Inspired Approaches for Integer Factorization. The 2015 International Conference on Soft Computing and Software Engineering (SCSE 2015), pp. 603-610.

Nitin, G. & Hasabe, R. P. (2015). A Comparison of Different Mother Wavelet for Fault Detection & Classification of Series Compensated Transmission Line. IJIRST- International Journal of Innovative Research in Science & Technology, Vol 1, pp. 78-86

Osowski, S. & Salat, R. (2002). Fault location in transmission line using hybrid neural network, COMPEL - The international journal of computation and mathematics in electrical and electronic engineering, Vol. 21 Issue: 1, pp.18-30, https://doi.org/10.1108/03321640210410715

Parhi, D.R., Das, H.C., Kumar, P.B., Muni, M.K. & Salony, K. (2019). Path optimization for navigation of a humanoid robot using hybridized fuzzy-genetic algorithm, International Journal of Intelligent Unmanned Systems, Vol. 7, Issue: 3, pp.112-119, https://doi.org/10.1108/IJIUS-11-2018-0032

Prince, J. & Bindu, V. R. (2014). Wavelet based transmission line fault Analysis. International Journal of Engineering and Innovation Technology (IJEIT), Vol 3, pp. 55-60.

Rao, R. & Jaya, (2016). A simple and new optimization algorithm for solving constrained and unconstrained optimization problems. International Journal of Industrial Engineering Computations, Vol 7, pp. 19-34.

Shou, Y. Y., Li, Y. & Lai, C. T. (2015). Hybrid particle swarm optimization for pre-emptive resource-constrained project scheduling. The international journal of Neurocomputing, Vol 148, pp. 122-128.

Sahoo, L., Bhunia, A.K. & Roy, D. (2014). Reliability optimization in stochastic domain via genetic algorithm, International Journal of Quality & Reliability Management, Vol. 31 Issue: 6, pp.698-717, https://doi.org/10.1108/IJQRM-06-2011-0090

Sallam, A. A., & Malik, O. P. (2011). Electric Distribution Systems, John Wiley & Sons, New Jersey.

Samson, R. S., Sundar, R., Amutha, A. & Nithiyananthan, K. (2016). Visual state estimation calculator model for three phase power network. Journal of Energy and Power Engineering, Vol 10, pp. 497-503.

Sanseverino, E.R., Campoccia, A., Di Silvestre, M.L. & Zizzo, G. (2012). A simple unsynchronized two-end algorithm for faults location and identification in electrical distribution systems, COMPEL - The international journal for computation and mathematics in electrical and electronic engineering, Vol. 31 Issue: 2, pp.636-655, https://doi.org/10.1108/03321641211200626

Sarlak, M. & Shahrtash, S.M. (2011). SVM-based method for high-impedance faults detection in distribution networks, COMPEL - The international journal for computation and mathematics in electrical and electronic engineering, Vol. 30, Issue: 2, pp.431-450, https://doi.org/10.1108/03321641111101014

Sheng, B., Deng, C., Wang, Y. & Xie, S. (2016). Improved multi-faults diagnosis for CNC machine tools. Mechatronics and Embedded Systems and Applications (MESA), 12th IEEE/ASME International Conference on IEEE, pp. 1-6.

Sing, T. Y. et al., (2016). Cluster Analysis Based Fault Identification Data Mining Models for 3 Phase Systems. International Journal of Innovation Scientific Research, Vol 24, pp.16-25.

Smriti, K. & Dharmendra, K. S. (2014). Simulation of fault Detection for protection of Transmission line using neural network. International Journal of Science, Engineering and Technology Research (IJSETR), Vol 3, pp.50-57.

Soroudi, A., Siano, P. & Keane, A. (2016). Optimal DR and ESS Scheduling for Distributed Losses Payments Minimization under Electricity Price Uncertainty. IEEE Trans Smart Grid, Vol 6, pp.261-272.

Tan, Y. (2015). Local Outlier Factor Based Data Mining Model for Three Phase Transmission Lines Fault Identification. International Journal of Computer Applications, Vol 130, pp. 17-23.

Tleis, N. (2008), Power Systems Modelling and Fault Analysis Theory and Practice, Elsevier, Oxford

Umasankar & Nithiyananthan, K. (2016). Environmental Friendly Voltage Up-gradation Model For Urban Electrical Distribution Power Systems. International Journal of Electrical and Computer Engineering, Vol 6, pp 88-96.

Varun, J., Dias, N., Arulselyan, G. & Pushpakumar, G. (2016). Fault Simulations on a Distribution Network through a GUI. International Journal of Innovative Research in Electrical, Electronics, Instrumentation and Control Engineering, Vol 4, pp.55-64.

Vitorino, L. N., Ribeiro, F. S. & Bastos-Filho, C. J. A. (2015). A mechanism based on artificial bee colony to generate diversity in particle swarm optimization. The international journal of Neurocomputing, Vol 148, pp. 39-45.

Yao, Y., Wang, Y., Xing, L. & Xu, H. (2015). An optimization method of technological processes to complex products using knowledge-based genetic algorithm, Journal of Knowledge Management, Vol. 19 Issue: 1, pp.82-94, https://doi.org/10.1108/JKM-11-2014-0454

Yudong, M., Hua, J., & Sidan, D. (2014). Two-way cyclotomc orthogonal space-time transmission scheme for asynchronous cooperative systems. The international journal of Computing, Networking and Communications (IJCNC), Vol 6, pp. 686-690.

Zhang, N., Kang, C., Xia, Q. & Liang, J. (2014). Modelling conditional forecast error for wind power in generation scheduling. IEEE Trans Power Systems, Vol 2, pp.1316-1324.

Zhang, Y. et al., (2014). Artificial intelligence and its applications. The international journal of Mathematics Problems in Engineering, Vol 8, pp. 25-37.

Zhang, Y. et al., (2014). Swarm intelligence and its applications. The Scientific world Journal, Vol 11, pp. 54-64.

Zhang, Y. et al., (2017). Intelligent early warning of power system dynamic insecurity risk towards optimal accuracy-earliness tradeoff. IEEE Trans Industrial Informatics, Vol 13, pp. 2544-2554.

Zhang, Y., Gong, D., Hu, Y. & Zhang, W. (2015). Feature selection algorithm based on bare bones particle swarm optimization. The international journal of Neurocomputing, Vol 148, pp. 150-157.

Zhu, J. (2015), Optimization of Power System Operation, Second Edition, IEEE Press, John Wiley & Sons, New Jersey, NJ